Zoosyst. Evol. 101 (1) 2025, 141–171 | DOI 10.3897/zse.101.136177

PENSOFT

MUSEUM FÜR NATURKUNDE BERLIN

Species delimitation of newly collected spiders of the genus *Pseudopoda* (Araneae, Sparassidae) from Honghe Hani and Yi Autonomous Prefecture, Yunnan, China: An integrated morphological and molecular approach

Jianshuang Zhang[1*], Tianqin Pan[1*], He Zhang[2,3,4], Yuanqian Xing[1], Hao Yu[1], Yang Zhong[2]

1 *The State Key Laboratory of Southwest Karst Mountain Biodiversity Conservation of Forestry Administration, School of Life Sciences, Guizhou Normal University, Guiyang, Guizhou, China*

2 *School of Nuclear Technology and Chemistry & Biology, Hubei University of Science and Technology, Xianning, Hubei, China*

3 *Guo Shoujing Innovation College, Xingtai University, Xingtai, Hebei, China*

4 *Hebei Province Sweet Potato Breeding and Application Technology Innovation Center, Xingtai, Hebei, China*

https://zoobank.org/29911097-4CEB-47ED-8CF4-13B5D1737E10

Corresponding author: Yang Zhong (hubeispider@aliyun.com)

Academic editor: Danilo Harms ♦ **Received** 2 September 2024 ♦ **Accepted** 9 January 2025 ♦ **Published** 29 January 2025

Abstract

A further study of the spider genus *Pseudopoda* Jäger, 2000, from Honghe Hani and Yi Autonomous Prefecture, Yunnan, southwest China, is presented. A total of six species are here addressed based on morphology and five methods of molecular species delimitation, increasing the number of known species of the genus in this area from 10 to 13. They comprise three new species, namely *P. xiaozhua* J. Zhang, H. Yu & Y. Zhong, **sp. nov.** (♂♀), *P. yangae* J. Zhang, H. Zhang & Y. Zhong, **sp. nov.** (♂♀), and *P. ying* J. Zhang, H. Zhang & Y. Zhong, **sp. nov.** (♂), and three known species: *P. huanglianensis* Zhang, Jäger & Liu, 2023, *P. mamillaris* Zhang, Jäger & Liu, 2023, and *P. oliviformis* Zhang, Jäger & Liu, 2023. The males of the three known species are described for the first time. Detailed descriptions, diagnoses, photographs of the six species, and a distribution map for all 13 *Pseudopoda* species in Honghe Prefecture are provided. The DNA barcodes of the six species were obtained for species delimitation, sex matching, and future use.

Key Words

Biodiversity, DNA barcoding, huntsman spider, molecular species delimitation, morphology, new species, southwest China

Introduction

Pseudopoda Jäger, 2000, is the largest genus of the family Sparassidae Bertkau, 1872, currently including 261 extant species and having a broad distribution across South, East, and Southeast Asia (Wu et al. 2024; WSC 2025). Currently, a total of 158 *Pseudopoda* species are known from China, approximately 60% of the globally recognized species, making it the country with the most *Pseudopoda* species (Chang et al. 2024; Wu et al. 2024; WSC 2025). However, the diversity of this genus in China is still not fully discovered, as a considerable number of species have been described in recent years (WSC 2025).

Most *Pseudopoda* species have been described in detail, alongside high-quality illustrations, with 67 species clearly assigned to nine species groups to facilitate

* These authors contributed equally to this work.

species recognition (Jäger 2001; Zhang et al. 2017; Li et al. 2019; Zhang et al. 2019; Zhang et al. 2023a). Despite this, the genus remains inadequately studied, particularly in terms of its α-taxonomy. We have to consider the following phenomena: (1) The collection of paired mature specimens is very difficult in the field, resulting in more than half of *Pseudopoda* species being reported from a single sex (55 from males only, 80 from females only) (WSC 2025); (2) most *Pseudopoda* species exhibit a typical sympatric distribution pattern, especially in certain biodiversity hotspots (such as the Gaoligong Mountains and the Himalayan region, etc.), where they show high local species richness (Jiang et al. 2018; Zhang et al. 2023a: MAP1–MAP6). For example, at least 20 species can be found in Nujiang Lisu Autonomous Prefecture and 19 species in Baoshan City (both of which are part of the Gaoligong Mountains in China) (Jäger and Vedel 2007; Zhang et al. 2013a, b; Jiang et al. 2018; Zhang et al. 2023a), and more than 60 species have been described from the Himalayas and neighboring mountains) (Jäger 2001; Zhang et al. 2023a: MAP3); (3) morphologically, some species exhibit extraordinary intraspecific variation but low-level interspecific variation (Jäger 2001; Cao et al. 2016; Gong et al. 2023; Zhang et al. 2023a); (4) nearly 200 species cannot be readily assigned to any of the existing species groups, requiring comparisons of diagnostic illustrations from over 200 species for accurate identification of *Pseudopoda* species (Zhang et al. 2023a; for details, see section 'Comments on this genus' in the taxonomic accounts below). For these reasons, the α-taxonomy of *Pseudopoda* likely suffers from common taxonomic errors, such as over-splitting (e.g., a single species being subdivided into two or more similar species, or conspecific males and females being described as separate species), over-lumping (e.g., cryptic species being overlooked), and incorrect species assignments of individuals or populations (e.g., adults being mismatched). Undoubtedly, when reporting *Pseudopoda* species that are sympatrically distributed within a very limited range, we should exercise extreme caution and preferably adopt an integrative taxonomic approach. Fortunately, rapid species delimitation using a few or even a single locus (such as COI) as a barcode has already been successfully applied to various spider taxa in recent years, including several genera of Liphistiidae (Xu et al. 2015; 2017), Leptonetidae (*Leptonetela*) (Wang et al. 2017), Thomisidae (*Phrynarachne*) (Xu et al. 2022), Pholcidae (*Pholcus*) (Yao et al. 2021), and Sparassidae (*Pseudopoda*) (Cao et al. 2016), etc. However, recent studies on the genus *Pseudopoda* have continued to rely primarily on morphological characteristics rather than integrating DNA barcode data (Jiang et al. 2018; Deng et al. 2023; Zhang et al. 2023a).

The Honghe region reaches an elevation of 3074 meters and is home to some of the best-preserved humid evergreen broadleaf primeval forests in China, recognized as one of the three major biodiversity conservation hotspots in the country (Zhang et al. 2023b). It is well known that *Pseudopoda* is frequently found in moist, warm forests in high-altitude areas (Jäger 2001; Jäger et al. 2015; Jiang et al. 2018; Zhang et al. 2023a). However, *Pseudopoda* is poorly represented in Honghe Prefecture, with only 10 species, seven of which were described by Zhang et al. (2023a). Only two have been reported based on both sexes; one is known only from males, and the remaining seven are known only from females (Table 1).

A recent field collection in Honghe Prefecture was carried out in April, 2024 (Fig. 1). During this field exploration, we came across some spider specimens from the genus *Pseudopoda* that belong to at least six morphospecies. Sympatric distribution and high intraspecific morphological variation in certain species pose significant challenges for sexual pairing and species identification. We therefore generated DNA barcode data to devise a specimen phylogeny and used the five molecular species delimitation methods to test the morphology-based species identification. We then used the consensus results to delimit and diagnose the newly collected *Pseudopoda* spiders from Honghe Hani and Yi Autonomous Prefecture.

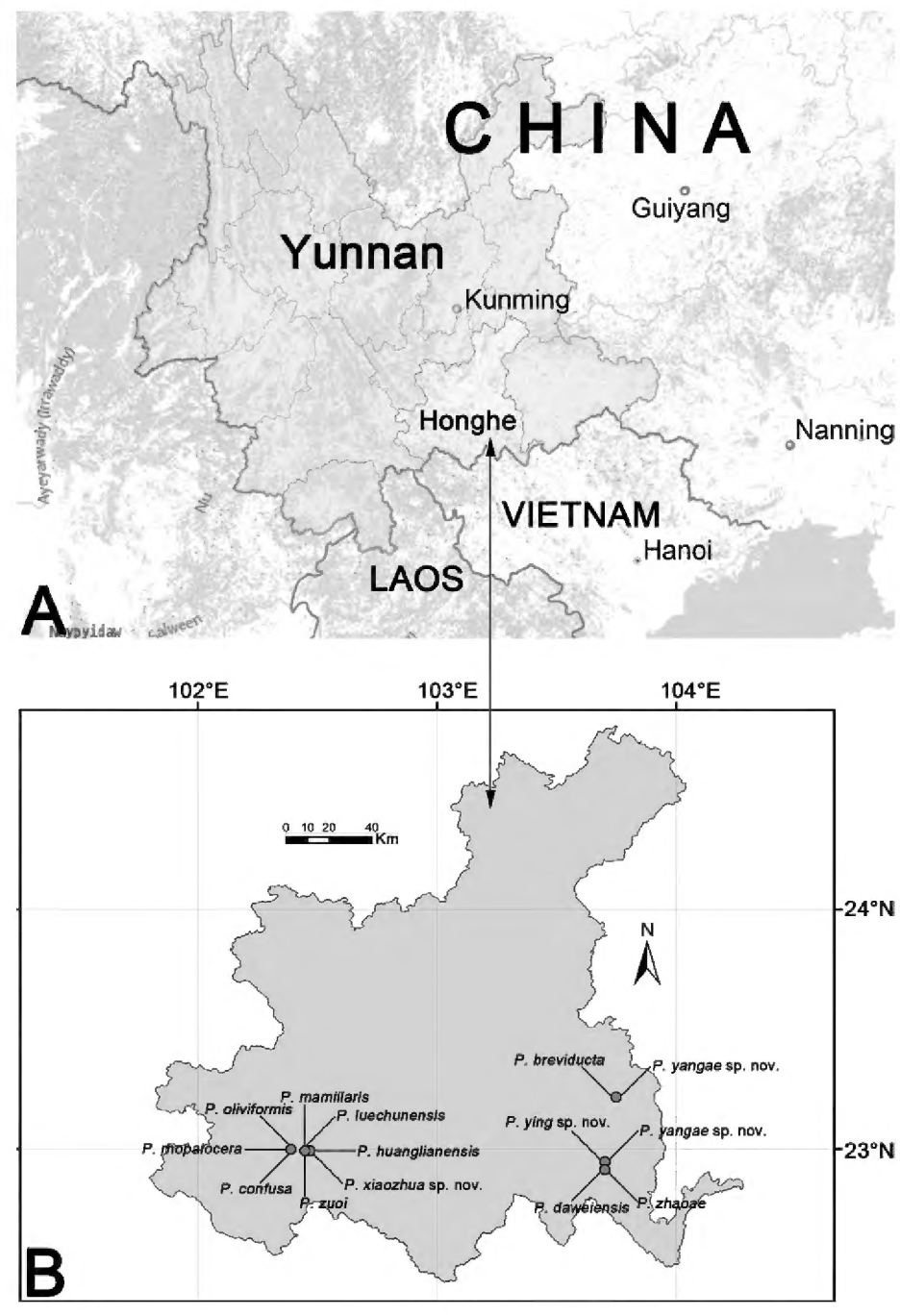

Figure 1. Locality of Honghe Hani and Yi Autonomous Prefecture (**A**) and distribution records (**B**) of *Pseudopoda* species in Honghe Prefecture.

Table 1. Checklist of *Pseudopoda* species from Honghe Hani and Yi Autonomous Prefecture.

	Species name	Authorship	Known sex	References
1	*P. breviducta*	Zhang, Zhang & Zhang, 2013	♂	Zhang et al. 2013a; female described in the original paper, considered misidentified in present paper
2	*P. confusa*	Jäger, Pathoumthong & Vedel, 2006	♂♀	Jäger et al. 2006; Zhang et al. 2023a
3	*P. daweiensis*	Zhang, Jäger & Liu, 2023	♀	Zhang et al. 2023a
4	*P. huanglianensis*	Zhang, Jäger & Liu, 2023	♂♀	Zhang et al. 2023a; male supplemented in present paper
5	*P. luechunensis*	Zhang, Jäger & Liu, 2023	♂	Zhang et al. 2023a
6	*P. mamillaris*	Zhang, Jäger & Liu, 2023	♂♀	Zhang et al. 2023a; male supplemented in present paper
7	*P. oliviformis*	Zhang, Jäger & Liu, 2023	♂♀	Zhang et al. 2023a; male supplemented in present paper
8	*P. rhopalocera*	Yang, Chen, Chen & Zhang, 2009	♀	Yang et al. 2009; Zhang et al. 2023a
9	*P. zhaoae*	Zhang, Jäger & Liu, 2023	♀	Zhang et al. 2023a
10	*P. zuoi*	Zhang, Jäger & Liu, 2023	♀	Zhang et al. 2023a
11	*P. xiaozhua* sp. nov.	J. Zhang, H. Yu & Y. Zhong	♂♀	present paper
12	*P. yangae* sp. nov.	J. Zhang, H. Zhang & Y. Zhong	♂♀	present paper
13	*P. ying* sp. nov.	J. Zhang, H. Zhang & Y. Zhong	♂	present paper

Materials and methods

Taxon sampling

Specimens in this study were collected alive by hand and directly fixed in absolute ethanol, and then the right legs were removed to be stored at −80 °C for subsequent DNA extraction. The remainder of the specimens was preserved in 80% ethanol for identification and morphological examination. A total of 26 adults were obtained, examined, and processed for DNA extraction. However, we were unable to obtain high-quality DNA extractions from three samples. Finally, we sampled 23 individuals for molecular species delimitation (Table 2). All voucher specimens (including types of the three new species) are deposited in the Museum of Guizhou Normal University, Guiyang, China.

Molecular protocols

Total genomic DNA was extracted using the Cell & Tissue Genomic DNA Isolation Kit (Bioteke, Beijing, China), following the manufacturer's protocols. We amplified cytochrome c oxidase subunit I (COI) using the primer pairs LCO1490/HCO2198 (Folmer et al. 1994) and standard polymerase chain reaction (PCR) settings (Cao et al. 2016). PCR products were sent to the Beijing Tsingke Biotech Co., Ltd. (Chongqing, China) for sequencing using the same PCR primers. We manually edited the sequences using Geneious Prime 2024 (Kearse et al. 2012), translated nucleotide sequences into amino acids to check for stop codons, and ensured the proper configuration of codon positions.

Phylogenetic analyses

For phylogenetic analyses, the COI data of 23 specimens of *Pseudopoda* were used as the in-group. In order to root the tree, we included two specimens, one of *Sinopoda anguina* Liu, Li & Jäger, 2008, and one of *S. pengi* Song & Zhu, 1999 (Cao et al. 2016) from GenBank, as the outgroup (Table 2). We performed maximum-likelihood (ML) analyses using IQ-TREE 2.3.1 (Minh et al. 2020) based on the best COI substitution model (GTR+I+G) in jMODELTEST 2.1.10 (Darriba et al. 2012). Branch supports were estimated with ultrafast bootstrapping with 1000 replicates (Hoang et al. 2018). The Bayesian-inference (BI) analysis in MrBayes 3.2.1 (Ronquist et al. 2012) was performed for Markov chain Monte Carlo (MCMC) with one independent chain for 50 million generations. The first 10% of trees from each run were discarded as burn-in. Finally, we used FigTree 1.4.4 (Rambaut 2012) to visualize and manipulate trees and used Photoshop CC 2018 to summarize them.

Molecular species delimitation

In order to delimit six putative morphospecies of *Pseudopoda* based on an accompanying morphological study of the genus, we conducted two genetic distance-based methods: the DNA barcoding gap (Barrett and Hebert 2005) and the ABGD (Puillandre et al. 2012), and three methods based on the inferred tree—the GMYC (Pons et al. 2006), the P ID (Liberal), and mPTP (Kapli et al. 2017).

As the P ID (Liberal) and DNA barcoding gap (Barrett and Hebert 2005) require a priori designation. We assigned 23 *Pseudopoda* individuals to six putative species based on a combination of phylogenetic topology and morphological characteristics. In the DNA barcoding gap, we examined the overlap between the interspecies and intraspecies Kimura two-parameter (K2P) and uncorrected p-distance for each candidate species calculated in MEGA X (Kumar et al. 2018). The P ID (Liberal) method tests different species delimitation relying on defining the putative species groups. We used BI tree as a guide tree to test species hypothesis (Xu et al. 2017).

The other three methods that we used do not require terminals to be assigned to putative species. ABGD calculates all pairwise distances in the data set, evaluates intraspecific divergences, and then sorts

Table 2. Samples used in species delimitation: specimen label, taxon name, sample collection locality with coordinates, and GenBank accession numbers.

Specimen code	Genus and species	Locality	Country	Coordinates	Elevation (m a.s.l.)	COI GenBank accession
YNZY013	*Pseudopoda huanglianensis*	Mount Huanglianshan, Luechun County, Honghe Autonomous Prefecture, Yunnan Pro.	China	22.99°N, 102.46°E	1940	PQ871005
YNZY014	*Pseudopoda huanglianensis*	Mount Huanglianshan, Luechun County, Honghe Autonomous Prefecture, Yunnan Pro.	China	22.99°N, 102.46°E	1940	PQ871006
YNZY024	*Pseudopoda huanglianensis*	Mount Huanglianshan, Luechun County, Honghe Autonomous Prefecture, Yunnan Pro.	China	22.99°N, 102.46°E	1940	PQ871007
YNZY025	*Pseudopoda huanglianensis*	Mount Huanglianshan, Luechun County, Honghe Autonomous Prefecture, Yunnan Pro.	China	22.99°N, 102.46°E	1940	PQ871008
YNZY009	*Pseudopoda mamillaris*	Martyr Cemetery, Luechun County, Honghe Autonomous Prefecture, Yunnan Pro.	China	22.99°N, 102.45°E	1940	PQ871009
YNZY010	*Pseudopoda mamillaris*	Martyr Cemetery, Luechun County, Honghe Autonomous Prefecture, Yunnan Pro.	China	22.99°N, 102.45°E	1940	PQ871010
YNZY023	*Pseudopoda mamillaris*	Martyr Cemetery, Luechun County, Honghe Autonomous Prefecture, Yunnan Pro.	China	22.99°N, 102.45°E	1940	PQ871011
YNZY011	*Pseudopoda oliviformis*	Martyr Cemetery, Luechun County, Honghe Autonomous Prefecture, Yunnan Pro.	China	22.99°N, 102.45°E	1934	PQ871012
YNZY012	*Pseudopoda oliviformis*	Martyr Cemetery, Luechun County, Honghe Autonomous Prefecture, Yunnan Pro.	China	22.99°N, 102.45°E	1934	PQ871013
YNZY015	*Pseudopoda oliviformis*	Martyr Cemetery, Luechun County, Honghe Autonomous Prefecture, Yunnan Pro.	China	22.99°N, 102.45°E	1934	PQ871014
YNZY016	*Pseudopoda oliviformis*	Martyr Cemetery, Luechun County, Honghe Autonomous Prefecture, Yunnan Pro.	China	22.99°N, 102.45°E	1934	PQ871015
YNZY003	*Pseudopoda xiaozhua* sp. nov.	Mount Huanglianshan, Luechun County, Honghe Autonomous Prefecture, Yunnan Pro.	China	22.99°N, 102.46°E	1940	PQ871018
YNZY004	*Pseudopoda xiaozhua* sp. nov.	Mount Huanglianshan, Luechun County, Honghe Autonomous Prefecture, Yunnan Pro.	China	22.99°N, 102.46°E	1940	PQ871019
YNZY018	*Pseudopoda xiaozhua* sp. nov.	Mount Huanglianshan, Luechun County, Honghe Autonomous Prefecture, Yunnan Pro.	China	22.99°N, 102.46°E	1940	PQ871020
YNZY001	*Pseudopoda yangae* sp. nov.	Mount Daweishan, Pingbian County, Honghe Autonomous Prefecture, Yunnan Pro.	China	22.94°N, 103.70°E	2365	PQ871021
YNZY002	*Pseudopoda yangae* sp. nov.	Mount Daweishan, Pingbian County, Honghe Autonomous Prefecture, Yunnan Pro.	China	22.94°N, 103.70°E	2365	PQ871022
YNZY005	*Pseudopoda yangae* sp. nov.	Mount Daweishan, Pingbian County, Honghe Autonomous Prefecture, Yunnan Pro.	China	22.94°N, 103.70°E	2365	PQ871023
YNZY006	*Pseudopoda yangae* sp. nov.	Mount Daweishan, Pingbian County, Honghe Autonomous Prefecture, Yunnan Pro.	China	22.94°N, 103.70°E	2365	PQ871024
YNZY017	*Pseudopoda yangae* sp. nov.	Mount Daweishan, Pingbian County, Honghe Autonomous Prefecture, Yunnan Pro.	China	22.94°N, 103.70°E	2365	PQ871025
YNZY020	*Pseudopoda yangae* sp. nov.	Mount Daweishan, Pingbian County, Honghe Autonomous Prefecture, Yunnan Pro.	China	22.94°N, 103.70°E	2365	PQ871026
YNZY021	*Pseudopoda yangae* sp. nov.	Mount Daweishan, Pingbian County, Honghe Autonomous Prefecture, Yunnan Pro.	China	22.94°N, 103.70°E	2365	PQ871027
YNZY007	*Pseudopoda ying* sp. nov.	Mount Daweishan, Pingbian County, Honghe Autonomous Prefecture, Yunnan Pro.	China	22.94°N, 103.70°E	2365	PQ871016
YNZY026	*Pseudopoda ying* sp. nov.	Mount Daweishan, Pingbian County, Honghe Autonomous Prefecture, Yunnan Pro.	China	22.94°N, 103.70°E	2365	PQ871017
S261	*Sinopoda anguina*	Yaojiaping Protection Station, Yunnan Pro.	China	25.96°N, 98.72°E	2588	KY096645
S457	*Sinopoda pengi*	Xishan Mountain, Yunnan Pro.	China	24.99°N, 102.62°E	2025	KY096644

the terminals into candidate species with calculated P-values. We performed on a web server (https://bio-info.mnhn.fr/abi/public/abgd/), using three different models: Jukes-Cantor (JC69; Jukes and Cantor 1969), K2P (Kimura 1980), and simple distance (p-distance; Nei and Kumar 2000). We analysed the data using two different values for the parameters P_{min} (0.001 and 0.0001), P_{max} (0.1 and 0.2), and relative gap width ($X = 1$ or 1.5), with the other parameters set to default values. We used BI tree as a guide tree to test species hypotheses (Xu et al. 2017). The mPTP analysis was run for MCMC analysis of 2 runs, each of 100 million steps, logging every one million steps and ignoring the first 2 million steps. Start each run from a random delimitation. The GMYC methodology (Pons et al. 2006) analysis was conducted using the single-threshold model in the "splits" package (Ezard et al. 2009) for R 4.2.2 (R Development Core Team 2024). An ultrametric gene tree for the GMYC analysis was converted using BEAST 2.6.7 (Bouckaert et al. 2014). Analyses were run for 50 million MCMC steps and discarded as "burn-in" 10% of the trees in each chain.

Morphological protocols

Specimens were examined using an Olympus SZX7 stereomicroscope. Further details were studied under a CX41 compound microscope. Besides new materials, specimens of all ten known species recorded from Honghe prefecture were re-examined for comparison, including types of seven species described by Zhang et al. (2023a).

Left male palps were examined and illustrated after dissection. Epigynes were removed and cleared in a warm 10% potassium hydroxide (KOH) solution. Images were captured with a Canon EOS 70D digital camera mounted on an Olympus CX41 compound microscope and assembled using Helicon Focus 6.80 image stacking software (Khmelik et al. 2005). All measurements were obtained using an Olympus SZX7 stereomicroscope and are given in millimetres. Eye diameters were measured at the widest part. The total body length does not include the chelicerae or spinnerets. Leg lengths are given as total length (femur, patella + tibia, metatarsus, tarsus). The number of macrosetae is listed for each segment in the following order: prolateral, dorsal, retrolateral, and ventral (in femora and patellae, ventral spines are absent, and the fourth digit is omitted in the setation formula). All species mentioned in this paper have 3 promarginal and 4 retromarginal cheliceral teeth. The ratio between palpal tibia length and cymbium was calculated by measuring both parts in a retrolateral view (as in Zhang et al. 2023a: Fig. 3C) and dividing the value of the tibia length by the cymbial length value. The same method is used to calculate the ratios of dRTA to palpal tibia and vRTA to dRTA.

The distribution map was generated with ArcGIS 10.5 (ESRI Inc). The terminology used in the text and figure legends follows Zhang et al. (2023a) and Zhang et al. (2013a, b). Abbreviations used in the text or figures are given in Table 3.

Table 3. List of abbreviations used in the text or figures.

Male palp	
C = conductor	**CB** = cymbial bulge
Cy = cymbium	**dRTA** = dorsal branch/part of RTA
E = embolus	**EB** = embolic base
ET = embolic tip	**RTA** = retrolateral tibial apophysis
Sp = spermophor	**St** = subtegulum
T = tegulum	**TA** = tegular apophysis
Ti = tibia	**vRTA** = ventral branch/part of RTA
Epigyne	
AB = anterior band	**aEF** = anterior margin of epigynal field
amLL = anterior margin of lateral lobes	**amMF** = anterior margin of median field
CO = copulatory opening	**FD** = fertilization duct
FW = first winding	**LL** = lateral lobe
MF = median field of epigyne	**mmLL** = median margin of lateral lobes
MS = membranous sac	**PI** = posterior incision
pmLL = posterior margin of lateral lobes	**S** = spermatheca
SA = spermathecal appendage	
Ocular area	
AER = anterior eye row	**CH** = clypeus height
ALE = anterior lateral eye	**PER** = posterior eye row
AME = anterior median eye	**PLE** = posterior lateral eye
AME–ALE = distance between AME and ALE	**PME** = posterior median eye
AME–AME = distance between AMEs	**PME–PLE** = distance between PME and PLE
AME–PLE = distance between AME and PLE	**PME–PME** = distance between PMEs
AME–PME = distance between AME and PME	
Legs and body	
DS = dorsal shield of prosoma	**Fe** = femur
Mt = metatarsus	**OS** = Opisthosoma
Pa = patella	**Ti** = tibia
I, II, III, IV = legs I to IV	

Results and discussion

Based on traditional morphological characters and experience (matching of males and females we had hypothesized mainly on the basis of co-occurrence and compatibility of epigyne and male pedipalpal structures), all newly collected materials can be identified as at least six morphospecies: three of them belong to undescribed species new to science: *P. xiaozhu* sp. nov., *P. yangae* sp. nov., *P. ying* sp. nov.; the remaining three were identified as *P. huanglianensis*, *P. mamillaris*, and *P. oliviformis* based on comparison with the type specimens (previously described based on holotype females only, respectively). However, some morphological variations are exhibited by different individuals of both sexes of *P. yangae* sp. nov. (further details can be found in the following comments for *P. yangae* sp. nov.). Furthermore, we discovered drawings by Zhang et al. (2013a) of the *P. breviducta* paratype female that bore striking similarity to females of *P. yangae* sp. nov., while the males of the two species exhibited significant differences. We therefore generated DNA barcodes and used the five molecular species delimitation methods to test the morphology-based species identification and matching of sexes.

The COI matrix of 23 *Pseudopoda* individuals analyzed in this study had a sequence length of 633 bp, with 171 variable and 163 parsimony-informative sites (Table 2). For COI, phylogenetic inference from BI and ML analyses yielded similar topologies, with the node being highly supported (Fig. 2; posterior probability, PP = 1; bootstrap value, BS = 100). The trees clearly divided the samples into eight deeply divergent clades (Fig. 2).

When assigning six species of *Pseudopoda*, a distinct gap between intraspecific and interspecific genetic distances was found, ranging from 2.09 to 5.45% for K2P (Fig. 3A) and from 2.05 to 5.21% for p-distance (Fig. 3B). The lowest mean interspecific distance was 5.45% / 5.21% (K2P / uncorrected p-distance) found between *P. mamillaris* and *P. huanglianensis*, and the highest mean intraspecific distance (0.85% / 0.84% K2P / uncorrected p-distance) was estimated for *P. oliviformis*. Compared with the barcoding gap of 4.8% - 6.25%

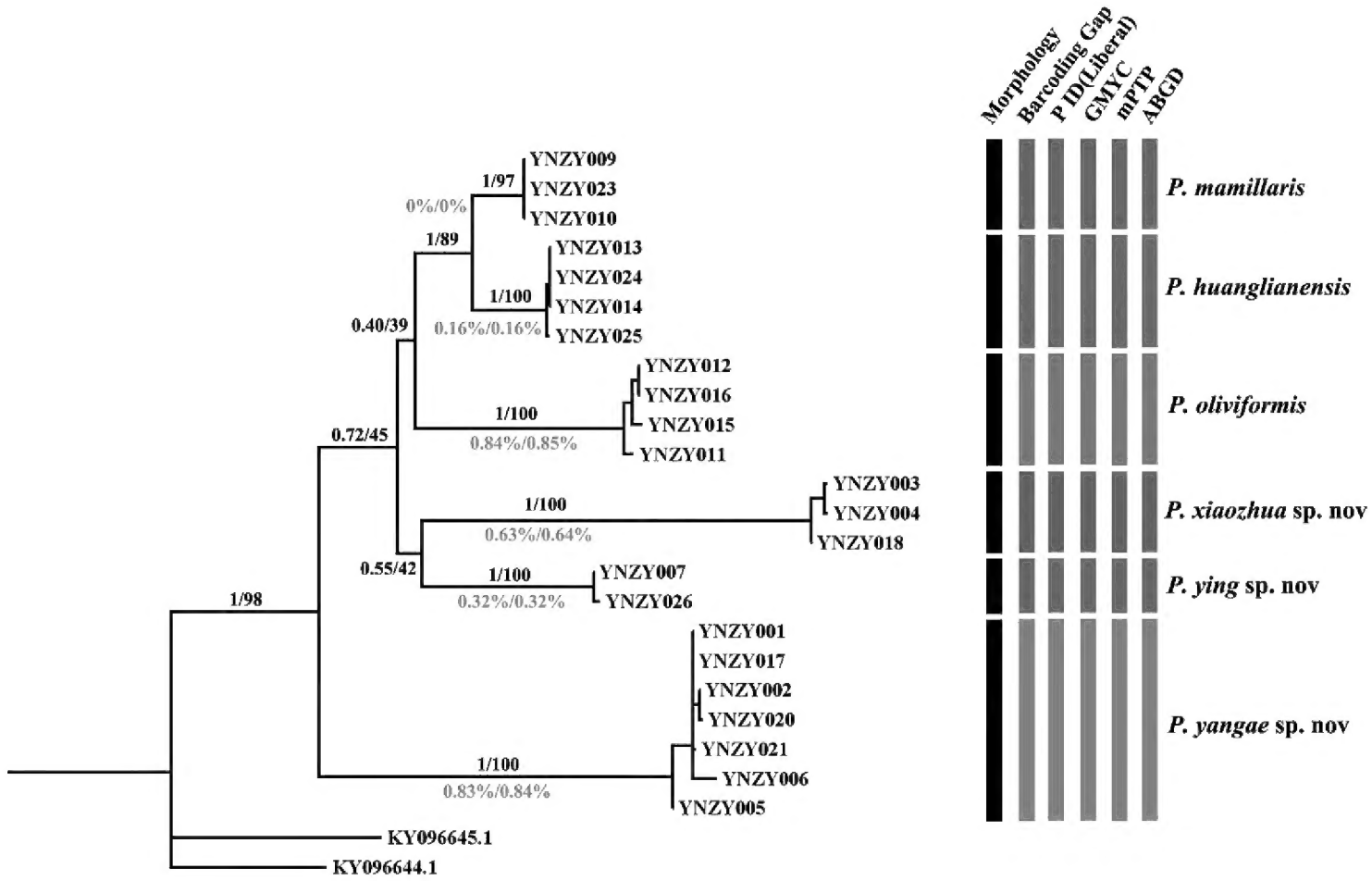

Figure 2. Bayesian CO1 gene tree for 23 terminals of *Pseudopoda* from Honghe Prefecture, with the results of five different species delimitation approaches, in addition to morphology (see legend). Numbers above branches show posterior probability and bootstrap supports (black), and values above show mean intraspecific (red), calculated as *Pseudopoda* p-distance/two-parameter (K2P). Species names (for species codes, see Table 2) according to consensus results of species delimitation approaches.

for the *Pseudopoda* genus (Cao et al. 2016), the gap is highly consistent with our barcoding gap results. Six species were identified by the barcoding gap range, of which three are known and three are new (Fig. 2).

In the ABGD results, different parameter combinations of both the initial and recursive partition yielded diverse outcomes (Table 4). The initial six species partition was consistent with those six morphospecies, while the recursive partition regime yielded more species (Fig. 2, Table 4). However, all analyses under different assumptions revealed the six hypothetical species, and this is entirely consistent with the morphological identification results (Fig. 2).

P ID (Liberal) is used to test species hypotheses based on the Bayesian inference tree (Xu et al. 2017). The mean probability, with the 95% confidence interval (CI) for the prediction, of making a correct identification of an unknown specimen. Our results revealed high P ID (Liberal) values ≥0.96 (0.81–1.0) (Table 5), thereby also supporting the taxonomy of six putative species (Fig. 2).

The mPTP can better accommodate the sampling- and population-specific characteristics of a broader range of empirical datasets compared to PTP analysis. Meanwhile, this method provides a Markov chain Monte Carlo (MCMC) sampling approach that allows the inference of delimitation support values (Kapli et al. 2017). The results of our mPTP analysis indicated that, when only monophyletic species are considered, the six hypothetical species are identified, as anticipated (Fig. 2). The mPTP model strongly supports the split for *P. ying* sp. nov, *P. yangae* sp. nov, and *P. xiaozhua* sp. nov and *P. oliviformis* (PP = 1.0). However, the posterior probability for *P. mamillaris* and *P. huanglianensis* was only 50%. This result may be attributed to genetic similarity, small sample sizes, or suboptimal genetic markers.

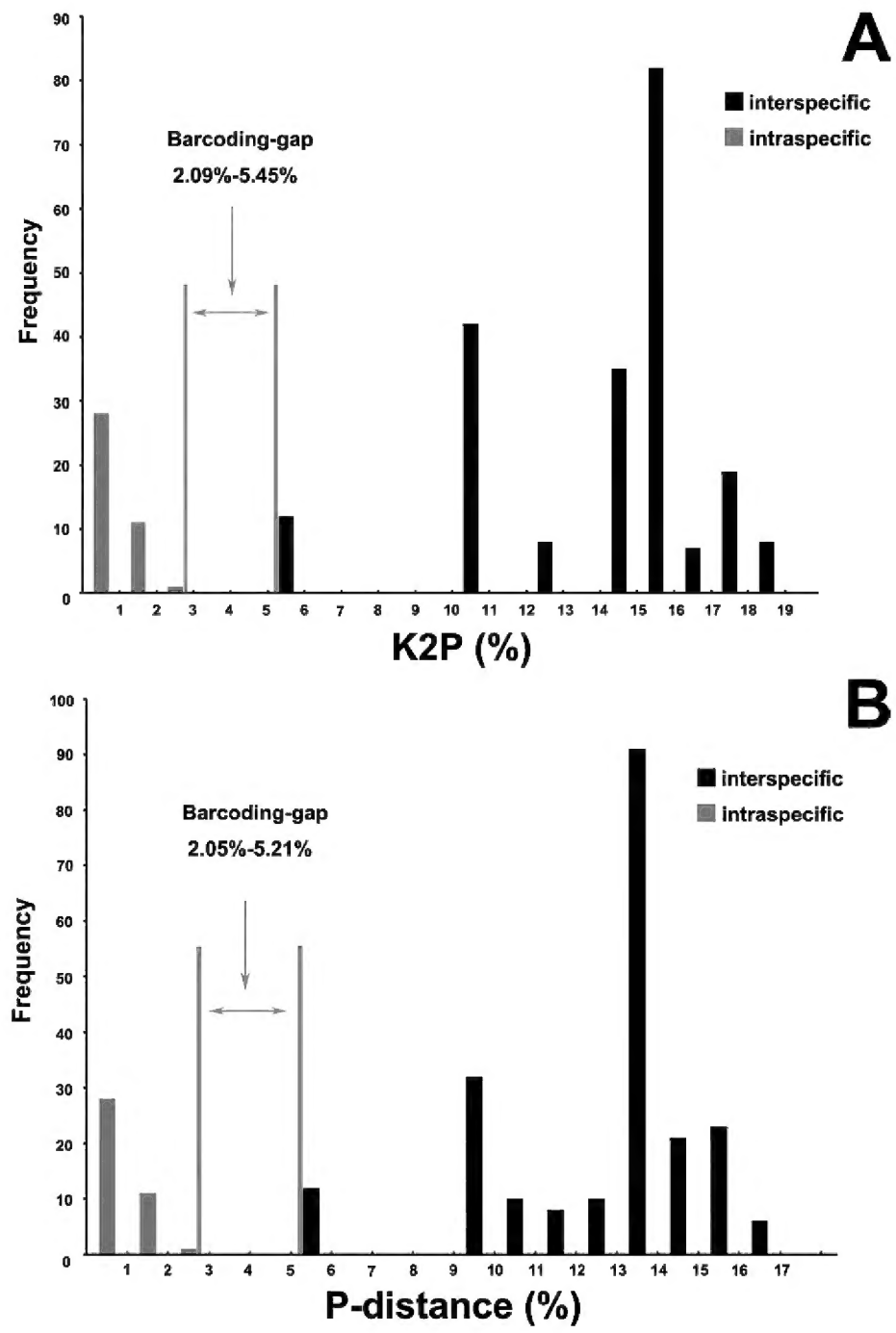

Figure 3. DNA barcoding gap for *Pseudopoda* from Honghe Prefecture. Histograms show the division of intraspecific (gray) and interspecific (black) CO1 sequence variation based on the Kimura two-parameter (K2P) (**A**) and uncorrected p-distance (**B**).

Table 4. Results of the automatic barcode gap discovery (ABGD) analysis.

Substitution model	P_{min}/P_{max}	X	Partiton	Prior intraspecific divergence (P)							
				0.001	0.0017	0.0028	0.0046	0.0077	0.0129	0.0215	0.0359
JC	0.001/0.1	1	Initial	6	6	6	6	6	6	6	6
			Recursive	8	8	8	6	6	6	6	6
K2P	0.001/0.1	1	Initial	6	6	6	6	6	6	6	6
			Recursive	8	8	8	7	6	6	6	6
Simple	0.001/0.1	1	Initial	6	6	6	6	6	6	6	6
			Recursive	8	8	8	6	6	6	6	6
JC	0.001/0.1	1.5	Initial	6	6	6	6	6	6	6	6
			Recursive	8	8	8	6	6	6	6	6
K2P	0.001/0.1	1.5	Initial	6	6	6	6	6	6	6	6
			Recursive	8	8	8	6	6	6	6	6
Simple	0.001/0.1	1.5	Initial	6	6	6	6	6	6	6	6
			Recursive	8	8	8	6	6	6	6	6
				0.0001	0.0002	0.0005	0.0013	0.0029	0.0068	0.1587	0.0369
JC	0.0001/0.2	1	Initial	6	6	6	6	6	6	6	6
			Recursive	8	8	8	8	8	6	6	6
K2P	0.0001/0.2	1	Initial	6	6	6	6	6	6	6	6
			Recursive	8	8	8	8	8	6	6	6
Simple	0.0001/0.2	1	Initial	6	6	6	6	6	6	6	6
			Recursive	8	8	8	8	8	6	6	6
JC	0.0001/0.2	1.5	Initial	6	6	6	6	6	6	6	6
			Recursive	8	8	8	8	8	6	6	6
K2P	0.0001/0.2	1.5	Initial	6	6	6	6	6	6	6	6
			Recursive	8	8	8	8	8	6	6	6
Simple	0.0001/0.2	1.5	Initial	6	6	6	6	6	6	6	6
			Recursive	8	8	8	8	8	6	6	6

JC, Jukes-Cantor substitution model; K2P, Kimura two-parameter substitution model; Simple, p-distance; *X*, relative gap width.

Table 5. Summary of the mean intraspecific and closest interspecific genetic distance, the mean probability with a 95% confidence interval, and the intra/interspecific ratio for the six putative species of *Pseudopoda*.

Putative species	Intraspecific K2P/*p*-distance	Closest interspecific K2P/*p*-distance	P ID (Liberal)	Closest P ID (Liberal) species	Intra/Inter
P. yangae sp. nov.	0.0084/0.0083	0.1498/0.1354	0.99 (0.93, 1.0)	*P. mamillaris*	0.05
P. ying sp. nov.	0.0032/0.0032	0.1074/0.0995	0.96 (0.81, 1.0)	*P. mamillaris*	0.03
P. xiaozhua sp. nov.	0.0064/0.0063	0.1525/0.1372	0.98 (0.84, 1.0)	*P. ying* sp. nov.	0.04
P. oliviformis	0.0085/0.0084	0.1063/0.0983	0.96 (0.85, 1.0)	*P. mamillaris*	0.08
P. mamillaris	0/0	0.0545/0.0521	0.98 (0.84, 1.0)	*P. huanglianensis*	0.04
P.huanglianensis	0.0016/0.0016	0.0545/0.0521	0.97 (0.86, 1.0)	*P. mamillaris*	0.04

As a species delimitation technique, the General Mixed Yule Coalescent (GMYC) produced the same results as the four methods mentioned above: six hypothetical species (Fig. 2). The single-threshold model GMYC resulted in six clusters and eight entities with different confidence intervals of 6-6 and 8-9, respectively (Table 6). Meanwhile, when visualizing the data as a tree in R, the results were consistent with those obtained from maximum likelihood (ML) and Bayesian inference (BI) analyses, with all methods displaying the same six branches (Fig. 2).

In conclusion, all analyses reported so far support six morphological species, with syntopic terminals being conspecific. Particularly for *P. yangae* sp. nov., the results from five molecular species delimitation analyses indicate that, despite considerable morphological variation among individuals, they should be classified as the same species: (1) Both the ABGD and GMYC methods, whether using multiple parameter settings or visualizing the data tree, support a single species (Fig. 2, Tables 4, 6); (2) these results are also supported by both the P ID (Liberal) and mPTP methods, with a P ID (Liberal) value of 0.99 (0.93, 1.0) (> 95%) (Table 5) and a posterior probability of one in mPTP; (3) our barcoding gap results (2.09% - 5.45% / 2.05% - 5.21% / K2P/uncorrected p-distance) further support that the average genetic distance (0.84% / 0.83% K2P/uncorrected p-distance) of *P. yangae* sp. nov. represents the intraspecific genetic distance (Fig. 2, 3). After careful re-examination, the variations were determined to be intraspecific differences. We confirm sex pairing accuracy of all six morphospecies based on an integrated morphological and molecular approach, including *P. yangae* sp. nov., and proposed that the male

Table 6. Results of the general mixed Yule-coalescent (GMYC) analyses (***$P < 0.001$).

Analysis	Clusters (CI)	Entities (EI)	Likelihood(null)	Likelihood (GMYC)	Likelihood ratio	Threshold
Single	6(6-6)	8(8-9)	125.1238	134.9478	19.64795	-0.009578187

and female of *P. breviducta* were not conspecific in the original paper. *P. breviducta* is still valid based only on the male holotype; the female of *P. breviducta* should be considered to belong to *P. yangae* sp. nov., in view of the following three facts: (1) *P. breviducta* was also collected from Daweishan Mt. of Honghe Prefecture, the type locality of *P. yangae* sp. nov.; (2) *P. yangae* sp. nov. exhibits high levels of intraspecific variation; (3) the male was chosen as the holotype of *P. breviducta*. Although we have not examined the paratype female of *P. breviducta*, the high-quality illustrations in the original paper, as well as the morphological and molecular evidence based on new materials from the type locality, leave no doubt that our identification is correct.

As can be concluded from the above, when identifying certain species of the genus *Pseudopoda*, relying solely on morphological characters may lead to over-splitting of species and mispairing, as exemplified by the case of *P. yangae* sp. nov. and *P. breviducta*. Nevertheless, our results indicate that even single-locus analyses based on the COI barcodes, when integrated with morphological data and collection experience, may provide sufficiently reliable species delimitation.

Taxonomic accounts

Family Sparassidae Bertkau, 1872
Subfamily Heteropodinae Thorell, 1873

Genus *Pseudopoda* Jäger, 2000

Type species. *Sarotes promptus* O. Pickard-Cambridge, 1885, from Murree (Pakistan) and Himachal Pradesh (India).

Diagnosis. See Zhang et al. (2023a) and Wu et al. (2024).

Distribution. Its distribution range extends west to Murree in Pakistan (approximately 73°E), east to the Ryukyu Islands in Japan (approximately 128°E), south to Kaeng Krachan National Park in Phetchaburi Province, Thailand (approximately 13°N), and north to Taibaishan National Forest Park in Shaanxi Province, China (approximately 34°N). Also can refer to MAP1 in Zhang et al. (2023a).

Comments. Up to now, a total of nine *Pseudopoda* species groups have been proposed, and 67 species were clearly assigned. Among them, the *daliensis*-group (five species), *signata*-group (seven species), and *interpositia*-group (two species) were established based on both molecular and morphological characteristics by Zhang et al. (2017, 2019) and Li et al. (2019), respectively. The remaining six were all established by Jäger (2001) based on genitalic morphological characters to accommodate 42 species: the *diversipunctata*-group (three species), *latembola*-group (seven species), *martensi*-group (13 species), *parvipunctata*-group (eight species), *prompta*-group (nine species), and *schwendingeri*-group (two species). After the establishment of these species groups, at least 11 species were clearly assigned to these groups in the original papers: four were allocated to the *diversipunctata* group by Jäger et al. (2006) and Yang et al. (2022), four were allocated to the *martensi* group by Jäger (2008), Zhang et al. (2013b), and Caleb et al. (2018), two were allocated to the *prompta* group by Jäger (2008) and Zhang et al. (2023a), and one was allocated to the *schwendingeri* group by Jäger et al. (2015).

It is evident that the number of species clearly assigned to these species groups accounts for about a quarter of the total species in the genus. In contrast, the remaining nearly 200 species, including a large number of recently described species, cannot be allocated (Jiang et al. 2018; Deng et al. 2023; Gong et al. 2023; Zhang et al. 2023a; Chang et al. 2024; Wen et al. 2024; Wu et al. 2024). Sorting *Pseudopoda* species into species groups is highly challenging. The possible reasons for this have been discussed in detail in Zhang et al. (2023a) and will not be repeated here.

We have also attempted to group the six species treated in this paper based on both morphological and molecular data but were unable to do so. While *P. ying* sp. nov. can be clearly assigned to the *daliensis* group (as it exhibits typical features of the *daliensis* group and resembles *P. sicyoidea* Zhang, Jäger & Liu, 2017, the core species of this group, and the grouping is also supported by molecular data), the remaining five species cannot be assigned to any of the existing nine species groups. Furthermore, reviewing the species groups of the genus is not within the scope of this work. Therefore, we refrain from assigning species (except *P. ying* sp. nov.) to species groups in the current paper.

Pseudopoda huanglianensis Zhang, Jäger & Liu, 2023

Figs 1, 4–7, 28A

Pseudopoda huanglianensis Zhang, Jäger & Liu, in Zhang et al. 2023a: 138, figs 124A, C, 125A, B (♀).

Holotype. ♀ (CBEE, LJ202002838), China: • Yunnan Prov.: Honghe Hani and Yi Autonomous Prefecture, Luechun Co., Huanglianshan Mt., 22.99°N, 102.46°E, c. 1940 m, by hand, 13 VII 2020, R. Zhong et al. leg. Examined.

Material examined. • 2 ♂ 2 ♀ (YNZY013, YNZY014, YNZY024, YNZY025). Same locality as holotype, by hand, 16 IV 2024, Y. Zhong & S. Yang leg.

Diagnosis. Males of this species can be easily distinguished from those of all other congeners by the embolus (E) shaped like the lowercase letter 'y' in ventral view, the embolic tip (ET) strongly torqued along its length, with distinct subterminal torsion, and by the rhombic tip of conductor (C) (Figs 4A, 5A, B, 6A–C). In contrast, the embolus (E) and conductor (C) of all other species do not exhibit these characteristics. In most *Pseudopoda* species, such as *P. mamillaris* and *P. yangae* sp. nov., the embolic tip (ET) is not torqued (as shown in Figs 8A, 9A, B, 10A–C, 20A, 21A, B, 22A–C), or the embolic tip (ET) is moderately torqued with no distinct subterminal torsion, as in a few species like *P. oliviformis* and *P. xiaozhua* sp. nov. (as shown in Figs 12A, 13A, B, 14A–C, 17A, B, 18C). Female of

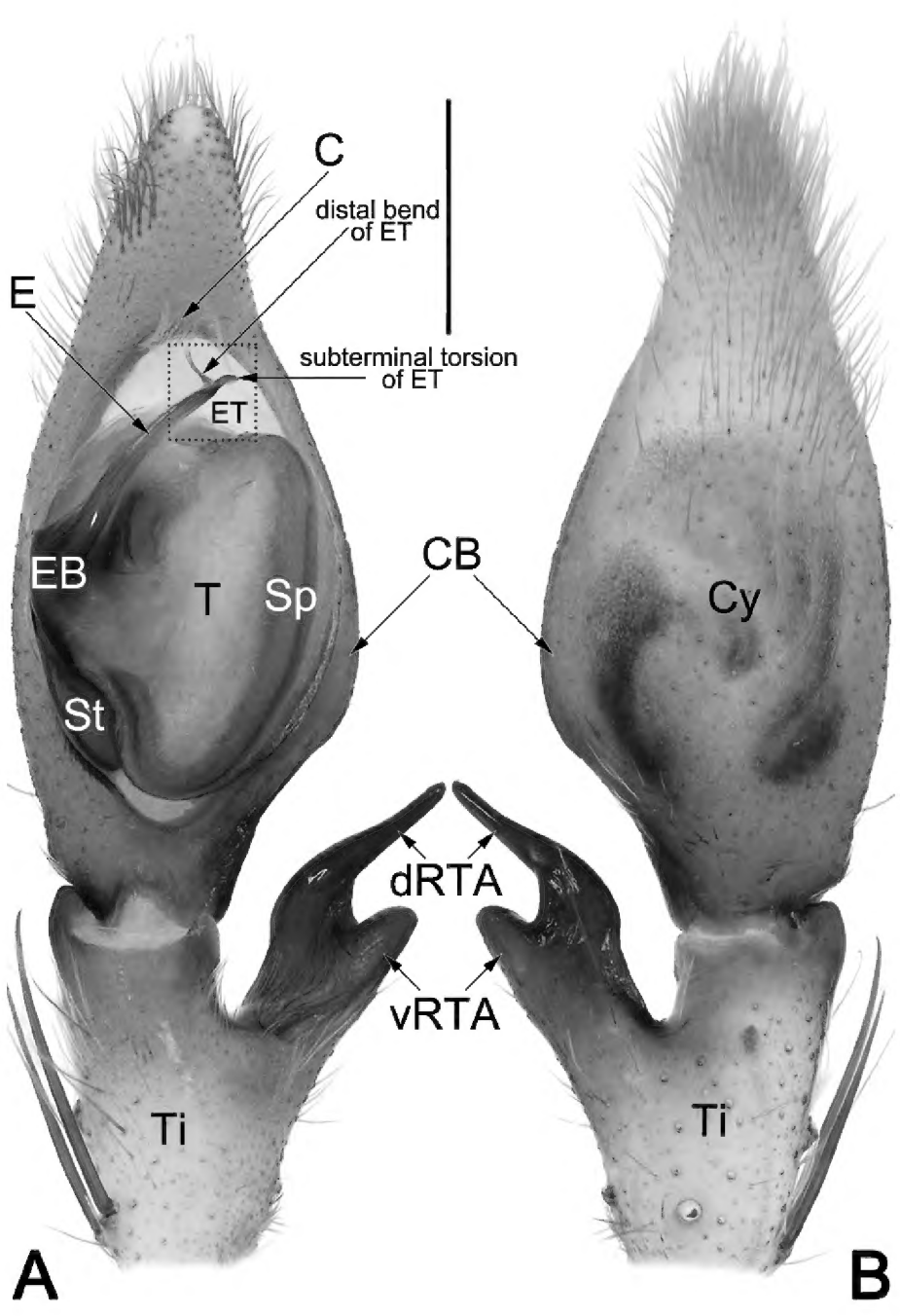

Figure 4. Male palp of the topotype of *Pseudopoda huanglianensis*. **A.** Ventral; **B.** Dorsal. Abbreviations: C = conductor; CB = cymbial bulge; Cy = cymbium; dRTA = dorsal branch of RTA; E = embolus; EB = embolic base; ET = embolic tip; Sp = spermophor; St = subtegulum; T = tegulum; Ti = palpal tibia; vRTA = ventral part of RTA. Scale bar: 0.5 mm (equal for **A, B**).

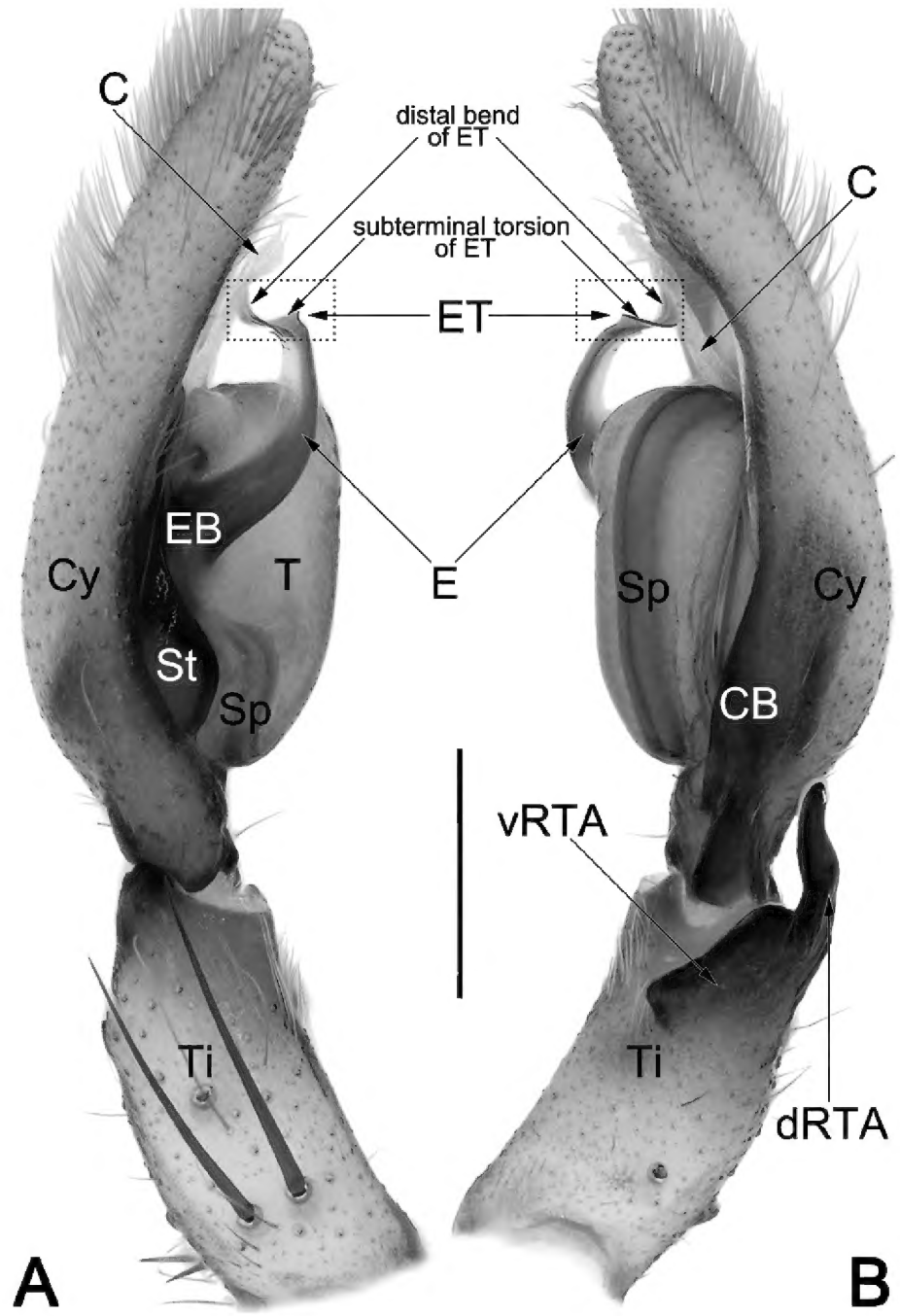

Figure 5. Male palp of the topotype of *Pseudopoda huanglianensis*. **A.** Prolateral; **B.** Retrolateral. Abbreviations: C = conductor; CB = cymbial bulge; Cy = cymbium; dRTA = dorsal branch of RTA; E = embolus; EB = embolic base; ET = embolic tip; Sp = spermophor; St = subtegulum; T = tegulum; Ti = palpal tibia; vRTA = ventral part of RTA. Scale bar: 0.5 mm (equal for **A, B**).

P. huanglianensis resembles that of *P. anfracta* Zhang, Jäger & Liu, 2023, in having the similarly shaped median field (MF) and the relatively sclerotized, nearly funnel-shaped first windings (FD), but can be recognised by the median field (MF) relatively narrower, ca. 2/5 epigyne width (vs. wider, more than 2/3 epigyne width) (cf. Fig. 7A, B and Zhang et al. 2023a: fig. 12A). Female also resembles that of *P. cangschana* Jäger & Vedel, 2007 (Zhang et al. 2023a: 50, figs 39A, B, 40C, D); see Zhang et al. (2023a) for the diagnosis.

Description. Male (YNZY013). Total length 7.1. Carapace 3.6 long, 3.5 wide, anterior width 1.7. Opisthosoma 3.5 long, 2.2 wide. ***Eye sizes and interdistances*:** AME 0.18, ALE 0.30, PME 0.24, PLE 0.30, AME–AME 0.10, AME–ALE 0.06, PME–PME 0.22, PME–PLE 0.24, AME–PME 0.25, ALE–PLE 0.25, CH AME 0.32, CH ALE 0.25. ***Spination*:** palp: 131, 101, 2111; Fe: I–II 323, III 322, IV 321; Pa: I–IV 101; Ti: I–II 2228, III 2226, IV 2126; Mt: I–II 2024, III–IV 3036. ***Measurements of palp and legs*:** palp 4.9 (1.6, 0.7, 0.8, 1.8), I 15.3 (4.3, 1.9, 4.1, 3.6, 1.4), II 16.5 (4.5, 1.9, 4.3, 4.2, 1.6), III 12.8 (3.9, 1.3, 3.3, 3.2, 1.1), IV 14.9 (4.4, 1.4, 3.6, 4.1, 1.4). Cheliceral furrow with ~34 denticles.

Colouration in ethanol **(Fig. 6D, E)**. DS light brown, lateral bands and margin slightly darker, clothed with fine setae; median band bright yellowish-brown, not distinctly delimited to lateral bands, with indistinct Ψ-shaped markings starting from behind PER, almost reaching indistinct cervical groove; fovea and striae distinctly marked. Cheliceral base coloured similarly to median band, with red fangs. Sternum uniformly light brown. Endites light brown. Labium coloured similarly to endites. Legs yellowish-brown, with numerous brown spots, and covered with short spines. OS elongate-oval; dorsum with median band starting from behind pedicel, reaching 4/5 of abdomen length, with two pairs of circular dots on each side; median band with diamond-shaped anterior part, cross-shaped stem, and '␣'-shaped, black posterior part, all three parts fused; dorsum with transverse yellow line located posterior to median band; ventral OS marked with numerous brown spots.

Palp **(Figs 4, 5, 6A–C, 28A)**. Femur and patella unmodified. Tibia (Ti) relatively long, ca. 1/2 cymbium length, with retrolateral apophysis (RTA) arising mesially to distally; RTA bifurcated, with ventral part (vRTA) and dorsal branch (dRTA): dRTA finger-like, slightly curved

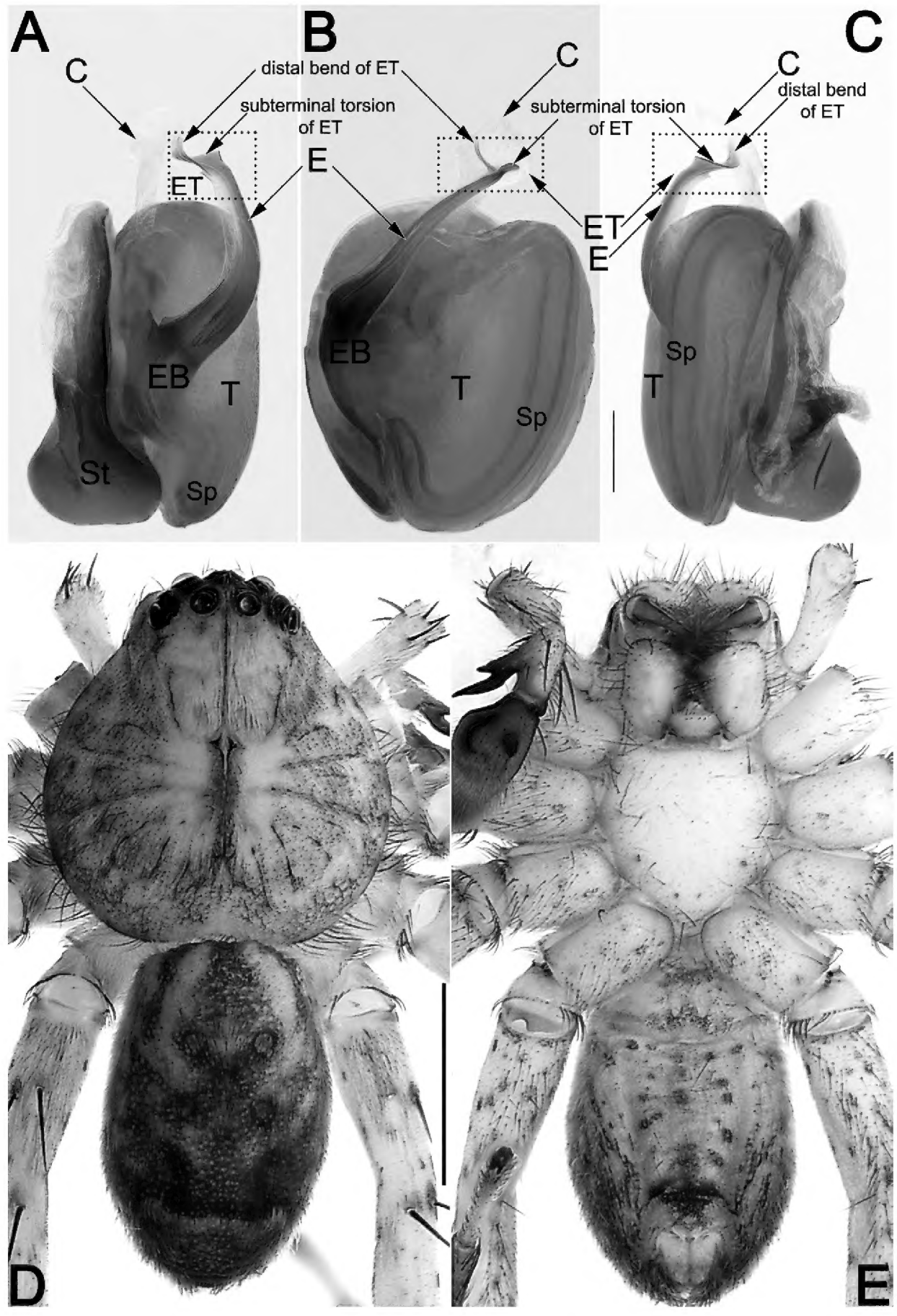

Figure 6. *Pseudopoda huanglianensis*, male topotype, palpal bulb (**A–C**) and habitus (**D, E**). **A.** Prolateral; **B.** Ventral; **C.** Retrolateral; **D.** Dorsal; **E.** Ventral. Abbreviations: C = conductor; E = embolus; EB = embolic base; ET = embolic tip; Sp = spermophor; St = subtegulum; T = tegulum. Scale bars: 0.2 mm (equal for **A–C**); 1 mm (equal for **D, E**).

and tapering, ca. 3/4 tibia length, extending to cymbial base; vRTA laminar, humble, and broad in retrolateral view, with blunt, round apex. Cymbium (Cy) approximately 2.4 times as long as wide, retrolaterally with indistinct bulge (CB). Tegulum (T) nearly egg-shaped, ca. 1.3× longer than wide, relatively flat, marginally with distinct, ɔ-shaped spermophor (Sp) in ventral view. Embolus (E) shaped like the lowercase letter 'y' in ventral view, ca. as long as tegulum (T), arising from tegulum at nearly the 8–9 o'clock position, terminating at ca. 11:30 o'clock position; the proximal first half of embolus (E) columnar, while the second half thin and flat, ribbon-shaped; embolic tip (ET) strongly torqued along its length, with subterminal torsion and distal, rostrate bend. Conductor (C) membranous, ca. 1/2 of embolus length, inserted anterodorsally on tegulum, extending obliquely, the latter half of conductor (C) widens and diamond-shaped, directing prolaterally.

Female (YNZY025). Total length 9.1. Carapace 4.1 long, 3.8 wide, anterior width 2.3. Opisthosoma 5.0 long, 3.6 wide. ***Eye sizes and interdistances*:** AME 0.22, ALE 0.34, PME 0.25, PLE 0.34, AME–AME 0.14, AME–ALE 0.08, PME–PME 0.32, PME–PLE 0.34, AME–PME 0.32, ALE–PLE 0.32, CH AME 0.35, CH ALE 0.26. ***Spination*:** palp: 131, 101, 2121, 1014; Fe: I–II 323, III 322, IV 321; Pa: I–IV 101; Ti: I–II 2228, III–IV 2126; Mt: I–II 2024, III–IV 3036. ***Measurements of palp and legs*:** palp 5.4 (1.7, 0.9, 1.1, 1.7), I 14.4 (4.3, 1.8, 3.3, 3.7, 1.3), II 15.1 (4.4, 2.0, 3.8, 3.6, 1.3), III 12.0 (3.7, 1.5, 2.9, 2.8, 1.1), IV 14.0 (3.9, 1.8, 3.6, 3.4, 1.3). Cheliceral furrow with ~50 denticles. Colouration in ethanol as in males, but body slightly darker (Fig. 7D, E; see Zhang et al. (2023a) for others described).

***Epigyne* (Fig. 7A–C).** Epigynal field ca. 1.25× wider than long; anterior margin (aEF) distinctly delimited,

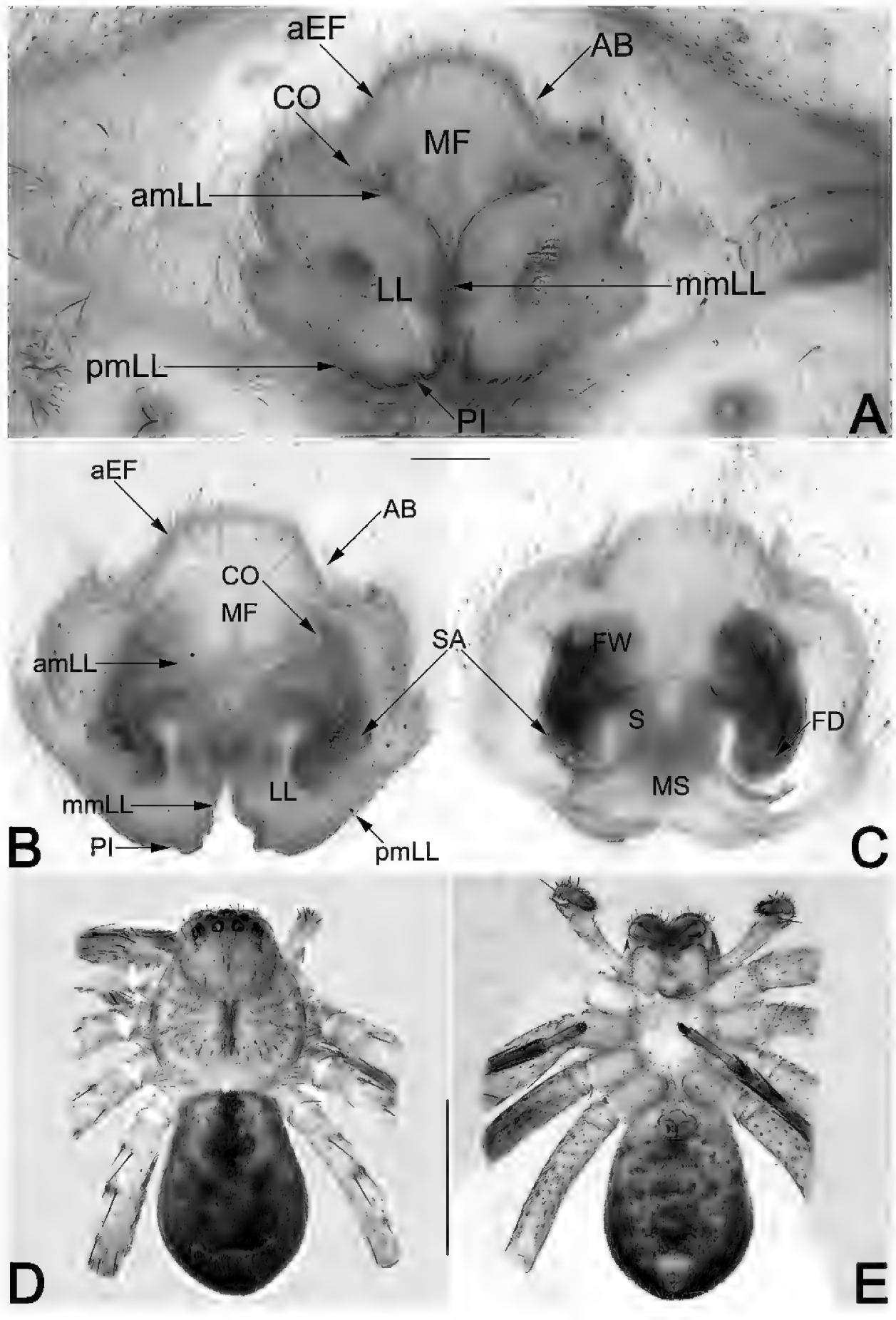

Figure 7. *Pseudopoda huanglianensis*, female topotype, epigyne (**A–C**) and habitus (**D, E**). **A.** Intact, ventral; **B.** Cleared and macerated, ventral; **C.** Cleared and macerated, dorsal; **D.** Dorsal; **E.** Ventral. Abbreviations: AB = anterior band; aEF = anterior margin of epigynal field; amLL = anterior margin of lateral lobes; CO = copulatory opening; FD = fertilization duct; FW = first winding; LL = lateral lobe; MF = median field of epigyne; mmLL = median margin of lateral lobes; MS = membranous sac; PI = posterior incision; pmLL = posterior margin of lateral lobes; S = spermatheca; SA = spermathecal appendage. Scale bars: 0.2 mm (equal for **A–C**); 2 mm (equal for **D, E**).

mesially distinctly recurved; anterior bands (AB) indistinct. Median field (MF) shaped like a ginkgo leaf (more or less fan-shaped), ca. 2/5 epigyne length and 2/5 epigyne width. Lateral lobes (LL) nearly as wide as long, slightly converged along the axis; anterior margins (amLL) slightly recurved; median margins (mmLL) touching each other along middle line in anterior half; posterior margins (pmLL) with distinct incision (PI). Copulatory openings (CO) indistinct, located at basolateral borders of median field (MF). First windings (FW) weakly sclerotized, nearly funnel-shaped; starting from near copulatory openings (CO), descending obliquely, posteriorly with U-turns; two first windings (FW) separated by ca. 0.75× diameters. Spermathecae (S) represented by thick, '∩'-shaped tubes, forming letter 'm'; laterally covered by first windings (FW) and with globular appendage (SA), medially exposed and touching each other along middle line in posterior half. Membranous sac (MS) nearly trapeziform, located at posterior portion of vulva; anterior margin recurved, separated from epigastric fold by ca. 1/4 epigyne length, reaching contact point of spermathecae; posterior margin nearly straight, close to epigastric fold. Fertilization ducts (FD) acicular, membranous, ca. 1/2 length of first windings.

Distribution. Known only from the type locality (Fig. 1).

Pseudopoda mamillaris Zhang, Jäger & Liu, 2023

Figs 1, 8–11, 28B

Pseudopoda mamillaris Zhang, Jäger & Liu, in Zhang et al. 2023a: 176, figs 159A, C, 160A, B (♀).

Holotype. ♀ (CBEE, LJ202002615), China: • Yunnan Pro.: Honghe Hani and Yi Autonomous Prefecture, Luechun Co., Martyr Cemetery, 22.99°N, 102.45°E, c. 1940 m, by hand, 11 VII 2020, R. Zhong et al. leg. Examined.

Material examined. • 2♂, 2♀ (YNZY009, YNZY010, YNZY022, YNZY023), same locality as holotype, by hand, 15 IV 2024, Y. Zhong & S. Yang leg.

Diagnosis. Male of *P. mamillaris* is similar to that of *P. platembola* Jäger, 2001, in having a similar sickle-shaped embolus (E) and petal-shaped conductor (C). However, it can be distinguished from the latter by the following characteristics: (1) in ventral view, embolus (E) is apically rugged and as wide as its middle section (vs. apically not rugged, pointed) (cf. Figs 8A, 10B, and Jäger 2001: figs 35b, g, i); (2) dorsal branch of RTA (dRTA) tip not curved (vs. slightly or distinctly curved) (cf. Figs 8A, B, 9B, 28B, and Jäger 2001: figs 35a–c, f–h); (3) RTA inserted closer to cymbium (Cy), both dRTA and vRTA separated from cymbium (Cy) by approximately half of the tibial (Ti) diameter (vs. inserted farther, both dRTA and vRTA separated from cymbium (Cy) by more than one tibial (Ti) diameter) (cf. Figs 8A, B and Jäger 2001: figs 35b, g). For the female diagnosis, see Zhang et al. (2023a).

Description. Male (YNZY009). Total length 7.3. Carapace 3.6 long, 3.5 wide, anterior width 1.8. Opisthosoma 3.8 long, 2.6 wide. ***Eye sizes and interdistances*:** AME 0.19, ALE 0.30, PME 0.23, PLE 0.31, AME–AME 0.14, AME–ALE 0.06, PME–PME 0.23, PME–PLE 0.26, AME–PME 0.28, ALE–PLE 0.23, CH AME 0.32, CH ALE 0.27. ***Spination*:** palp: 131, 101, 2111; Fe: I–III 323, IV 321; Pa: I–III 101, IV 100; Ti: I–II 2226, III–IV 2126; Mt: I–II 2024, III–IV 3036. ***Measurements of palp and legs*:** palp 5.2 (1.6, 0.9, 1.0, 1.7), I 15.3 (4.4, 1.5, 3.8, 4.2, 1.4), II 15.9 (4.5, 1.9, 4.2, 3.8, 1.5), III 13.1 (3.8, 1.4, 3.4, 3.3, 1.2), IV 14.7 (4.0, 1.7, 4.0, 3.6, 1.4). Cheliceral furrow with ~26 denticles.

***Colouration in ethanol* (Fig. 10D, E)**. DS yellowish brown, with numerous dark spots; lateral bands and margin slightly darker, clothed with thin hairs; median band bright yellowish-brown, without distinct pattern, not distinctly delimited to lateral bands; fovea and radial grooves distinctly marked. Cheliceral base yellowish white, with red fangs. Sternum uniformly yellowish. Endites and labium reddish orange, darker distally. Legs coloured as DS, with numerous brown spots, and covered by short spines. OS elongate-oval; dorsum with indistinct median band starting from behind pedicel, extending to 4/5 of abdomen length, almost reaching the indistinct transverse yellow line; median band anteriorly represented by a longitudinal brown line, with two light brown and reniform patches on each side, the latter half distinctly widened and not clearly delimited,

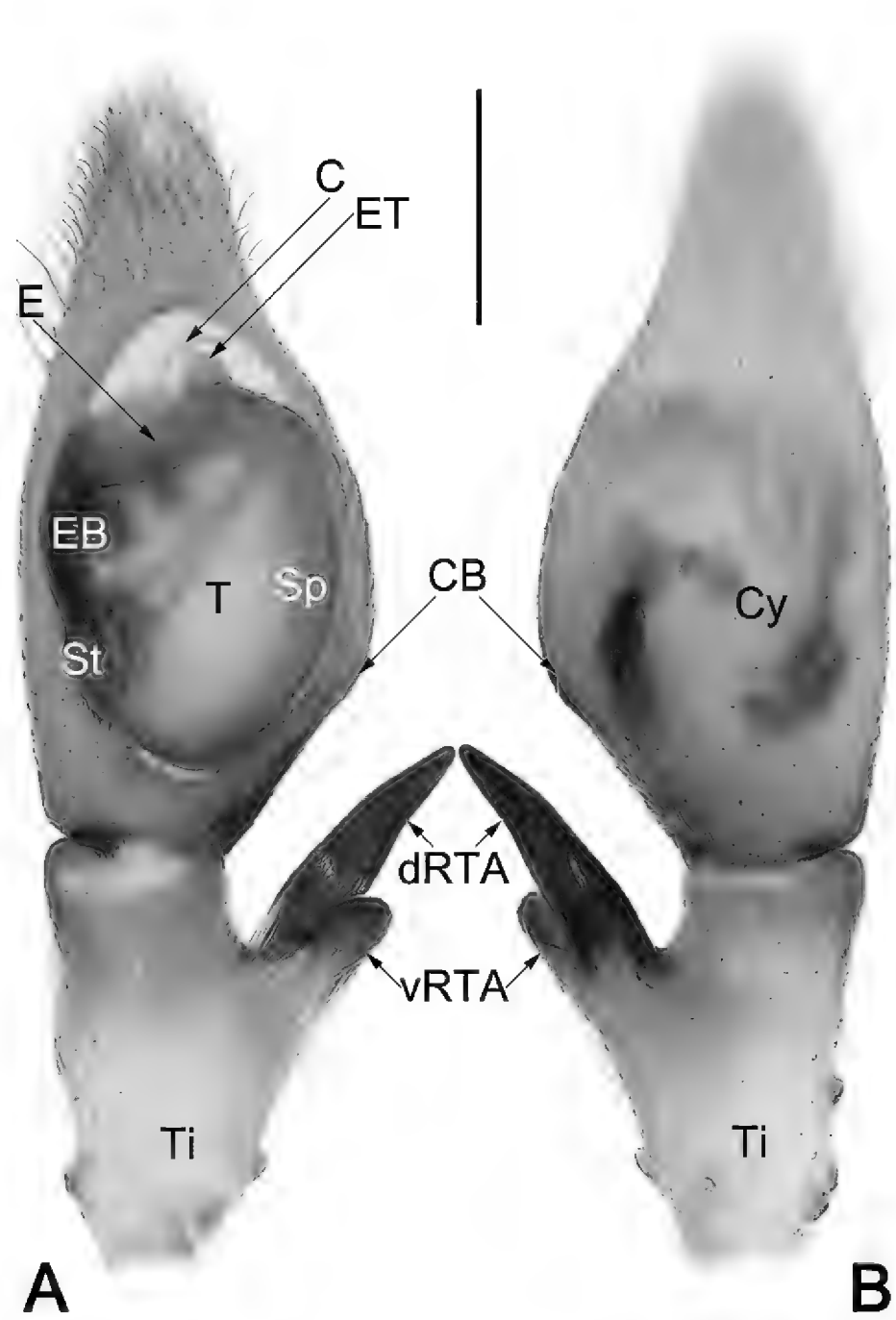

Figure 8. Male palp of the topotype of *Pseudopoda mamillaris*. **A.** Ventral; **B.** Dorsal. Abbreviations: C = conductor; CB = cymbial bulge; Cy = cymbium; dRTA = dorsal branch of RTA; E = embolus; EB = embolic base; ET = embolic tip; Sp = spermophor; St = subtegulum; T = tegulum; Ti = palpal tibia; vRTA = ventral branch of RTA. Scale bar: 0.5 mm (equal for **A, B**).

with three pairs of circular spots located at lateral part; ventral OS basically yellowish, centrally marked with three pairs of purplish dots.

***Palp* (Figs 8, 9, 10A–C, 28B)**. Femur and patella unmodified. Tibia (Ti) moderately long, ca. 3/5 cymbium length, with retrolateral apophysis (RTA) arising mesially; RTA bifurcated, ɔ-shaped in retrolateral view, both ventral and dorsal branches distinctly protruding: dorsal branch (dRTA) finger-like, slightly curved and tapering, ca. 3/5 of tibia length, extending to cymbial base; ventral branch (vRTA) thumb-like, relatively short, ca. 1/2 length of dRTA, apex round. Cymbium (Cy) ca. 1.9× longer than wide, cymbial bulge (CB) indistinct. Tegulum (T) oval, ca. 1.2× longer than wide, posteriorly slightly bulged, slightly excavated on prolatero-apical side to accommodate embolus (E) and conductor (C); spermophor (Sp) sinuate, forming a loop along tegular margin. Embolus (E) wide and flattened, nearly Ƨ-shaped in ventral view, ca. 3/4 of tegulum length and 1/6–1/5 of tegulum width; the embolic base (EB) situated prolateral on the tegulum (ca. 9–10 o'clock on tegulum); the free part of the embolus (E) sickle-shaped; the embolic tip (ET) apically rugged, terminated at ca. 12 o'clock position. Conductor

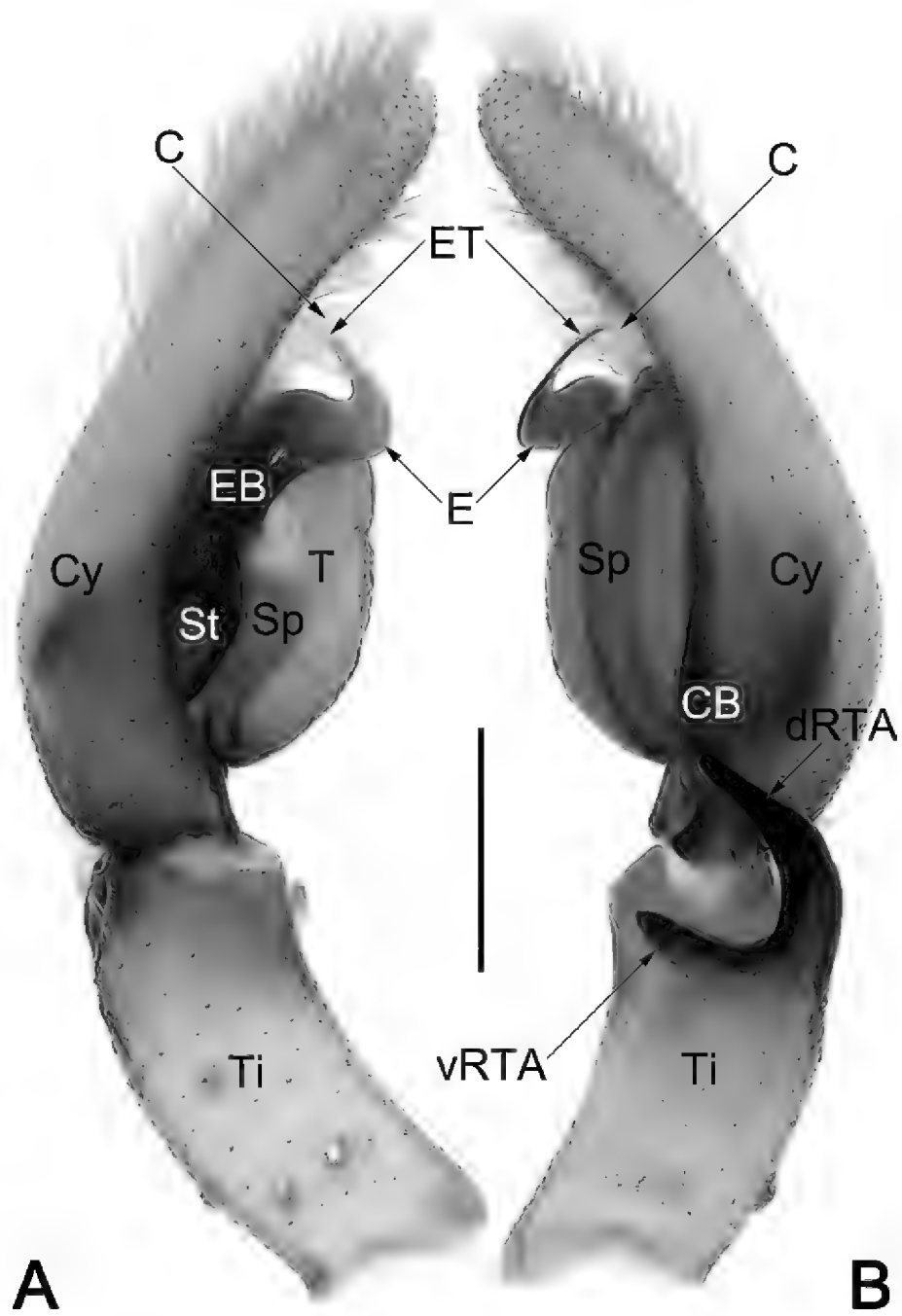

Figure 9. Male palp of the topotype of *Pseudopoda mamillaris*. **A.** Prolateral; **B.** Retrolateral. Abbreviations: C = conductor; CB = cymbial bulge; Cy = cymbium; dRTA = dorsal branch of RTA; E = embolus; EB = embolic base; ET = embolic tip; Sp = spermophor; St = subtegulum; T = tegulum; Ti = palpal tibia; vRTA = ventral branch of RTA. Scale bar: 0.5 mm (equal for **A, B**).

(C) membranous, ca. 1/3 of embolus length, thick, more or less petal-shaped, inserted apically (approximately 12 o' lock relative to tegulum), covering embolic tip (ET) in prolateral and ventral views.

Female (YNZY010). Total length 9.2. Carapace 3.8 long, 3.4 wide, anterior width 2.0. Opisthosoma 5.4 long, 4.0 wide. ***Eye sizes and interdistances*:** AME 0.20, ALE 0.31, PME 0.25, PLE 0.33, AME–AME 0.16, AME–ALE 0.06, PME–PME 0.21, PME–PLE 0.29, AME–PME 0.31, ALE–PLE 0.31, CH AME 0.32, CH ALE 0.23. ***Spination*:** palp: 131, 101, 2121, 1014; Fe: I–III 323, IV 321; Pa: I–IV 101; Ti: I–III 2026, IV 2126; Mt: I–II 2024, III 2026, IV 3036. ***Measurements of palp and legs*:** palp: 4.3 (1.3, 0.7, 0.9, 1.4), I 11.0 (3.4, 1.2, 2.6, 2.8, 1.0), II 12.1 (3.7, 1.6, 3.1, 2.6, 1.1), III 9.6 (2.9, 1.1, 2.4, 2.3, 0.9), IV 10.6 (3.1, 1.3, 2.7, 2.5, 1.0). Cheliceral furrow with ~26 denticles. Colouration in ethanol as in males, but body slightly darker (Fig. 11D, E; see Zhang et al. (2023a) for others described).

***Epigyne* (Fig. 11A–C).** Epigynal field ca. 1.27× wider than long; anterior margin (aEF) distinctly delimited, trilobate, anterolaterally with two large v-shaped incisions that are well separated by at ca. 2× widths; anterior bands (AB) indistinct, situated at the two incisions. Median field (MF) anterior margin invisible, large, ca. 1/2 epigyne length and as wide as epigyne. Lateral lobes (LL) nearly as wide as long; anterior margins (amLL) distinctly recurved; median margins (mmLL) entirely touching each other along the middle line; posterior margins (pmLL) distinctly procurved; posterior incision (PI) absent. Copulatory openings (CO) indistinct, located at basolateral borders of median field (MF). First windings (FW) hyaline, shaped like inverted triangles, starting from copulatory openings (CO), descending longitudinally, tapering posteriorly; two first windings (FW) separated by ca. one diameter. Spermatheca (S) nearly '∞'-shaped, consisting of inner part and lateral part; inner part spherical, touching median margin of lateral lobe (mmLL), entirely covered by membranous sac (MS) in dorsal view; lateral part shaped like water droplet, anterolaterally with globular appendage (SA), entirely covered by first winding (FW) in dorsal view. Membranous sac (MS) nearly trapeziform, located at posterior portion of vulva; anterior margin almost straight, ca. 1/3 epigyne width, separated from epigastric fold by ca. 2/5 epigyne length; posterior margin also nearly straight, ca. 2/3 epigyne width, reaching posterior margins of lateral lobes (pmLL). Fertilization ducts (FD) acicular, membranous, ca. 1/2 length of first windings.

Distribution. Known only from the type locality (Fig. 1).

Pseudopoda oliviformis Zhang, Jäger & Liu, 2023

Figs 1, 12–15, 28C

Pseudopoda oliviformis Zhang, Jäger & Liu, in Zhang et al. 2023a: 210, figs 191A, C, 192A, B (♀).

Holotype. ♀ (CBEE, LJ2140), China: • Yunnan Pro.: Honghe Hani and Yi Autonomous Prefecture, Luechun Co., Martyr Cemetery, 22.99°N, 102.45°E, c. 1934 m, by hand, 30 X 2015, Y. Zhong & Y. Zhu leg. Examined.

New material examined. • 2 ♂, 2 ♀ (YNZY011, YNZY012, YNZY015, YNZY016), same locality as holotype, by hand, 15 IV 2024, Y. Zhong & S. Yang leg.

Diagnosis. Both sexes of *P. oliviformis* resemble those of *P. zixiensis* Zhao & Li, 2018 in the general shape of the male palp, the epigynal plate, and vulva. The palps of the two species share the similarly shaped embolus (E), which has a torsional tip, and the finger-like dorsal branch of RTA (dRTA), but differ in the following: (1) ventral branch of RTA (vRTA) subtriangular, apex sharp in retrolateral view (vs. humble and broad, with a blunt apex) (cf. Fig. 13B and Jiang et al. 2018: fig. 34C); (2) retrolateral rim of embolus (E) distinctly curved in ventral view (vs. almost straight) (cf. Figs 12A, 13A, B, 14A–C and Jiang et al. 2018: figs 35A, B); (3) embolic projection absent (vs. present) (cf. Figs 12A, 13A, 14B and Jiang et al. 2018: figs 34B, 35A). Female resembles *P. zixiensis* in having the similarly shaped lateral lobes (LL) and the spherical spermathecae (S), but can be recognised by:

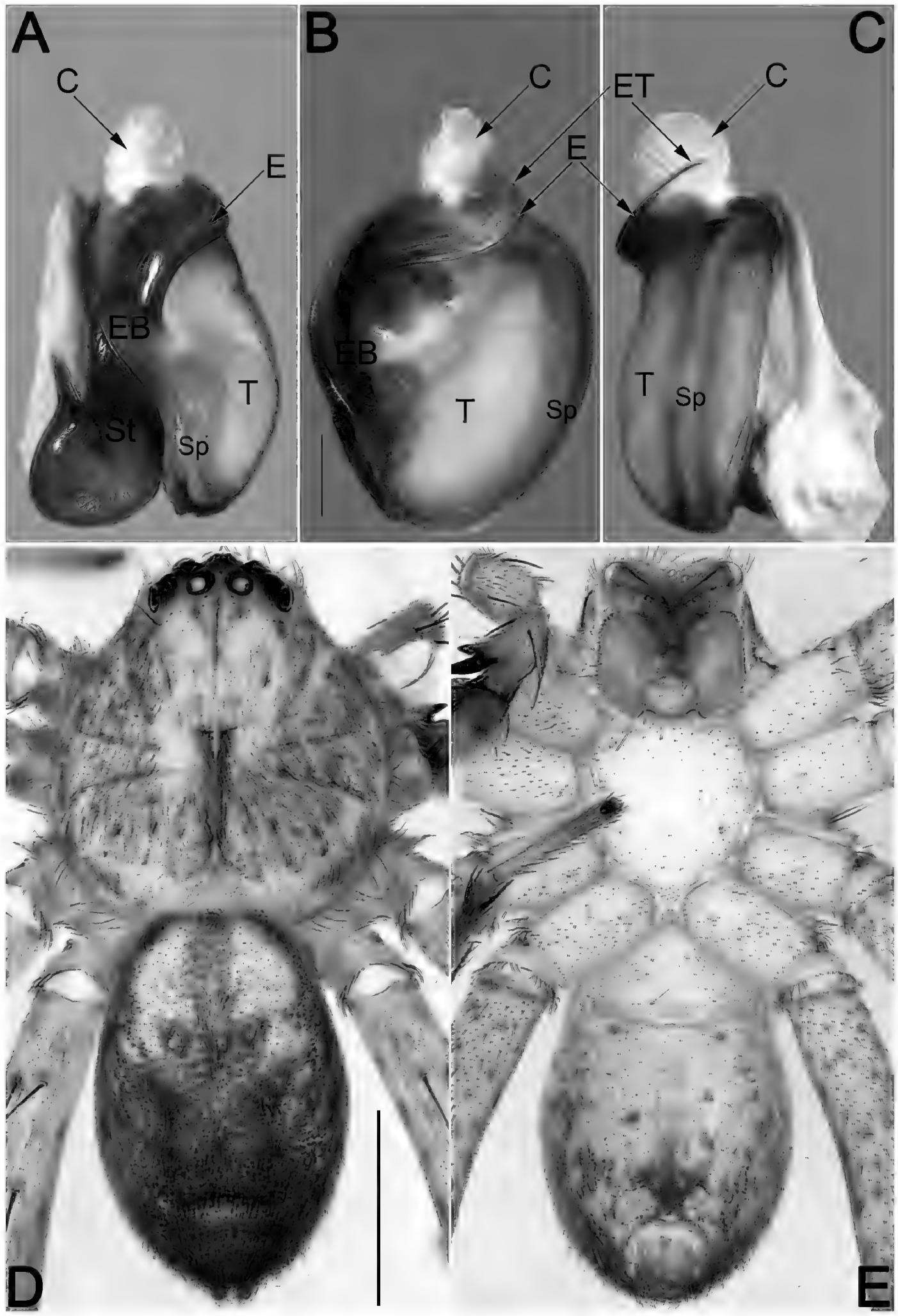

Figure 10. *Pseudopoda mamillaris*, male topotype, palpal bulb (**A–C**) and habitus (**D, E**). **A.** Prolateral; **B.** Ventral; **C.** Retrolateral; **D.** Dorsal; **E.** Ventral. Abbreviations: C = conductor; E = embolus; EB = embolic base; ET = embolic tip; Sp = spermophor; St = subtegulum; T = tegulum. Scale bars: 0.2 mm (equal for **A–C**); 1 mm (equal for **D, E**).

(1) anterior band (AB) and anterior margin of epigynal field (aEF) indistinct (vs. both distinct) (cf. Fig. 15A, B and Jiang et al. 2018: fig. 36A); (2) posterior margins of lateral lobes (pmLL) with distinct posterior incision (PI) on each side, respectively (vs. PI absent) (cf. Fig. 15A, B and Jiang et al. 2018: fig. 36A); (3) spermathecae (S) surface smooth, without coiling ducts embedded (vs. surface wrinkled, with coiling ducts embedded) (cf. Fig. 15C and Jiang et al. 2018: fig. 36B).

Description. Male (YNZY011). Total length 8.4. Carapace 4.3 long, 4.4 wide; anterior width 2.3. Opisthosoma 4.1 long, 2.6 wide. ***Eye sizes and interdistances*:** AME 0.21, ALE 0.34, PME 0.27, PLE 0.32, AME–AME 0.13, AME–ALE 0.05, PME–PME 0.26, PME–PLE 0.32, AME–PME 0.34, ALE–PLE 0.30, CH AME 0.42, CH ALE 0.33. ***Spination*:** palp: 131, 101, 2101; Fe: I–III 323, IV 321; Pa: I–IV 101; Ti: I–II 2026, III–IV 2126; Mt: I–II 1014, III 2026, IV 3036. ***Measurements of palp and legs*:** palp 5.9 (2.0, 1.0, 1.1, 1.8), I 19.1 (5.0, 2.0, 5.2, 5.1, 1.8), II 20.2 (5.5, 2.0, 5.5, 5.2, 2.0), III 16.1 (4.6, 1.7, 4.1, 4.2, 1.5), IV 18.4 (5.3, 1.6, 4.5, 5.2, 1.8). Cheliceral furrow with ~42 denticles.

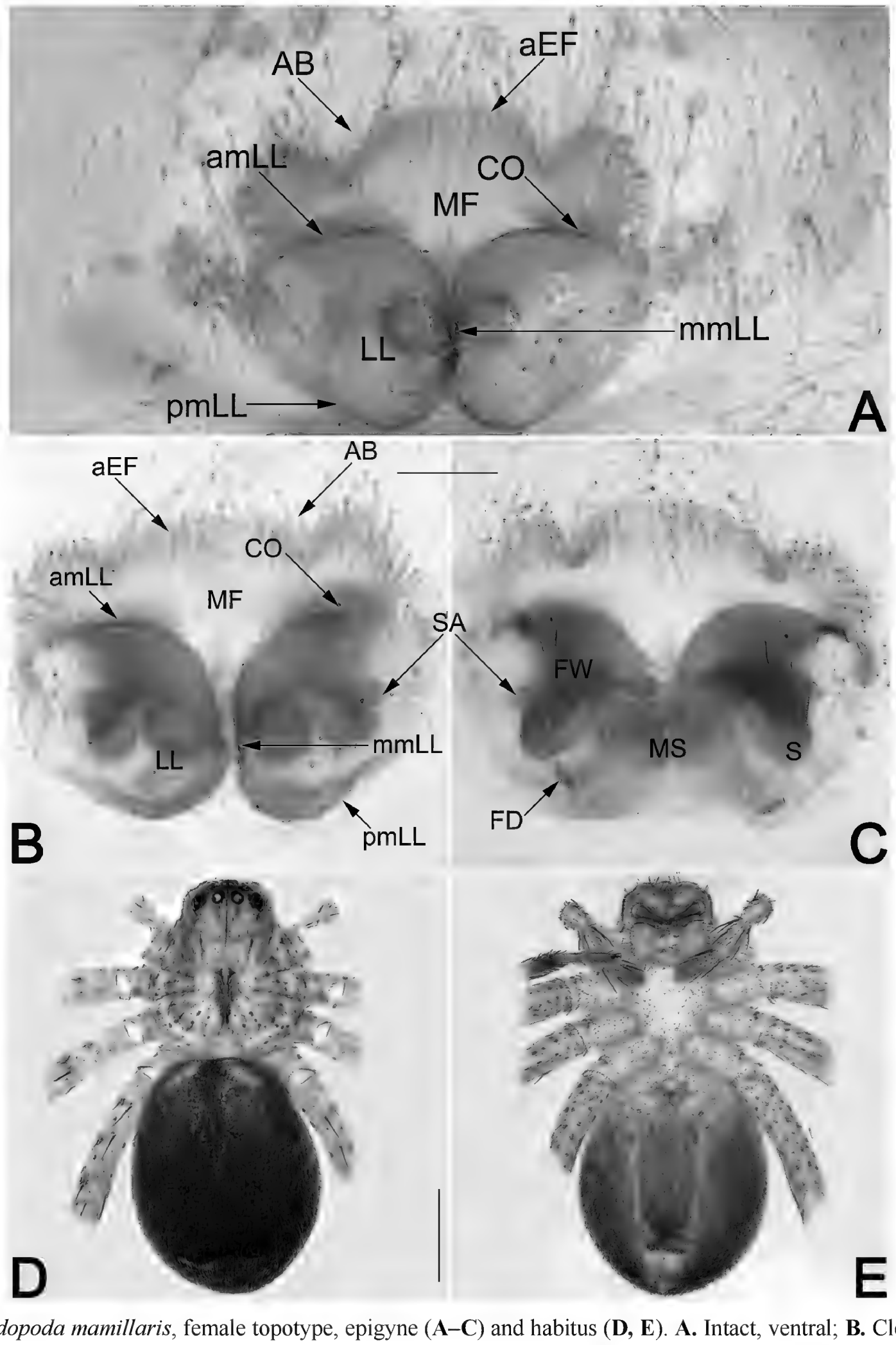

Figure 11. *Pseudopoda mamillaris*, female topotype, epigyne (**A–C**) and habitus (**D, E**). **A.** Intact, ventral; **B.** Cleared and macerated, ventral; **C.** Cleared and macerated, dorsal; **D.** Dorsal; **E.** Ventral. Abbreviations: AB = anterior band; aEF = anterior margin of epigynal field; amLL = anterior margin of lateral lobes; CO = copulatory opening; FD = fertilization duct; FW = first winding; LL = lateral lobe; MF = median field of epigyne; mmLL = median margin of lateral lobes; MS = membranous sac; pmLL = posterior margin of lateral lobes; S = spermatheca; SA = spermathecal appendage. Scale bars: 0.2 mm (equal for **A–C**); 2 mm (equal for **D, E**).

Colouration in ethanol **(Fig. 14D, E)**. DS yellowish white, with numerous indistinct, irregularly shaped patches; lateral bands and margin slightly darker, relatively smooth, sparsely covered with hairs; median band bright yellowish, with distinct Ψ-shaped markings starting from behind PME, almost reaching reddish fovea; fovea and radial furrows distinctly marked. Cheliceral base coloured as DS, cheliceral fang red. Sternum mainly yellowish, with two pairs of indistinct dots located at lateral parts. Endites and labium yellowish, slightly darker on inner margin. Legs coloured as DS, with numerous black spots, and bearing short spines. OS oval; dorsum anteriorly with nearly '⊓'-shaped bright region, centrally with indistinct '♀'-shaped median band, posteriorly with large ')('-shaped black pattern located on both sides of median band, distally marked with more or less semicircular transverse yellow band; venter of OS centrally with inverted trapezoidal black patch.

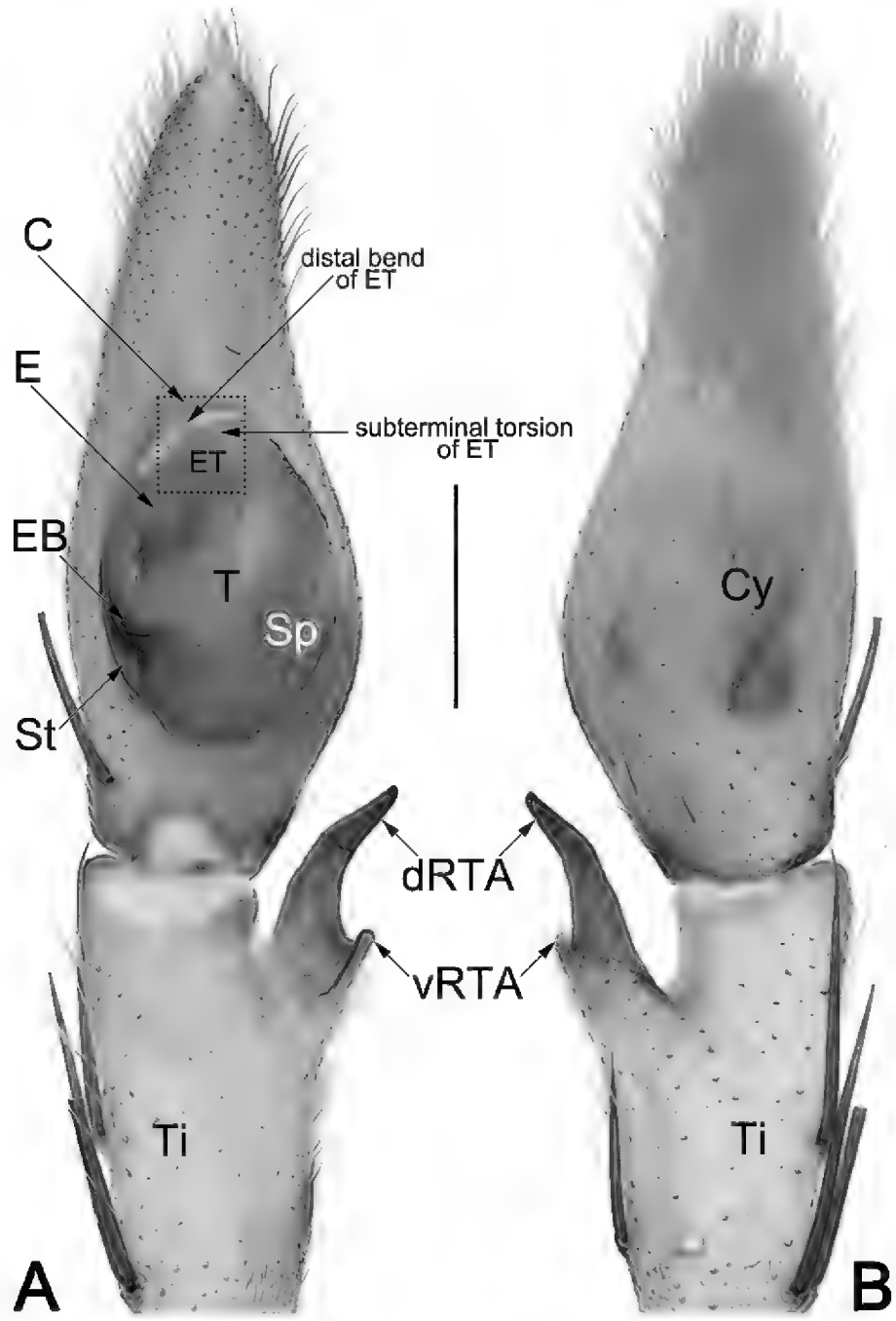

Figure 12. Male palp of the topotype of *Pseudopoda oliviformis* **A.** Ventral; **B.** Dorsal. Abbreviations: C = conductor; Cy = cymbium; dRTA = dorsal branch of RTA; E = embolus; EB = embolic base; ET = embolic tip; Sp = spermophor; St = subtegulum; T = tegulum; Ti = palpal tibia; vRTA = ventral part of RTA. Scale bar: 0.5 mm (equal for **A, B**).

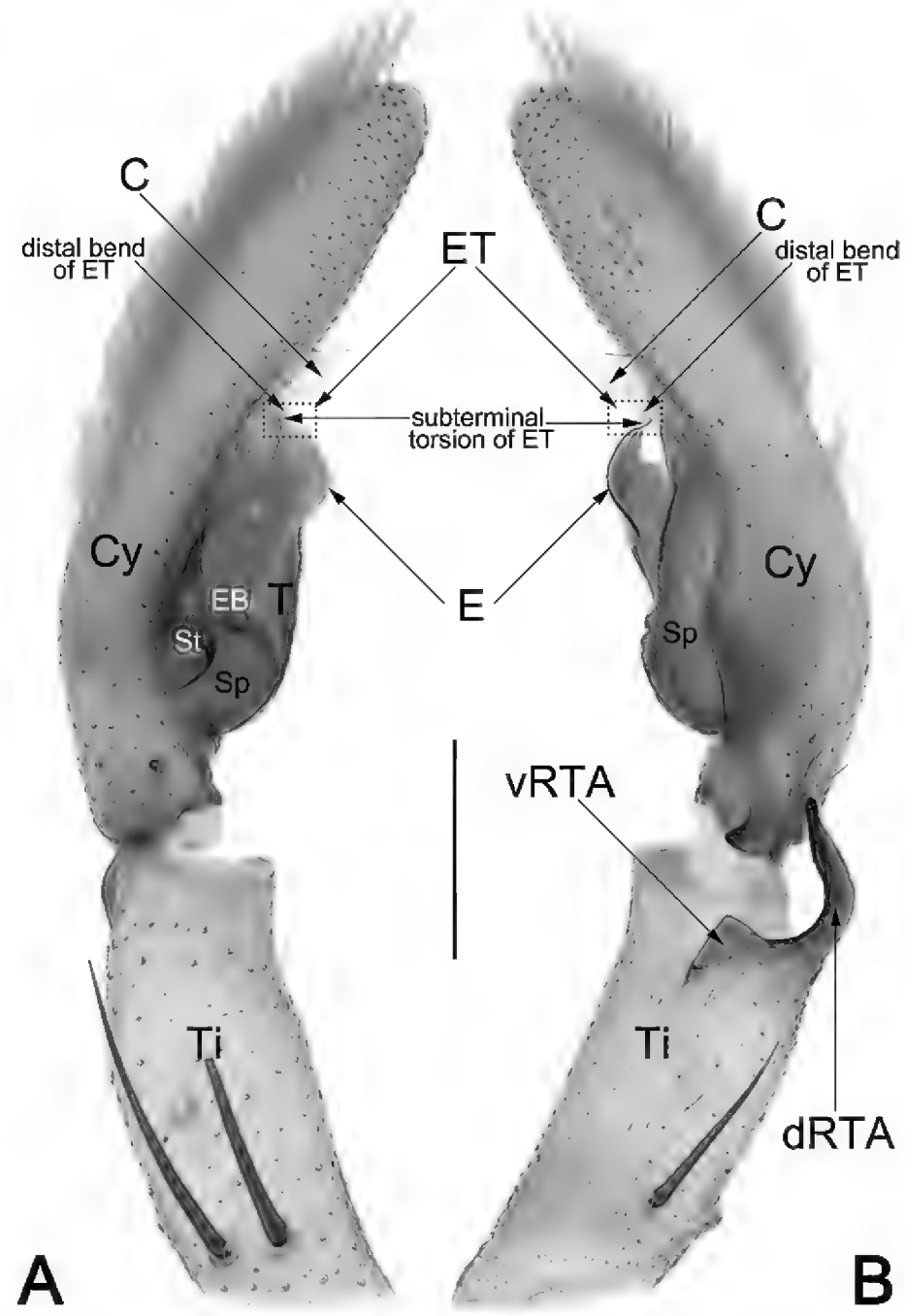

Figure 13. Male palp of the topotype of *Pseudopoda oliviformis* **A.** Prolateral; **B.** Prolateral. Abbreviations: C = conductor; Cy = cymbium; dRTA = dorsal branch of RTA; E = embolus; EB = embolic base; ET = embolic tip; Sp = spermophor; St = subtegulum; T = tegulum; Ti = palpal tibia; vRTA = ventral part of RTA. Scale bar: 0.5 mm (equal for **A, B**).

***Palp* (Figs 12, 13, 14A–C, 28C)**. Femur and patella unmodified. Tibia (Ti) moderately long, ca. 2/3 cymbium length, with retrolateral apophysis (RTA) arising mesially; RTA bifurcated, with ventral part (vRTA) and dorsal branch (dRTA): dRTA ɔ-shaped in retrolateral view, curved and tapering, ca. 2/5 of tibia length, extending to cymbial base; vRTA represented by a distinctly short triangular lamina, ca. 1/3 length of dRTA, apex sharp. Cymbium (Cy) distinctly slender, ca. 2.7× longer than wide, cymbial bulge (CB) indistinct. Tegulum (T) oval, ca. 1.35× longer than wide, relatively flattened, proximally slightly bulged and prolapsed, slightly excavated on prolatero-apical side to accommodate embolus (E) and conductor (C); spermophor (Sp) sinuate, not distinct, oriented clockwise along the margin of the tegulum (T). Embolus (E) nearly Ƨ-shaped in ventral view, ca. 2/3 of tegulum length; embolic base (EB) situated meso-prolaterally on the tegulum (T) (approximately the 9 o'clock position); mesially broadened and flattened, nearly 1/2 of tegulum width; embolic tip (ET) distinctly narrowed, with subterminal torsion and distal beak-shaped bend, apex sharp, terminated at ~ 11 o'clock position. Conductor (C) membranous, irregularly shaped, inserted apically (at approximately 11–12 o'clock position relative to the tegulum).

Female (YNZY012). Total length 10.5. Carapace 4.3 long, 4.0 wide, anterior width 2.4. Opisthosoma 6.2 long, 4.8 wide. ***Eye sizes and interdistances*:** AME 0.21, ALE 0.34, PME 0.27, PLE 0.33, AME–AME 0.18, AME–ALE 0.07, PME–PME 0.28, PME–PLE 0.35, AME–PME 0.32, ALE–PLE 0.31, CH AME 0.40, CH ALE 0.35. ***Spination*:** palp: 131, 101, 2121, 1014; Fe: I–III 323, IV 321; Pa: I–IV 101; Ti: I–IV 2126; Mt: I–II 2024, III–IV 3036. ***Measurements of palp and legs*:** palp 5.6 (1.7, 0.9, 1.2, 1.8), I 15.2 (4.3, 1.9, 3.9, 3.7, 1.4), II 16.7 (4.8, 2.1, 4.3, 4.0, 1.5), III 13.6 (4.3, 1.8, 3.1, 3.2, 1.2), IV 14.7 (4.6, 1.4, 3.5, 4.0, 1.2). Cheliceral furrow with ~46 denticles. Colouration in ethanol as in males, but body slightly darker (Fig. 15D, E; see Zhang et al. (2023a) for others described).

***Epigyne* (Fig. 15A–C).** Epigynal field ca. 1.17× wider than long; anterior margin (aEF) indistinct, trilobate, anterolaterally with two large U-shaped incisions that are well separated by ca. one width; anterior bands (AB)

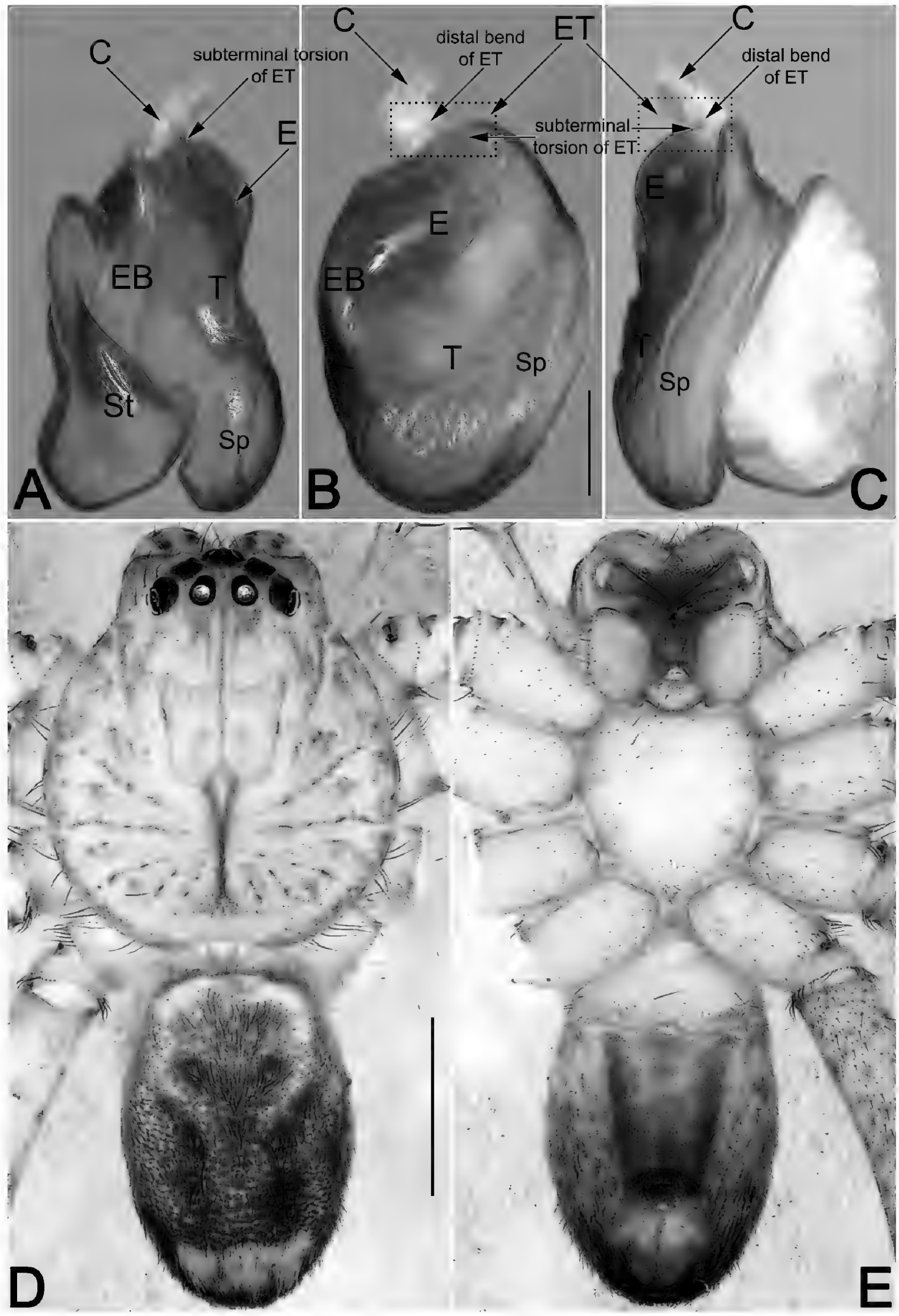

Figure 14. *Pseudopoda oliviformis*, male topotype, palpal bulb (**A–C**) and habitus (**D, E**). **A.** Prolateral; **B.** Ventral; **C.** Retrolateral; **D.** Dorsal; **E.** Ventral. Abbreviations: C = conductor; E = embolus; EB = embolic base; ET = embolic tip; Sp = spermophor; St = subtegulum; T = tegulum. Scale bars: 0.2 mm (equal for **A–C**); 1 mm (equal for **D, E**).

indistinct. Median field (MF) nearly fan-shaped, large, ca. 1/2 epigyne length and 2/3 epigyne width; anterior margin invisible, posteriorly with a circular patch anterior to lateral lobes (LL) with special surface structure of cuticle. Lateral lobes (LL) distinctly longer than wide; anterior margins (amLL) slightly recurved, almost straight, forming the letter 'V'; median margins (mmLL) entirely touching each other along the middle line; posterior margins (pmLL) '∧'-shaped, with distinct posterior incision (PI) on each side, respectively. Copulatory openings (CO) indistinct, located at basolateral borders of median field (MF). First windings (FW) membranous, tubular, slightly curved; starting from copulatory openings (CO), descending obliquely, then connecting with spermathecae at mid length of epigyne. Spermathecae (S) spherical, not subdivided, widely separated by ca. 1.5 diameters. Membranous sac (MS) large, nearly disc-shaped, located at posterior portion of

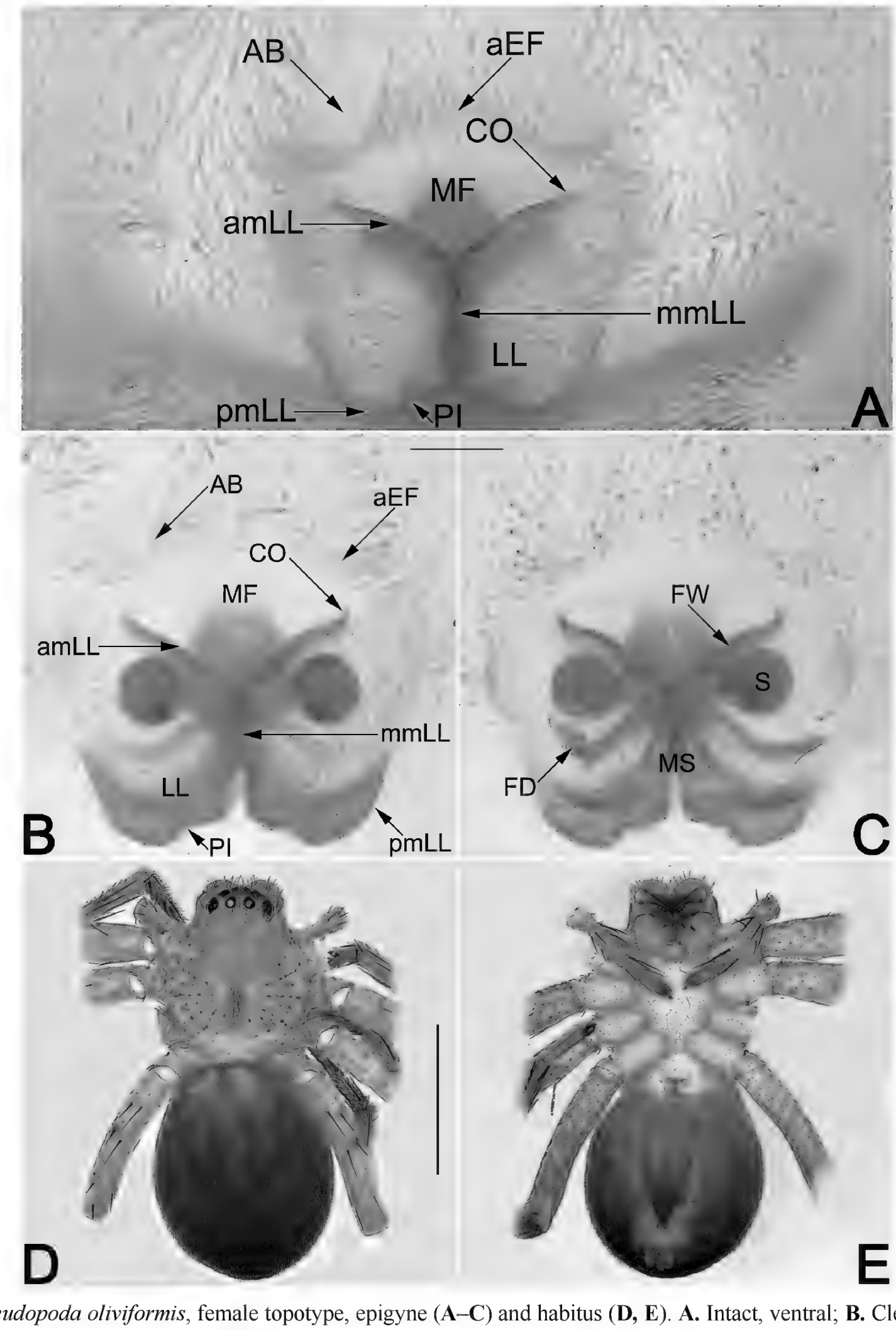

Figure 15. *Pseudopoda oliviformis*, female topotype, epigyne (**A–C**) and habitus (**D, E**). **A.** Intact, ventral; **B.** Cleared and macerated, ventral; **C.** Cleared and macerated, dorsal; **D.** Dorsal; **E.** Ventral. Abbreviations: AB = anterior band; aEF = anterior margin of epigynal field; amLL = anterior margin of lateral lobes; CO = copulatory opening; FD = fertilization duct; FW = first winding; LL = lateral lobe; MF = median field of epigyne; mmLL = median margin of lateral lobes; MS = membranous sac; PI = posterior incision; pmLL = posterior margin of lateral lobes; S = spermatheca. Scale bars: 0.2 mm (equal for **A–C**); 2 mm (equal for **D, E**).

vulva; anterior margin distinctly recurved, ca. 3/4 epigyne width, separated from epigastric fold by ca. 1/2 epigyne length, reaching cross point of anterior margins of lateral lobes (amLL); posterior margin distinctly procurved, as long as anterior margin, separated from epigastric fold by ca. 1/6 epigyne length. Fertilization ducts (FD) hyaline, slightly curved, relatively long, nearly 1/2 epigyne width; arising at central axis of vulva, extending laterally, terminating at lateral margin of epigynal field.

Distribution. Known only from the type locality (Fig. 1).

***Pseudopoda xiaozhua* J. Zhang, H. Yu & Y. Zhong, sp. nov.**

https://zoobank.org/9CD8CADF-8B6E-4F0F-847D-AB637785C6D4

Figs 1, 16–19, 28D

Holotype. ♂ (YNZY003), China: • Yunnan Pro.: Honghe Hani and Yi Autonomous Prefecture, Luechun Co., Huanglianshan Mt., 22.99°N, 102.46°E, c. 1940 m, by hand, 16 IV 2024, Y. Zhong & S. Yang leg. **Paratypes:** • 1 ♂ 2 ♀ (YNZY004, YNZY018, YNZY019), same data as holotype.

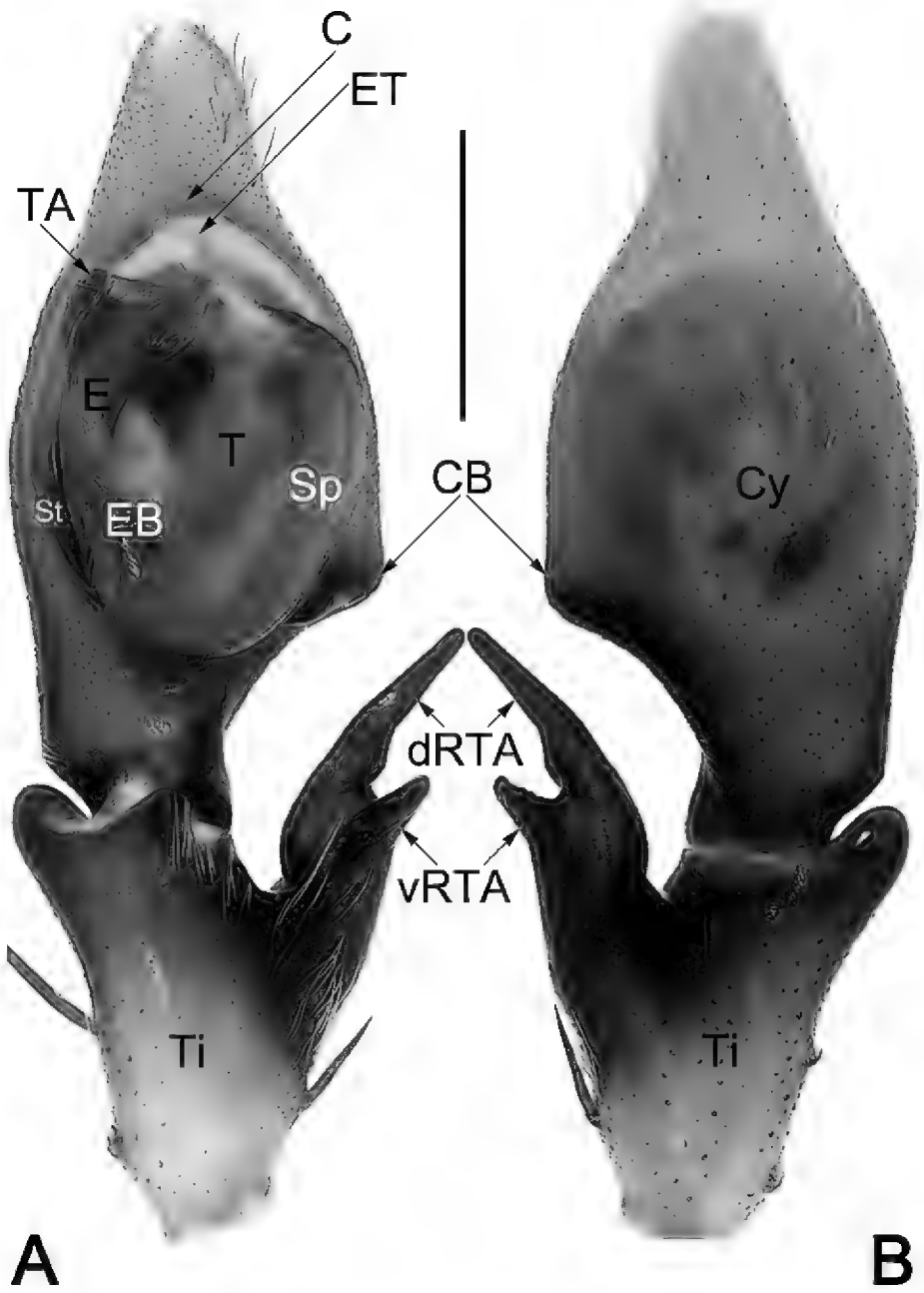

Figure 16. Male palp of the holotype of *Pseudopoda xiaozhua* sp. nov. **A.** Ventral; **B.** Dorsal. Abbreviations: C = conductor; CB = cymbial bulge; Cy = cymbium; dRTA = dorsal branch of RTA; E = embolus; EB = embolic base; ET = embolic tip; Sp = spermophor; St = subtegulum; T = tegulum; TA = tegular apophysis; Ti = palpal tibia; vRTA = ventral part of RTA. Scale bar: 1 mm (equal for **A, B**).

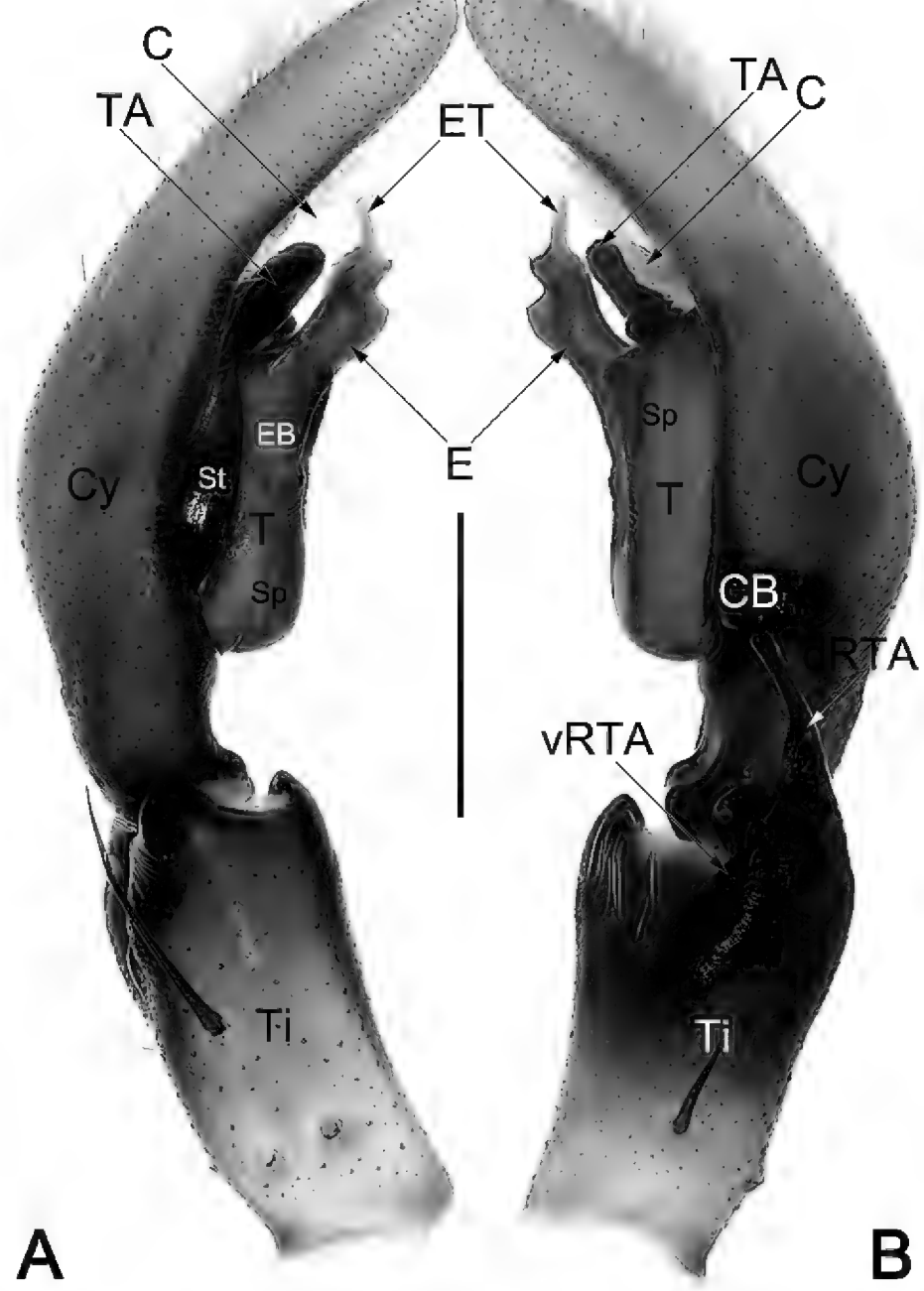

Figure 17. Male palp of the holotype of *Pseudopoda xiaozhua* sp. nov. **A.** Prolateral; **B.** Retrolateral. Abbreviations: C = conductor; CB = cymbial bulge; Cy = cymbium; dRTA = dorsal branch of RTA; E = embolus; EB = embolic base; ET = embolic tip; Sp = spermophor; St = subtegulum; T = tegulum; TA = tegular apophysis; Ti = palpal tibia; vRTA = ventral part of RTA. Scale bar: 1 mm (equal for **A, B**).

Etymology. The specific name is derived from the Chinese pinyin *xiǎo zhuǎ*, which means 'small claw', referring to the embolic tip, which is shaped like an unguiculus; noun in apposition.

Diagnosis. The males of new species can be easily distinguished from those of all other congeners by a combination of the following characters: (1) embolus (E) almost as long as tegulum (T), nearly column-shaped, distally with a small claw-shaped tip (ET), as in Figs 16A, 17A, B, 18A–C (vs. embolus (E) not as above); (2) tegulum (T) with a heavily sclerotised, strongly expanded tegular apophysis (TA), as in Figs 16A, 17A, B, 18A–C (vs. tegular apophysis (TA) absent). Female of *P. xiaozhua* sp. nov. is very similar to that of *P. mingshengi* Yang & Zhang, 2022 in the general appearance of the median field (MF) and vulva, but can be recognised by: (1) anterior margin of epigyne (aEF) with two small v-shaped incisions that are well separated by at least 3× widths (vs. two wide incisions closely spaced, aEF nearly W-shaped) (cf. Fig. 19A, B and Yang et al. 2022: figs 2D, 3D); (2) membranous sac (MS) disc-shaped, located at posterior portion of vulva, anterior margin not beyond the contact point of lateral lobes (LL) (vs. membranous sac (MS) triangular, located at central portion, posterior margin beyond the contact point) (cf. Fig. 19C and Yang et al. 2022: figs 2E, 3E).

Description. Male (YNZY003). Total length 10.9. Carapace 5.5 long, 5.2 wide; anterior width 2.7. Opisthosoma 5.4 long, 3.6 wide. ***Eye sizes and interdistances*:** AME 0.31, ALE 0.44, PME 0.36, PLE 0.42, AME–AME 0.19, AME–ALE 0.09, PME–PME 0.27, PME–PLE 0.41, AME–PME 0.37, ALE–PLE 0.37, CH AME 0.58, CH ALE 0.45. ***Spination*:** palp: 131, 101, 2101; Fe: I–III 323, IV 321; Pa: I–IV 101; Ti: I–II 2026, III–IV 2126; Mt: I–II 1014, III 2024, IV 3036. ***Measurements of palp and legs*:** palp 8.4 (2.7, 1.3, 1.4, 3.0), I 27.7 (7.4, 3.5, 6.3, 7.8, 2.7), II 30.3 (8.1, 3.0, 8.2, 8.3, 2.7), III 23.0 (6.5, 2.4, 6.0, 6.2, 1.9), IV 26.6 (7.6, 2.4, 6.5, 7.9, 2.2). Cheliceral furrow with ~50 denticles.

Colouration in ethanol **(Fig. 18D, E)**. DS yellowish brown, marked with numerous small spots along radial grooves, clothed with fine hairs; lateral bands and median band inconspicuous, not distinctly delimited; cervical groove not distinct, fovea and radial grooves distinct.

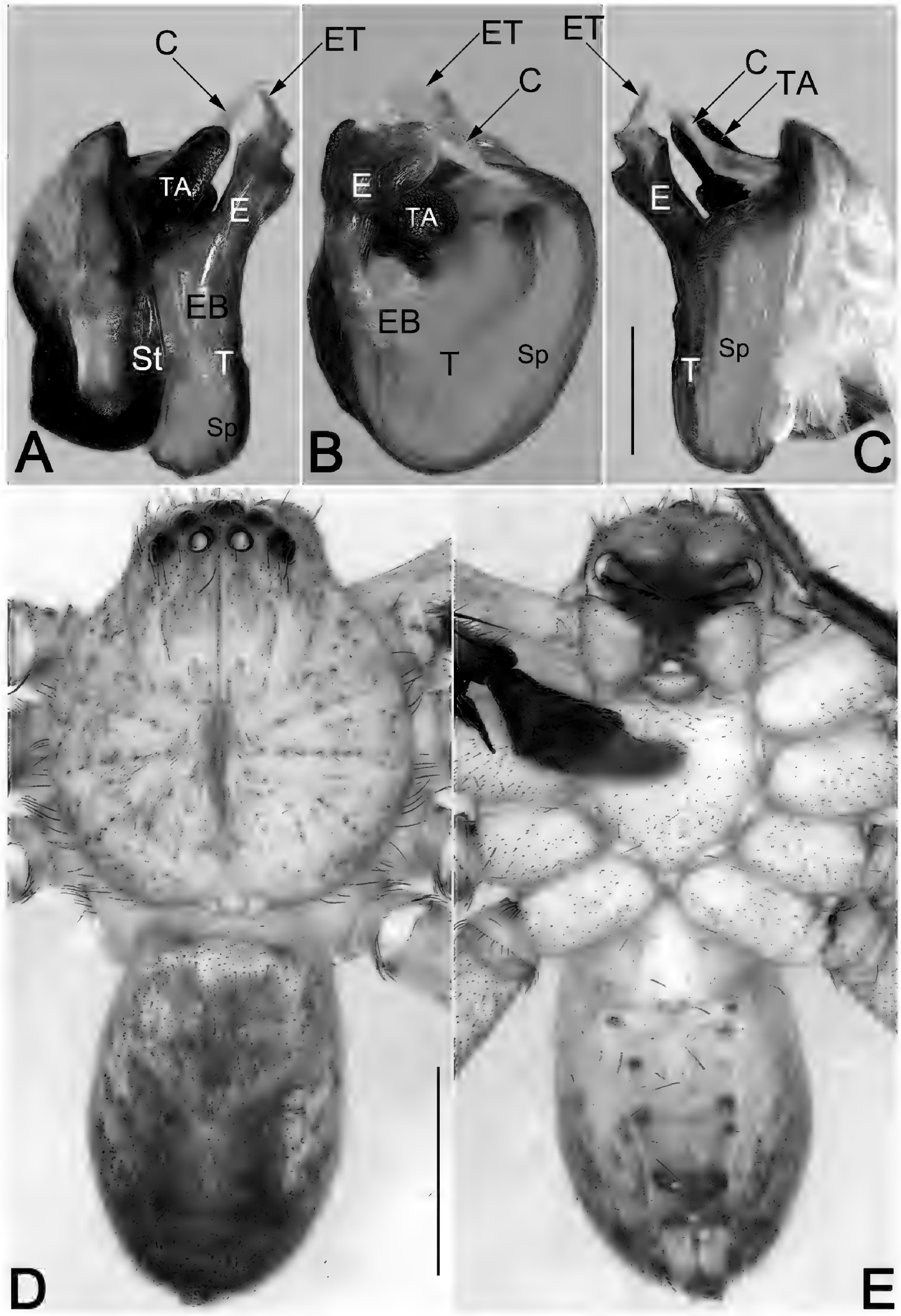

Figure 18. *Pseudopoda xiaozhua* sp. nov., male holotype, palpal bulb (**A–C**) and habitus (**D, E**). **A.** Prolateral; **B.** Ventral; **C.** Retrolateral; **D.** Dorsal; **E.** Ventral. Abbreviations: C = conductor; E = embolus; EB = embolic base; ET = embolic tip; Sp = spermophor; St = subtegulum; T = tegulum; TA = tegular apophysis. Scale bars: 0.5 mm (equal for **A–C**); 2 mm (equal for **D, E**).

Cheliceral base light brown, with red fang. Sternum yellowish-white, margin slightly darker. Endites and labium coloured as cheliceral base. Legs coloured as DS, with numerous spots, and bearing short spines. OS oval, dorsum laterally with bright patterns, centrally with Y-shaped median band, with a pair of circular dots on each side of the median band, posteriorly with large ‘)(‘-shaped black pattern, transverse line indistinct; venter of OS medially with a pair of diagonal broken lines.

Palp **(Figs 16, 17, 18A–C, 28D).** Femur and patella unmodified. Tibia (Ti) moderately long, ca. 2/5 cymbium length, with retrolateral apophysis (RTA) arising proximally to medially; RTA bifurcated, with ventral part (vRTA) and dorsal branch (dRTA): dRTA finger-like, distinctly long, nearly as long as tibia, almost reaching cymbial bulge (CB); vRTA humble and broad base and papilliform apex, ca.1/2 of dRTA length. Cymbium (Cy) ca. 2.1× longer than wide, basoretrolaterally with distinct, nearly

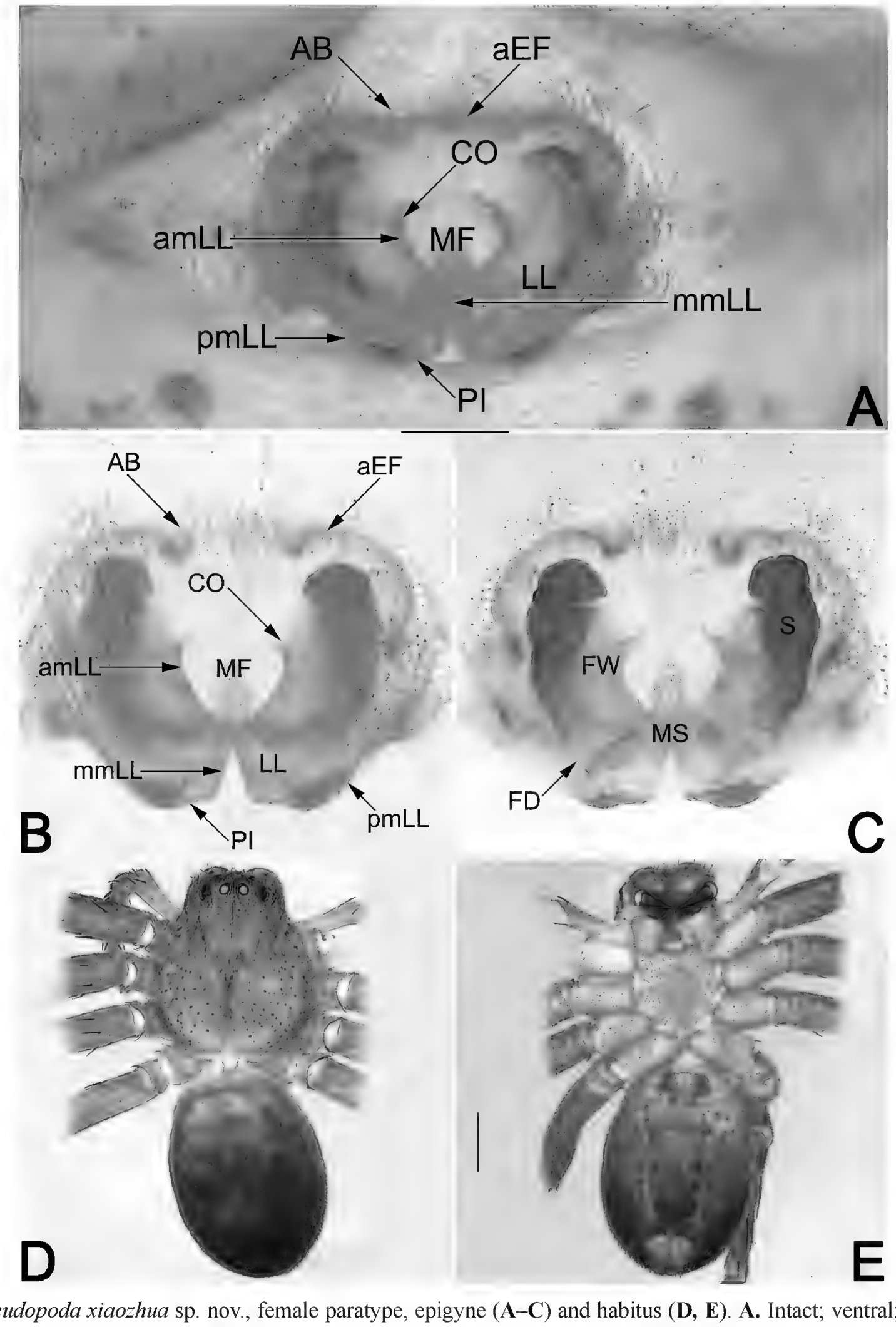

Figure 19. *Pseudopoda xiaozhua* sp. nov., female paratype, epigyne (**A–C**) and habitus (**D, E**). **A.** Intact; ventral; **B.** Cleared and macerated; ventral; **C.** Cleared and macerated; dorsal; **D.** Dorsal; **E.** Ventral. Abbreviations: AB = anterior band; aEF = anterior margin of epigynal field; amLL = anterior margin of lateral lobes; CO = copulatory opening; FD = fertilization duct; FW = first winding; LL = lateral lobe; MF = median field of epigyne; mmLL = median margin of lateral lobes; MS = membranous sac; PI = posterior incision; pmLL = posterior margin of lateral lobes; S = spermatheca. Scale bars: 0.2 mm (equal for **A–C**); 2 mm (equal for **D, E**).

triangular bulge (CB). Tegulum (T) egg-shaped, ca. 1.15× longer than wide, relatively flattened, prolatero-apically slightly excavated, with heavily sclerotised tegular apophysis (TA); spermophor (Sp) distinct, V-shaped in ventral view. Tegular apophysis (TA) strongly expanded, inserted at apico-prolateral portion of tegulum; proximally exposed and petal-shaped; mesially and distally digitiform, hidden behind embolus. Embolus (E) almost as long as tegulum (T); basally and mesially thick and robust, nearly column-shaped, originated at ~8–9 o'clock; embolic tip (ET) distinctly narrowed and curved, claw-shaped in ventral view, apex sharp, terminated at ~11 o'clock position. Conductor (C) membranous, ca. 1/2 of the embolus length, extending obliquely, arising at ca. 1 o'clock position from tegulum, terminating at c. 11 o'clock position; conductor (C) proximally narrowed, its tip widened, shaped like the membranous wing of hymenoptera, directed prolaterally and apically beyond embolic tip (ET).

Female (YNZY004). Total length 13.4. Carapace 6.3 long, 5.5 wide; anterior width 3.3. Opisthosoma 7.1 long, 5.1 wide. ***Eye sizes and interdistances*:** AME 0.32, ALE 0.47, PME 0.37, PLE 0.41, AME–AME 0.18, AME–ALE 0.07, PME–PME 0.32, PME–PLE 0.51, AME–PME 0.42, ALE–PLE 0.42, CH AME 0.63, CH ALE 0.51. ***Spination*:** palp: 131, 101, 2121, 1014; Fe: I–III 323, IV 321; Pa: I–IV 101; Ti: I–IV 2026; Mt: I–II 1014, III 2024, IV 3036. ***Measurements of palp and legs*:** palp 8.0 (2.5, 1.3, 1.7, 2.5), I 21.4 (6.4, 2.8, 5.1, 5.3, 1.8), II 22.4 (6.8, 2.6, 5.6, 5.7, 1.7), III 18.9 (6.0, 2.5, 4.8, 4.5, 1.1), IV 21.0 (6.5, 2.4, 5.3, 5.5, 1.3). Cheliceral furrow with ~56 denticles. Colouration in ethanol as in males, but generally distinctly darker (Fig. 19D, E).

***Epigyne* (Fig. 19A–C).** Epigynal field ca. 1.5× wider than long; anterior margin (aEF) trilobate, with two small v-shaped incisions that are well separated by at least 3× widths; anterior bands (AB) indistinct, situated at the two incisions. Median field (MF) nearly heart-shaped, relatively small, no more than 1/3 epigyne length and 1/4 epigyne width. Lateral lobes (LL) distinctly longer than wide, slightly converged on the central axis; anterior margins (amLL) distinctly procurved and delimited; median margins (mmLL) touching each other along the middle line in anterior half; posterior margins (pmLL) with incision (PI) on each side. Copulatory openings (CO) indistinct, located at anterolateral margins of median field (MF). First windings (FW) represented by translucent, membranous short tube, starting from near copulatory openings (CO), descending obliquely, moving laterally to basolateral surfaces of spermathecae (S), ca. 1/2 of epigyne length. Spermathecae (S) clavate, at least 2.7 longer than diameters; surface wrinkled, provided with several depressions and anterior hump; spermathecae (S) widely separated by ca. 2.4× diameters. Membranous sac (MS) disc-shaped, located at posterior portion of vulva; anterior margin separated from epigastric fold by ca. 1/3 epigyne length, reaching the contact point of median margins of lateral lobes (mmLL); posterior margin close to the epigastric fold. Fertilization ducts (FD) acicular, membranous, nearly 1/2 spermathecae length, proximally covered by membranous sac (MS).

Distribution. Presently known only from the type locality (Fig. 1).

Pseudopoda yangae J. Zhang, H. Zhang & Y. Zhong, sp. nov.

https://zoobank.org/C454FEC4-9705-4048-AA1B-93B34B8B314F

Figs 1, 20–24, 28E, F

Pseudopoda breviducta Zhang, Zhang & Zhang, 2013 in Zhang et al. 2013a: 279, figs 29–31, 35, 36 (♀ only, ♂ mismatched).

Holotype. ♂ (YNZY001), China: • Yunnan Pro.: Honghe Hani and Yi Autonomous Prefecture: Pingbian Co., Daweishan National Park, 22.94°N, 103.70°E, c. 2365 m, by hand, 14 IV 2024, Y. Zhong & S. Yang leg. **Paratypes:** • 3 ♂ 4 ♀ (YNZY002, YNZY005, YNZY006, YNZY008, YNZY017, YNZY020, YNZY021), same data as holotype.

Etymology. The specific name is dedicated to Ms. Siyu Yang (Xianning, China), collector of several specimens examined in this study.

Diagnosis. The males of the new species resemble those of *P. amelia* Jäger & Vedel, 2007; *P. putaoensis* Zhao & Li, 2018; and *P. zhangi* Fu & Zhu, 2008 in having a ɔ-shaped embolus (E) (Figs 20A, 22B; Jäger and Vedel 2007: figs 32, 33; Jiang et al. 2018: figs 18A, B, 19A, B; Fu and Zhu 2008: fig. 4), but differs by: (1) dorsal branch of RTA (dRTA) blade-shaped, reaching basal part of cymbium (Cy) (vs. distinctly shorter, not reaching cymbial base in *P. amelia*; finger-like in *P. putaoensis* and *P. zhangi*) (cf. Figs 20A, B, 21B, 28E, F and Jäger and Vedel 2007: figs 33, 34 and Jiang et al. 2018: figs 18B, C and Fu and Zhu 2008: figs 4, 5); (2) in retrolateral view, ventral branch of RTA (vRTA) claviform and distinctly protruding (vs. papilliform in *P. amelia*, laminar in *P. putaoensis* and *P. zhangi*, humble and barely protruding in *P. amelia*, *P. putaoensis* and *P. zhangi*) (cf. Figs 21B, 28E, F and Jäger and Vedel 2007: fig. 34 and Jiang et al. 2018: fig. 18C and Fu and Zhu 2008: fig. 5). Female of *P. yangae* sp. nov. is similar to that of *P. emei* F. Zhang, B. S. Zhang & Z. S. Zhang, 2013 by the similarly shaped median field (MF), but can be recognised by: (1) anterior bands (AB) indistinct (vs. distinct) (cf. Fig. 23A, B, D, E and Zhang et al. 2013b: fig. 25 and Jäger et al. 2015: figs 24, 29); (2) in dorsal view, lateral lobes (LL) without ridges, length of lateral margin of lateral lobes distinctly longer than that of median margin (mmLL) (vs. with distinct ridges, length of lateral margin almost equal to median margin) (cf. Fig. 23C, F and Zhang et al. 2013b: figs 26, 31 and Jäger et al. 2015: fig. 25); (3) first winding (FW) distinctly thinner, ca. 1/15–1/20 of epigyne width, widely separated by ca. 15–17× diameters (vs. relatively thicker, ca. 1/10–1/12 of epigyne width, separated by ca. 5× diameters) (cf. Fig. 23C, F and Zhang et al. 2013b: figs 26, 31 and Jäger et al. 2015: fig. 25); (4) first winding (FW) entirely covered by lateral lobes (LL) (vs. anterior half of first winding (FW) exposed, not covered by lateral lobes (LL)) (cf. Fig. 23C, F and Zhang et al. 2013b: figs 26, 31 and Jäger et al. 2015: fig. 25).

Description. Male (YNZY001). Total length 7.5. Carapace 3.9 long, 3.6 wide, anterior width 1.9. Opisthosoma 3.6 long, 2.4 wide. ***Eye sizes and interdistances*:** AME 0.19, ALE 0.31, PME 0.24, PLE 0.31, AME–AME 0.13, AME–ALE 0.04, PME–PME 0.20, PME–PLE 0.27, AME–PME 0.29, ALE–PLE 0.26, CH AME 0.29, CH ALE 0.20. ***Spination*:** palp: 131, 101, 2101; Fe: I–III 323, IV 321; Pa: I–IV 101; Ti: I–II 2126, III–IV 2226; Mt: I–II 1014, III 2024, IV 3036. ***Measurements of palp and legs*:** palp 6.0 (2.1, 1.0, 1.1, 1.8), I 19.2 (5.4, 1.8, 5.2, 5.1, 1.7), II 20.9 (5.7, 1.9, 5.8, 5.5, 2.0), III 15.3 (4.0, 1.4, 4.3, 4.1, 1.5), IV 17.6 (5.2, 1.6, 4.7, 4.5, 1.6). Cheliceral furrow with ~32 denticles.

***Colouration in ethanol* (Fig. 22D, E).** DS yellowish, marked with numerous small spots along radial grooves, lateral bands slightly darker, clothed with fine hairs; median band bright yellowish-brown, not distinctly

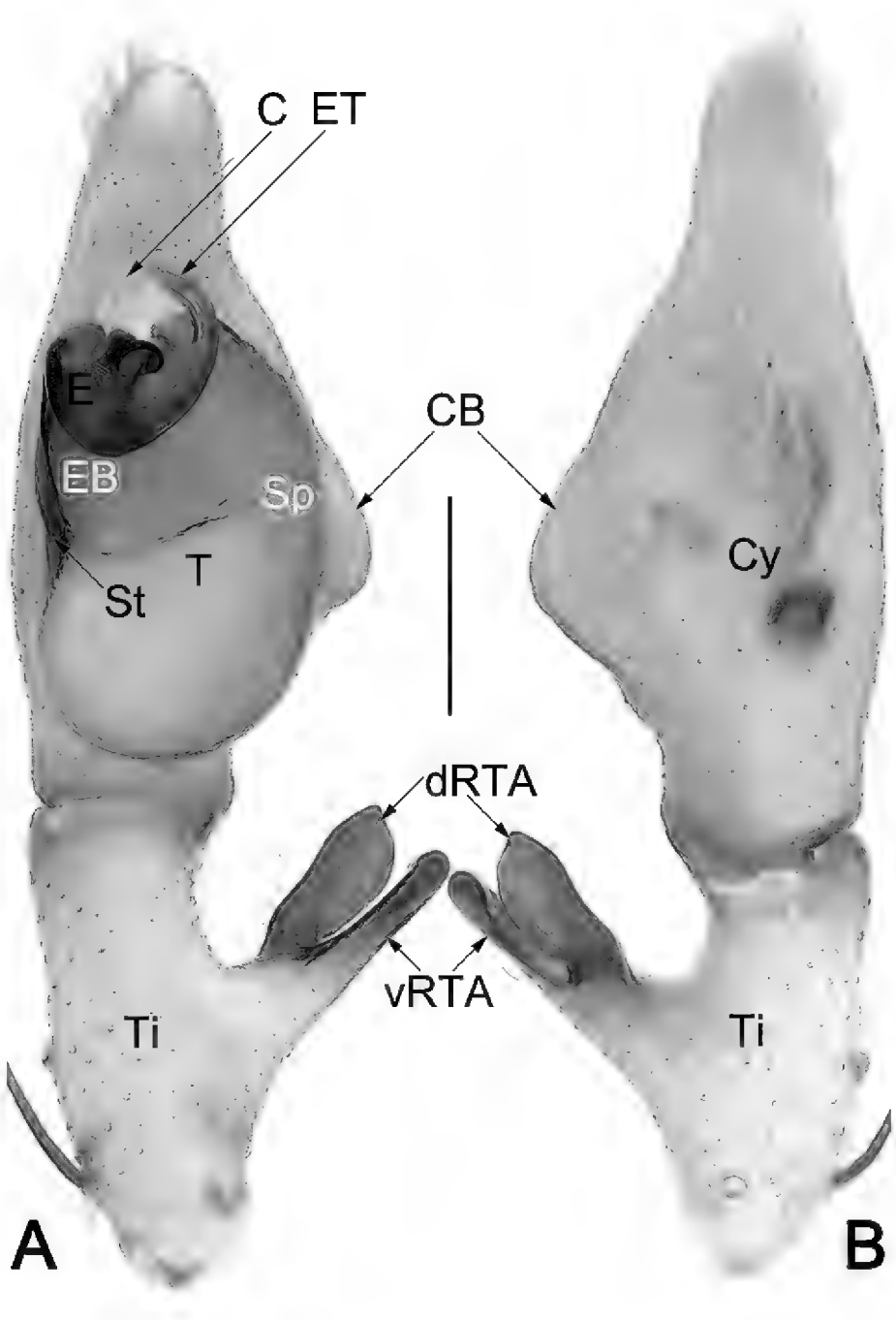

Figure 20. Male palp of the holotype of *Pseudopoda yangae* sp. nov. **A.** Ventral; **B.** Dorsal. Abbreviations: C = conductor; CB = cymbial bulge; Cy = cymbium; dRTA = dorsal branch of RTA; E = embolus; EB = embolic base; ET = embolic tip; Sp = spermophor; St = subtegulum; T = tegulum; Ti = palpal tibia; vRTA = ventral branch of RTA. Scale bar: 0.5 mm (equal for **A, B**).

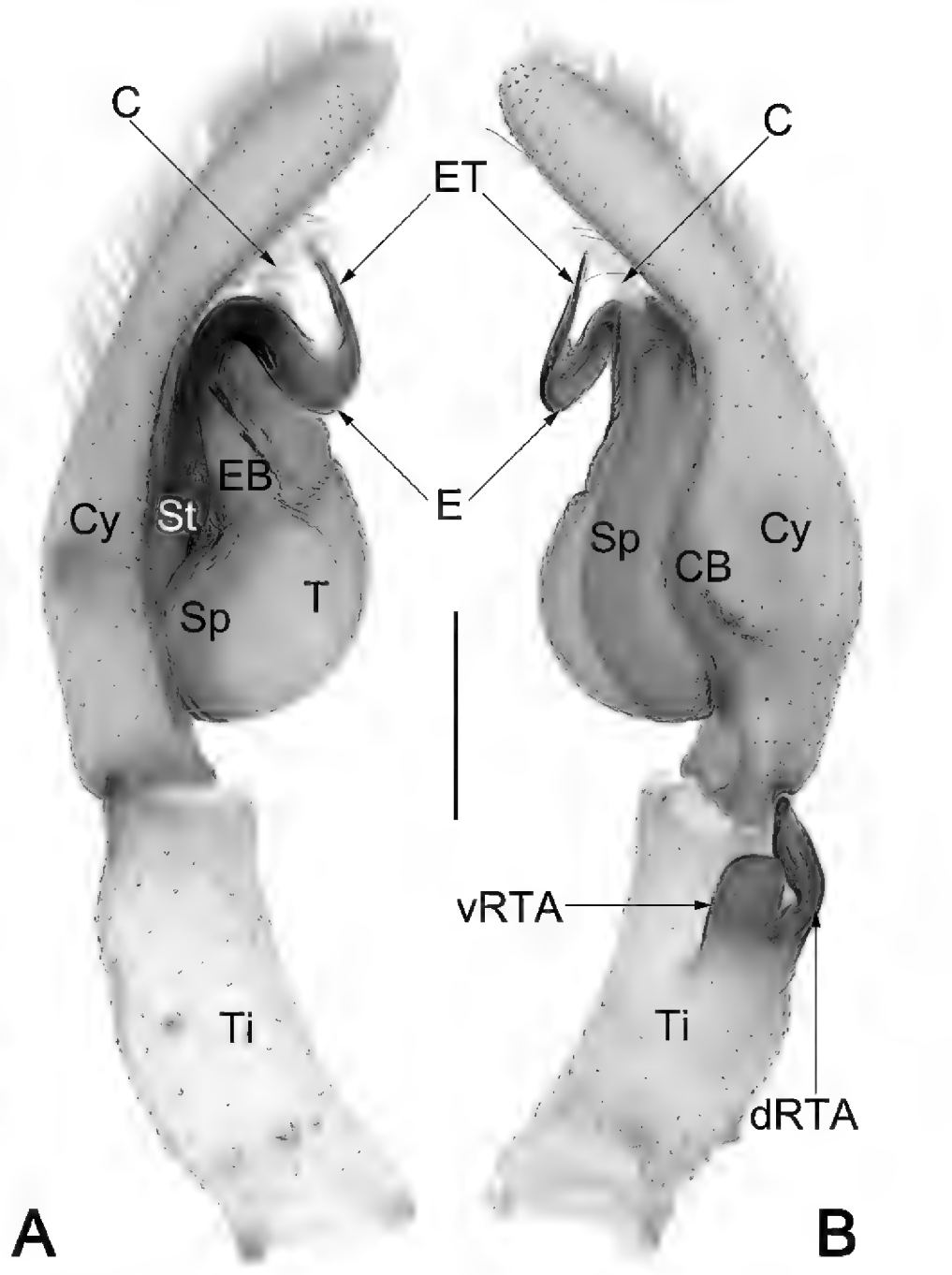

Figure 21. Male palp of the holotype of *Pseudopoda yangae* sp. nov. **A.** Prolateral; **B.** Retrolateral. Abbreviations: C = conductor; CB = cymbial bulge; Cy = cymbium; dRTA = dorsal branch of RTA; E = embolus; EB = embolic base; ET = embolic tip; Sp = spermophor; St = subtegulum; T = tegulum; Ti = palpal tibia; vRTA = ventral branch of RTA. Scale bar: 0.5 mm (equal for **A, B**).

delimited to lateral bands, with indistinct Ψ-shaped markings starting from behind PER, almost reaching fovea; fovea and striae distinctly marked. Cheliceral base yellowish white, fang reddish. Sternum yellowish white, margin slightly darker. Endites and labium light orange. Legs yellowish white, marked with numerous spots. OS oval, dorsum laterally with a pair of arc-shaped stripes, centrally with short, longitudinal median band, posteriorly with thick transverse line; venter of OS medially with a pair of indistinct, diagonal broken lines, posteriorly with triangular marking.

***Palp* (Figs 20, 21, 22A–C, 28E).** Femur and patella unmodified. Tibia (Ti) moderately long, ca. 2/3 cymbium length, with retrolateral apophysis (RTA) arising proximally to medially; RTA bifurcated, both ventral and dorsal branches distinctly protruding: dorsal branch (dRTA) blade-shaped, basally slightly curved, no more than 1/2 of the tibia length; ventral branch (vRTA) almost as long as dRTA, claviform, basally and distally slightly widened, medially slightly narrowed. Cymbium (Cy) ca. 2.1× longer than wide, retrolaterally with distinct blunt bulge (CB). Tegulum (T) elongate-oval, proximally strongly bulged and prolapsed, distinctly excavated on prolatero-apical side to accommodate embolus (E); spermophor (Sp) distinct, U-shaped in ventral view, oriented clockwise along tegular margin. Embolus (E) robust, slightly longer than tegulum, more or less ɔ-shaped in ventral view and Ƨ-shaped in prolateral view; embolic base (EB) broadened, inserted prolaterally (approximately 9 o'clock relative to tegulum); embolic tip (ET) distinctly curved, terminated at ~12 o'clock position, apex sharply pointed, directed prolaterally. Conductor (C) situated apically, irregularly shaped, covering embolic tip (ET) in prolateral and ventral views.

Female (YNZY002). Total length 9.7. Carapace 4.5 long, 4.3 wide, anterior width 2.5. Opisthosoma 5.2 long, 3.8 wide. ***Eye sizes and interdistances*:** AME 0.22, ALE 0.36, PME 0.28, PLE 0.34, AME–AME 0.20, AME–ALE 0.11, PME–PME 0.26, PME–PLE 0.39, AME–PME 0.38, ALE–PLE 0.37, CH AME 0.45, CH ALE 0.36. ***Spination*:** palp: 131, 101, 2121, 1014; Fe: I–III 323, IV 321; Pa: I–IV 101; Ti: I–II 2026, III–IV 2126; Mt: I–II 1014, III 2026, IV 3036. ***Measurements of palp and legs*:** palp 6.0 (1.9, 1.1, 1.2, 1.9), I 16.7 (4.8, 2.1, 4.3, 4.1, 1.4),

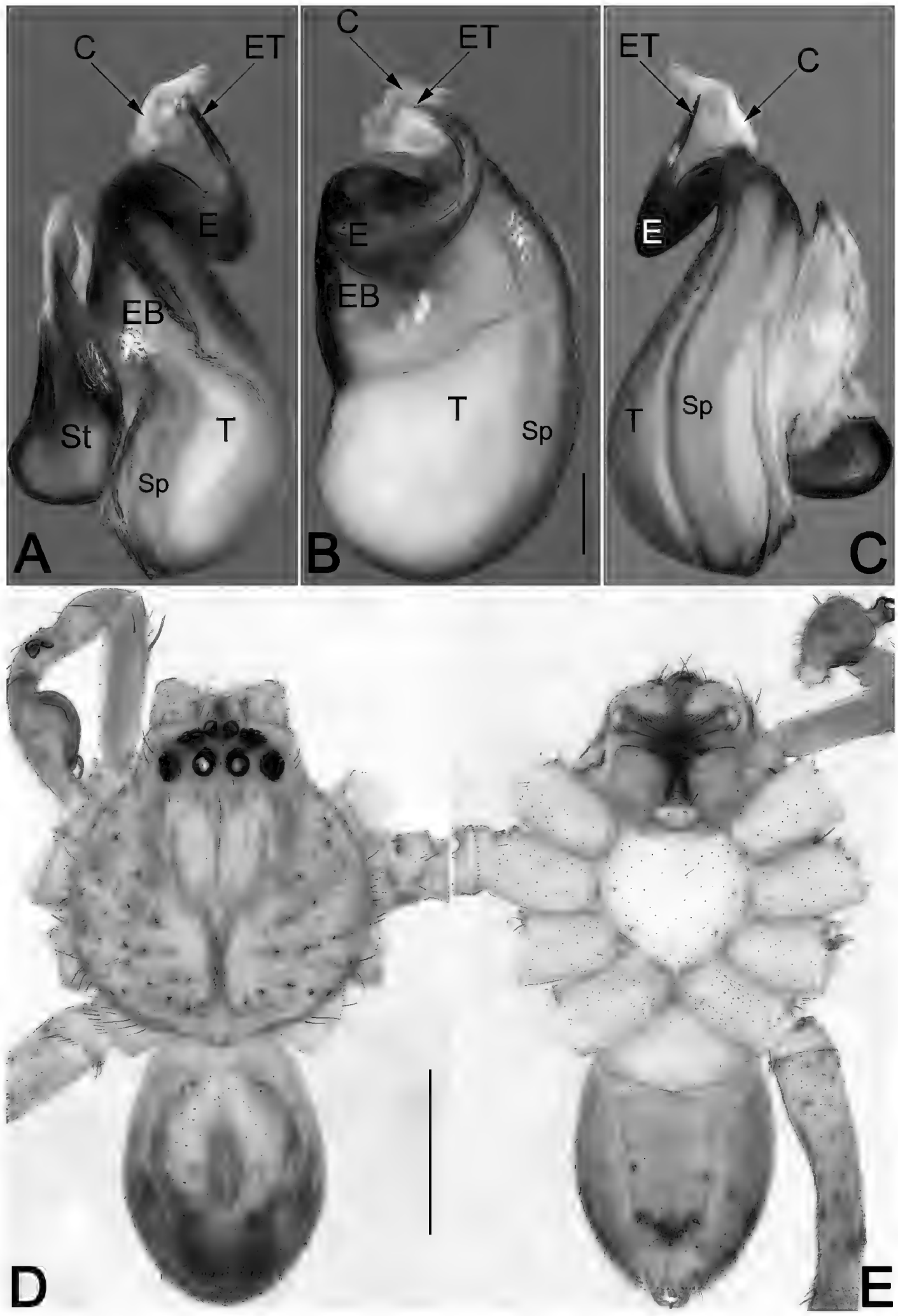

Figure 22. *Pseudopoda yangae* sp. nov., male holotype, palpal bulb (**A–C**) and habitus (**D, E**). **A.** Prolateral; **B.** Ventral; **C.** Retrolateral; **D.** Dorsal; **E.** Ventral. Abbreviations: C = conductor; E = embolus; EB = embolic base; ET = embolic tip; Sp = spermophor; St = subtegulum; T = tegulum. Scale bars: 0.2 mm (equal for **A–C**); 2 mm (equal for **D, E**).

II 17.6 (5.2, 2.2, 4.6, 4.2, 1.5), III 14.1 (4.4, 1.8, 3.5, 3.2, 1.3), IV 15.8 (4.9, 1.7, 3.8, 4.1, 1.5). Cheliceral furrow with ~44 denticles. Colouration in ethanol as in males, but generally distinctly darker (Fig. 24A, B).

Epigyne **(Fig. 23 A–C).** Epigynal field nearly as wide as long; anterior margin (aEF) recurved, without incision; anterior bands (AB) indistinct. Median field (MF) more or less cordiform, large, more than 1/2 epigyne length and 2/3 epigyne width, anterior margin (amMF) indistinct. Lateral lobes (LL) distinctly longer than wide; anterior margins (amLL) distinctly delimited, V-shaped; median margins (mmLL) touching each other along the middle line in anterior half; posterior margins (pmLL) curved, with distinct median indentation and distinct posterior incisions (PI) on each side. Copulatory openings (CO) indistinct, located at anterolateral borders of median field (MF). First windings (FW) entirely covered by lateral lobes (LL), represented by translucent, slightly curved long tubes, starting from near copulatory openings (CO), descending longitudinally, almost extending posteriorly to level of posterior parts of spermathecae (S), nearly as long as epigyne. Spermathecae (S) fist-shaped, ca. 1.5×

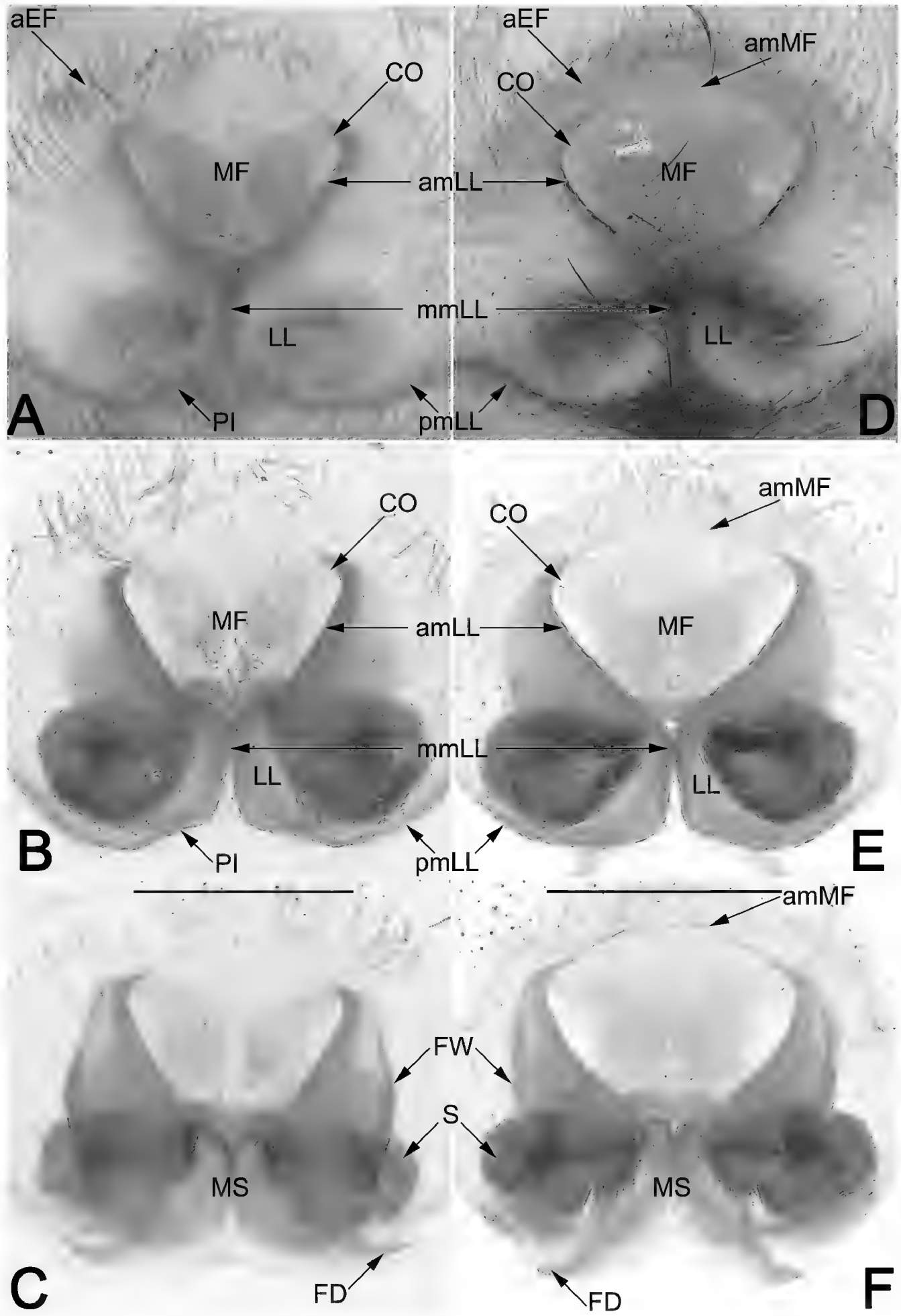

Figure 23. *Pseudopoda yangae* sp. nov., female paratypes, YNZY002 (**A–C**) and YNZY006 (**D–E**), epigyne, showing the intraspecific variations exhibited by different females, related to different degrees of sclerotization of amMF. **A, D.** Intact, ventral; **B, E.** Cleared and macerated, ventral; **C, F.** Cleared and macerated, dorsal. Abbreviations: aEF = anterior margin of epigynal field; amLL = anterior margin of lateral lobes; amMF = anterior margin of median field; CO = copulatory opening; FD = fertilization duct; FW = first winding; LL = lateral lobe; MF = median field of epigyne; mmLL = median margin of lateral lobes; MS = membranous sac; PI = posterior incision; pmLL = posterior margin of lateral lobes; S = spermatheca. Scale bars: 0.5 mm (equal for **A–C,** equal for **D–E**).

wider than long; relatively sclerotised, surface wrinkled, provided with several depressions and lateral hump; inner parts of the spermathecae covered by membranous sac (MS), separated by 0.3× widths. Membranous sac (MS) hyaline, nearly trapeziform, located at posterior portion of vulva; anterior margin separated from epigastric fold by ca. 1/2 epigyne length, beyond the contact point of lateral lobes (LL); posterior margin close to the epigastric fold. Fertilization ducts (FD) acicular, membranous, nearly 1/2 spermathecae length.

Distribution. Presently known only from the type locality (Fig. 1).

Comments. Both males and females exhibit some morphological variation among different individuals: for males, mostly related to different shapes of vRTA and dRTA (vRTA medially slightly narrowed, and dRTA apically more sharp in some males, such as in holotype, YNZY001 vs. vRTA medially more narrowed, dRTA apically more blunt in some males, such as in YNZY005; cf. Fig. 28E and Fig. 28F); for females, mostly related to different degrees

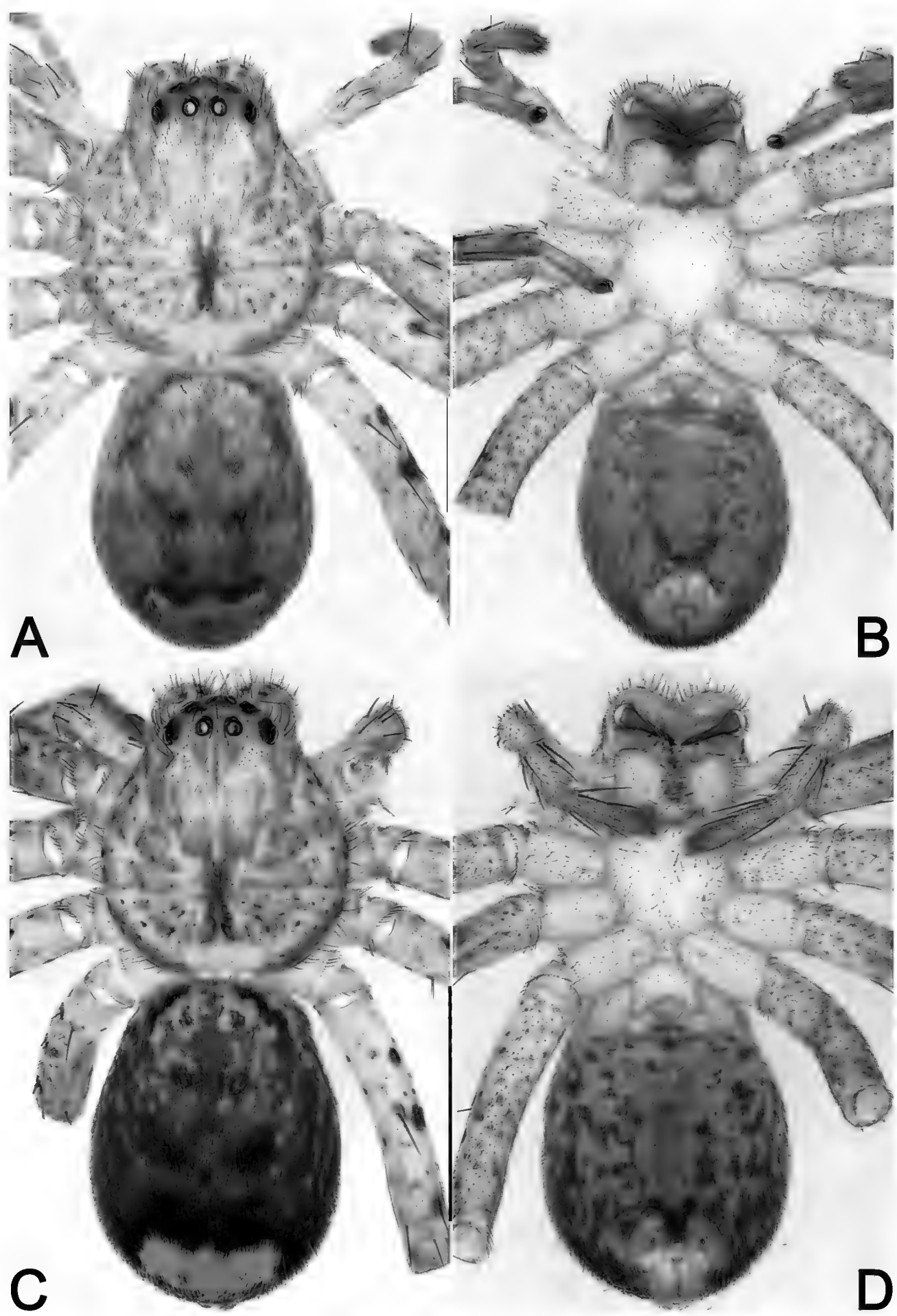

Figure 24. *Pseudopoda yangae* sp. nov., female paratypes, YNZY002 (**A, B**) and YNZY006 (**C, D**), habitus, showing the intraspecific variations exhibited by different females, related to different abdominal pattern. **A, C.** Dorsal; **B, D.** Ventral. Scale bars: 2 mm (equal for **A, B**; equal for **C, D**).

of sclerotization of amMF and curve of amLL (amMF indistinct, amLL relatively straight in some females, such as in YNZY002 vs. amMF distinct, amLL distinctly curved in some females, such as in YNZY006; cf. Fig. 23A, B and Fig. 23D, E), and the different abdominal pattern (dorsum of abdomen posteriorly with a narrow, W-shaped transverse line in some females, such as in YNZY002 vs. with a broad, W-shaped transverse band in some females, such as in YNZY006; cf. Fig. 24A and Fig. 24C). However, all molecular species delimitation analyses results show that the different individuals exhibiting considerable morphological variations should be classified as the same species (Fig. 2; for details see the results and discussion section). After careful examination, the variations listed above were determined to be intraspecific differences.

***Pseudopoda ying* J. Zhang, H. Zhang & Y. Zhong, sp. nov.**

https://zoobank.org/4A1B899F-AFF8-47BC-86FB-77A0DE4679C0

Figs 1, 25–27, 28G

Holotype. ♂ (YNZY007), China: • Yunnan Pro.: Honghe Hani and Yi Autonomous Prefecture: Pingbian Co., Daweishan National Park, 22.94°N, 103.70°E, c. 2365 m, by hand, 14 IV 2024, Y. Zhong & S. Yang leg. **Paratype:** • 1 ♂ (YNZY026), same data as holotype.

Etymology. The specific name is derived from the Chinese pinyin *'yìng'*, which means 'hard', referring to the conductor heavily sclerotized and well developed; adjective.

Diagnosis. Median-sized Sparassidae with body length of males 7.8 mm, belonging to the *daliensis* species

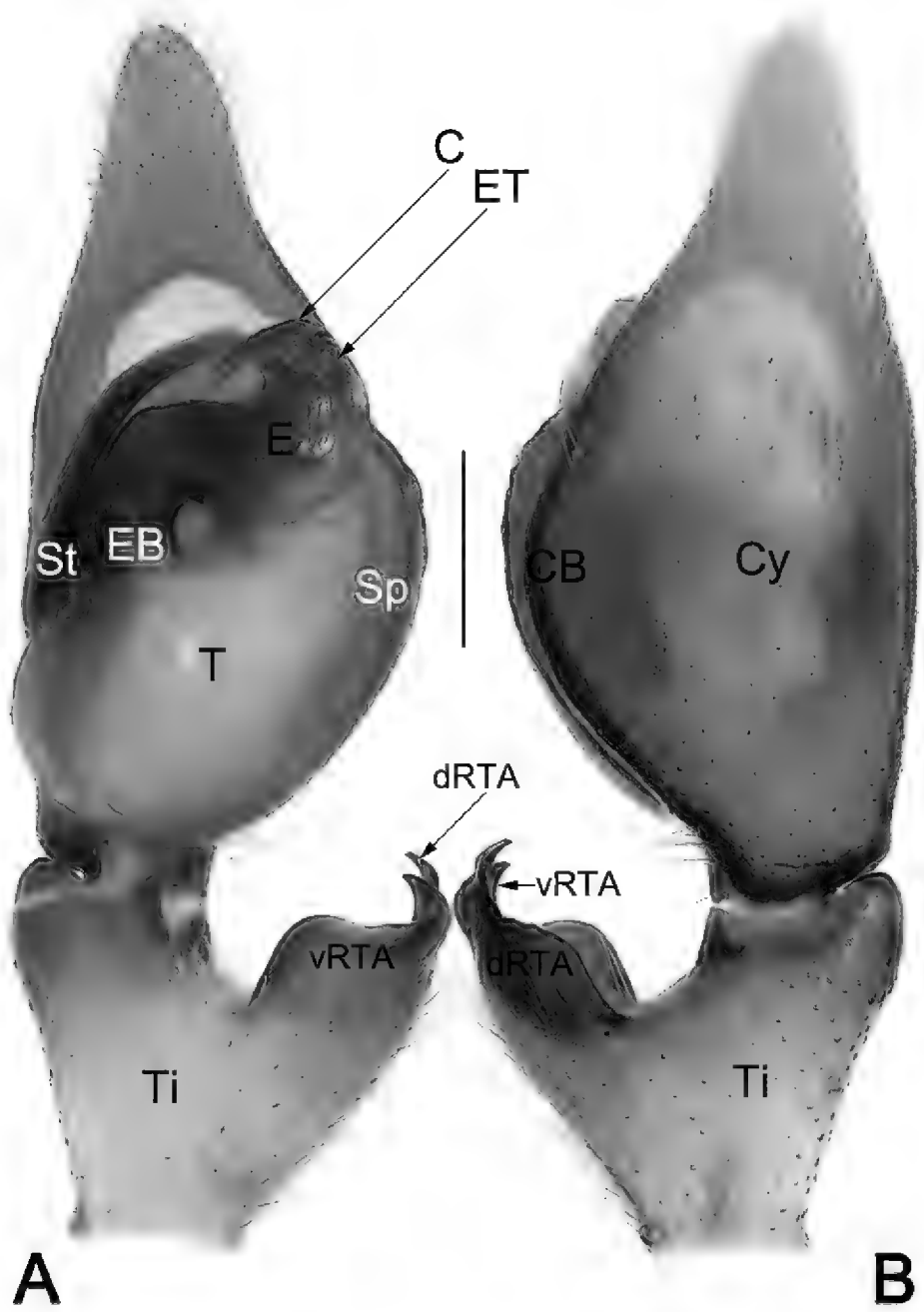

Figure 25. Male palp of the holotype of *Pseudopoda ying* sp. nov. **A.** Ventral; **B.** Dorsal. Abbreviations: C = conductor; CB = cymbial bulge; Cy = cymbium; dRTA = dorsal part of RTA; E = embolus; EB = embolic base; ET = embolic tip; Sp = spermophor; St = subtegulum; T = tegulum; Ti = palpal tibia; vRTA = ventral part of RTA. Scale bar: 0.5 mm (equal for **A, B**).

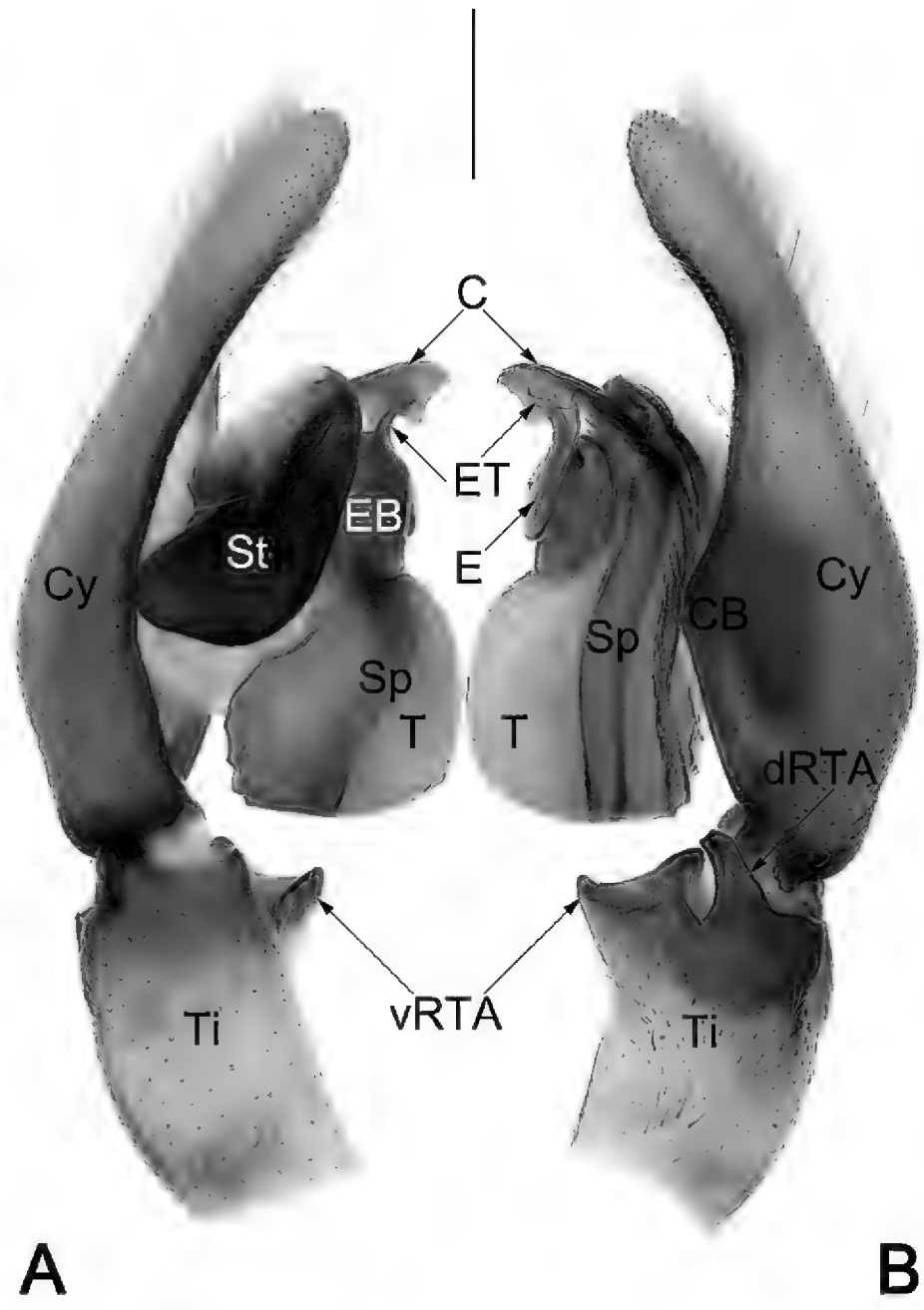

Figure 26. Male palp of the holotype of *Pseudopoda ying* sp. nov. **A.** Prolateral; **B.** Retrolateral. Abbreviations: C = conductor; CB = cymbial bulge; Cy = cymbium; dRTA = dorsal part of RTA; E = embolus; EB = embolic base; ET = embolic tip; Sp = spermophor; St = subtegulum; T = tegulum; Ti = palpal tibia; vRTA = ventral part of RTA. Scale bar: 0.5 mm (equal for **A, B**).

group. Male of the new species can be easily distinguished from all other congroupers, with the exception of *P. sicyoidea*, by having similar palp with ƨ-shaped, wide embolus (E), and broad ventral part of RTA (vRTA) with two distinct margins that resemble mountains, but can be distinguished by: (1) conductor (C) exhibits high degree of sclerotization (vs. membranous) (cf. Figs 25A, 26A, B, 27A–C and Zhang et al. 2017: 274, figs 13A, 14A); (2) embolic tip (ET) blunt, slightly curved, directing prolatero-distally, terminating at c. 12 o'clock position (vs. sharp and peak-shaped, distinctly curved, directing proximally, terminating at c. 10–11 o'clock position) (cf. Figs 25A, 27B and Zhang et al. 2017: 274, figs 12A, 14A).

Description. Male (YNZY007). Total length 7.8. Carapace 3.9 long, 3.6 wide, anterior width 2.0. Opisthosoma 3.9 long, 2.4 wide. ***Eye sizes and interdistances*:** AME 0.28, ALE 0.35, PME 0.29, PLE 0.30, AME–AME 0.18, AME–ALE 0.07, PME–PME 0.24, PME–PLE 0.36, AME–PME 0.34, ALE–PLE 0.28, CH AME 0.34, CH ALE 0.28. ***Spination*:** palp: 131, 101, 2101; Fe: I–III 323, IV 321; Pa: I–IV 101; Ti: I–IV 2226; Mt: I–II 1014, III 2026, IV 3036. ***Measurements of palp and legs*:** palp 6.0 (2.1, 0.7, 1.1, 2.1) I 24.3 (7.7, 2.0, 6.7, 6.2, 1.7); II 28.0 (7.9, 2.7, 8.2, 7.1, 2.1); III 19.6 (5.7, 1.7, 5.5, 5.2, 1.5); IV 23.4 (7.3, 1.4, 6.2, 6.7, 1.8). Cheliceral furrow with ~26 denticles.

***Colouration in ethanol* (Fig. 27D, E)**: DS yellowish brown, darker anteriorly and marginally; median band bright yellowish-brown, distinctly delimited to black lateral bands, with distinct Ψ-shaped markings starting from behind PER, almost reaching distinct fovea; fovea and radial grooves distinctly marked. Cheliceral base yellowish white, with red fangs. Sternum yellowish white, marked with numerous purplish spots. Endites and labium coloured as sternum. Legs dark yellowish-brown, with numerous brown spots, and covered by short spines. OS elongate-oval, dorsum anteriorly with median band, reaching 4/5 of abdomen length; median band consisting of cross-shaped anterior stripe and nearly square-shaped posterior stripe, the two stripes fused; ventral OS medially with V-shaped markings.

***Palp* (Figs 25, 26, 27A–C, 28G).** Femur and patella unmodified. Tibia (Ti) relatively short, ca. 2/5 cymbium length, with retrolateral apophysis (RTA) arising proximally to mesially; RTA subdivided, with ventral part (vRTA) and dorsal part (dRTA): dRTA basally wide,

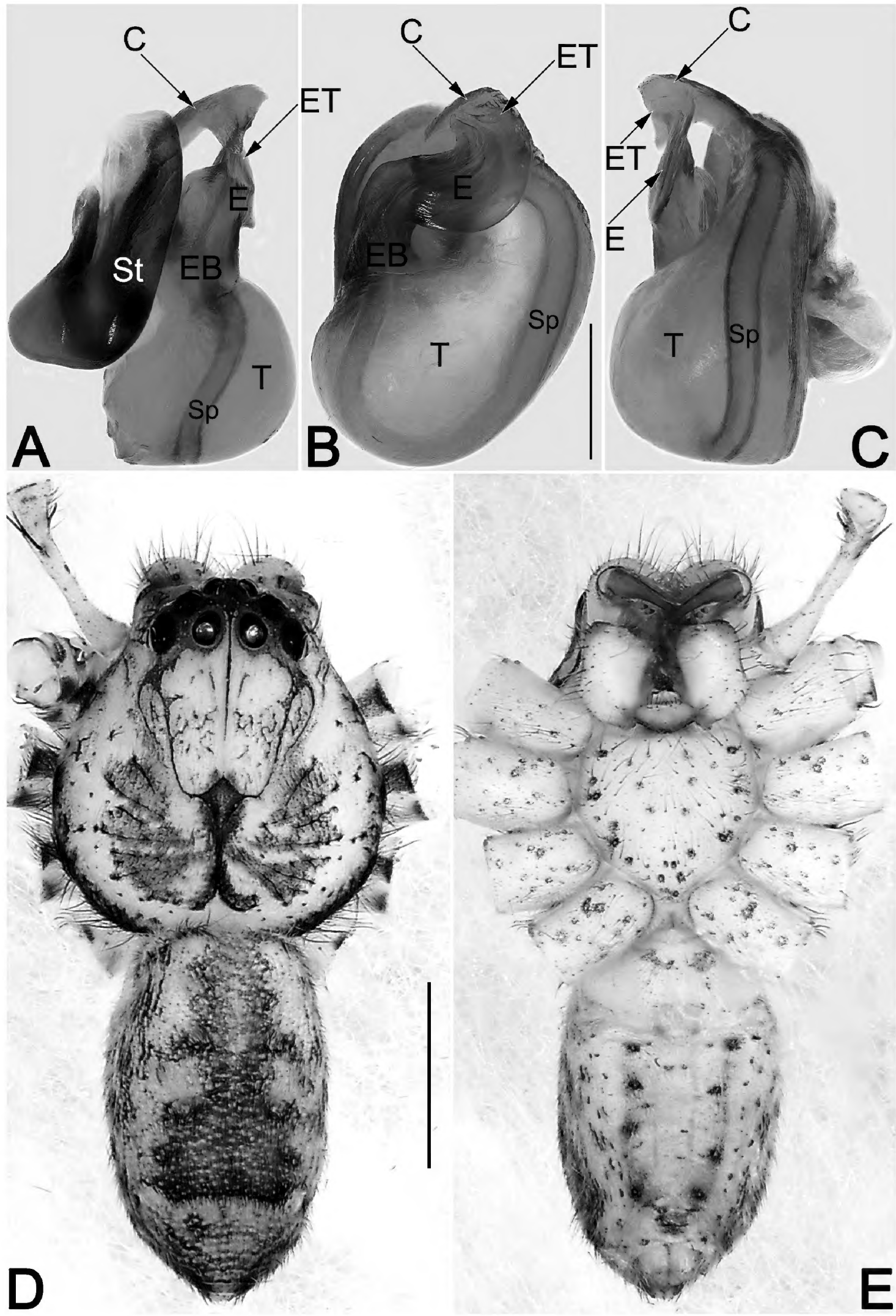

Figure 27. *Pseudopoda ying* sp. nov., male holotype, palpal bulb (**A–C**) and habitus (**D, E**). **A.** Prolateral; **B.** Ventral; **C.** Retrolateral; **D.** Dorsal; **E.** Ventral. Abbreviations: C = conductor; E = embolus; EB = embolic base; ET = embolic tip; Sp = spermophor; St = subtegulum; T = tegulum. Scale bars: 0.5 mm (equal for **A–C**); 1 mm (equal for **D, E**).

mesially and distally narrowed, apex nearly triangular, ca. 1/2 length of tibia; vRTA broad and slightly shorter than dRTA, with two distinct margins that look like mountains, among them the dorsal margin with quadrilateral-shaped apophysis. Cymbium (Cy) relatively short and wide, ca. 2.1× longer than wide, retrolaterally with a large bulge (CB). Tegulum (T) elongate-oval, ca. 1.3× longer than wide, strongly bulged and prolapsed. Spermophor (Sp) sinuate, forming a loop along tegular margin. Embolus (E) broad, ca. 4/5 of tegulum length, and wider than 1/2 of tegulum width, ƨ-shaped in ventral view, arising at approximately the 8–9 o'clock position, terminating at c. 12 o'clock position; embolic tip (ET) wide and blunt, apex rugged. Conductor (C) heavily sclerotized, c. 1/2 of the embolus length, originating at 12–1 o'clock position portion of tegulum; the base of conductor (C) relatively narrow, inserted dorsally to embolus; the tip of conductor (C) relatively wide and extending above apex of embolus.

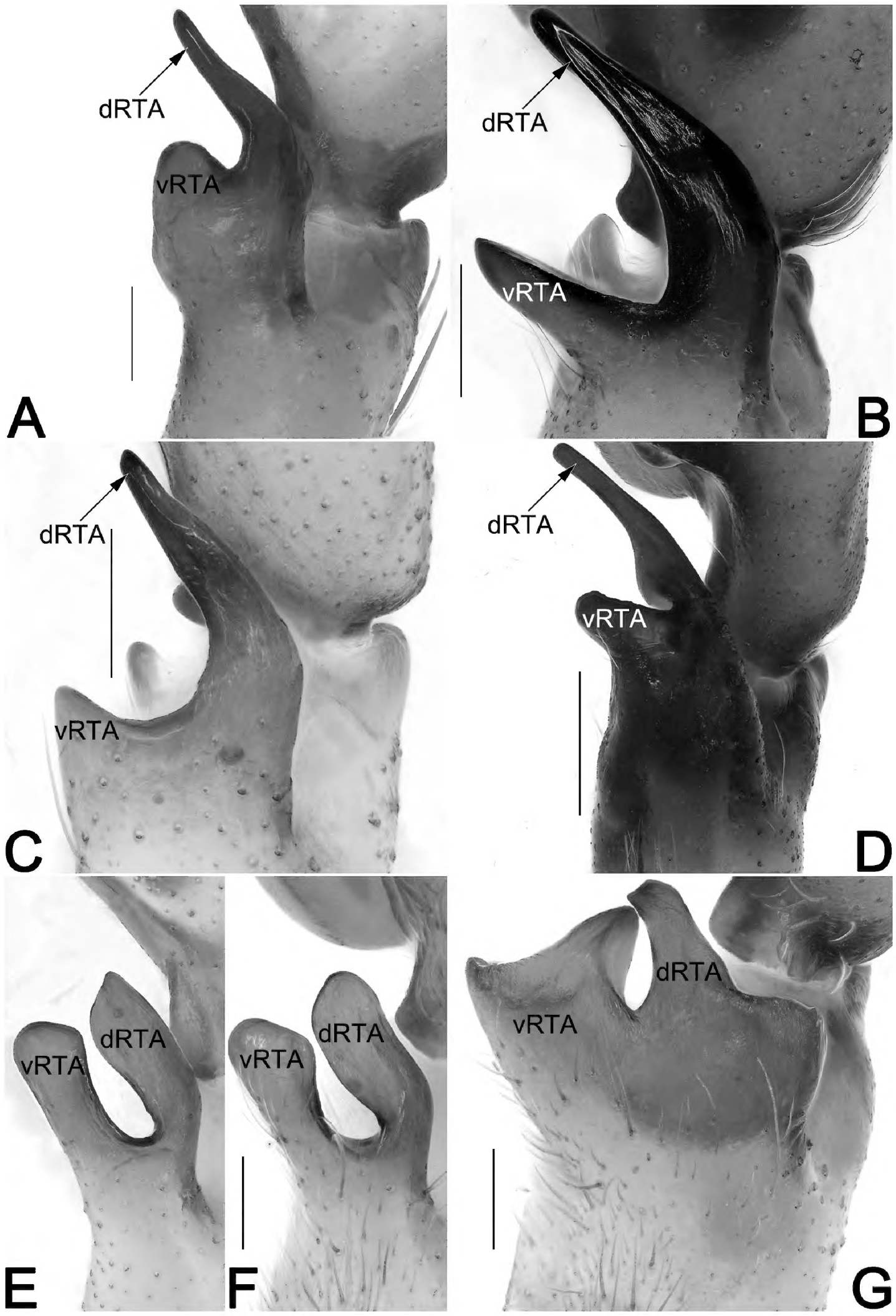

Figure 28. RTA of *Pseudopoda* spp. treated in this paper, retrolateral-dorsal **A.** *P. huanglianensis*; **B.** *P. mamillaris*; **C.** *P. oliviformis*; **D.** *P. xiaozhua* sp. nov.; **E, F.** *P. yangae* sp. nov., YNZY001 (**E**) and YNZY005 (**F**), showing the intraspecific variations exhibited by different males, related to different shapes of vRTA and dRTA; **G.** *P. ying* sp. nov. Abbreviations: dRTA = dorsal branch/part of RTA; vRTA = ventral branch/part of RTA. Scale bars: 0.2 mm (**A–C, G,** equal for **E, F**); 5 mm (**D**).

Female. Unknown.

Comments. A total of four *Pseudopoda* species are known only from females in Honghe Prefecture: *P. daweiensis*, *P. rhopalocera*, *P. zhaoae*, and *P. zuoi* (Table 1). However, none of them could be matched with *P. ying* sp. nov. due to their different habitus: abdomen with a distinct median band, which consists of a cross-shaped anterior stripe and a nearly square-shaped posterior stripe in *P. ying* sp. nov. vs. abdominal median band indistinct and not as above in *P. daweiensis*, *P. rhopalocera*, *P. zhaoae*, and *P. zuoi* (cf. Fig. 21D and Zhang et al. 2023a: figs 85A, 206A, 278A, 282A and Yang et al. 2009: fig. F). Moreover, males of *P. ying* sp. nov. exhibit typical *daliensis*-group features (diagnosis of *P. daliensis*-group, see Zhang et al. 2017: 273) and resemble the core species of the *daliensis*-group, such as *P. sicyoidea*, for their characteristic embolus and RTA (for a detailed diagnosis, see above). In contrast, females of *P. daweiensis*,

P. rhopalocera, *P. zhaoae* and *P. zuoi* exhibit the following distinctive suite of characters, here contrasted with the corresponding condition in *daliensis*-group: amLL distinctly oblique in *P. daweiensis* and *P. zuoi* (vs. amLL almost transversal to body length axis in *daliensis*-group species) (cf. Zhang et al. 2023a: figs 84A, 281A and Zhang et al. 2017: figs 2B, 4C, 6A, 9A, 12B, 14C, 16A, 17A); spermathecae covered by first windings in *P. rhopalocera*, located internally to first windings in *P. zhaoae*, not extending laterally beyond first winding (vs. extending laterally beyond first winding in *daliensis*-group species) (cf. Zhang et al. 2023a: figs 205B, 277C and Zhang et al. 2017: figs 2D, 4D, 6D, 9D, 12D, 14D, 16B, 17B). Therefore, we can rule out the possibility that the above four species are conspecific with *P. ying* sp. nov.

Distribution. Presently known only from the type locality (Fig. 1).

Acknowledgements

We are especially grateful to Danilo Harms (Hamburg, Germany), the subject editor. We thank two anonymous reviewers for providing constructive comments on the manuscript. This work was supported by the National Natural Sciences Foundation of China (NSFC-32360123/32060113/32300378/32000303), the Joint Fund of the National Natural Science Foundation of China and the Karst Science Research Center of Guizhou Province (Grant No. U1812401), the Natural Sciences Foundation of Hubei Province (2024AFC060), the Natural Sciences Foundation of Xianning City (2022ZRKX063), and the Scientific Research Project of Education Department of Hubei Province (Q20222806).

References

Barrett RDH, Hebert PDN (2005) Identifying spiders through DNA barcodes. Canadian Journal of Zoology 83(3): 481–491. https://doi.org/10.1139/z05-024

Bouckaert R, Heled J, Kuhnert D, Vaughan T, Wu CH, Xie D, Suchard MA, Rambaut A, Drummond AJ (2014) BEAST 2: a software platform for Bayesian evolutionary analysis. PLoS Computational Biology 10: e1003537. https://doi.org/10.1371/journal.pcbi.1003537

Caleb JTD, Mondal K, Kumar V (2018) A new species of the huntsman spider genus *Pseudopoda* Jäger (Araneae, Sparassidae) from the Eastern Himalayas, India. Halteres 9: 170–175. https://doi.org/10.5281/zenodo.1462247

Cao XW, Liu J, Chen J, Zheng G, Kuntner M, Agnarsson I (2016) Rapid dissemination of taxonomic discoveries based on DNA barcoding and morphology. Scientific Reports 6: 37066. https://doi.org/10.1038/srep37066

Chang J, Zhang H, Liu J, Zhu Y, Liu CY, Chen K, Hu CH (2024) Three new species of *Pseudopoda* Jäger, 2000 (Araneae, Sparassidae, Heteropodinae) from Qizimeishan National Nature Reserve of Hubei, China. ZooKeys 1214: 143–160. https://doi.org/10.3897/zookeys.1214.130101

Darriba D, Taboada GL, Doallo R, Posada D (2012) jModelTest 2: more models, new heuristics and parallel computing. Nature methods 9(8): 772. https://doi.org/10.1038/nmeth.2109

Deng MQ, Zhong Y, Irfan M, Wang LY (2023) Four new species of the spider genus *Pseudopoda* Jäger, 2000 (Sparassidae) from Yintiaoling Natural Reserve of Chongqing, China. Zootaxa 5257(1): 5–16. https://doi.org/10.11646/zootaxa.5257.1.3

Ezard T, Fujisawa T, Barraclough TG (2009) SPLITS: species' limits by threshold statistics. R Package Version 1.0-11.

Folmer O, Black M, Hoeh W, Lutz R, Vrijenhoek R (1994) DNA primers for amplification of mitochondrial cytochrome c oxidase subunit I from diverse metazoan invertebrates. Molecular Marine Biology and Biotechnology 3: 294–299.

Fu YN, Zhu MS (2008) A new species of the genus *Pseudopoda* from China (Araneae, Sparassidae). Acta Zootaxonomica Sinica 33: 657–659.

Gong LJ, Zeng MY, Zhong Y, Yu HL (2023) A new species of *Pseudopoda* (Araneae, Sparassidae) from China, with the description of different and distinctive internal ducts of the female vulva. Zookeys 1159: 189–199. https://doi.org/10.3897/zookeys.1159.97463

Hoang DT, Chernomor O, von Haeseler A, Minh BQ, Vinh LS (2018) UFBoot2: Improving the Ultrafast Bootstrap Approximation. Molecular Biology and Evolution 35(2): 518–522. https://doi.org/10.1093/molbev/msx281

Jäger P (2001) Diversität der Riesenkrabbenspinnen im Himalaya -- die Radiation zweier Gattungen in den Schneetropen (Araneae, Sparassidae, Heteropodinae). Courier Forschungsinstitut Senckenberg 232: 1–136.

Jäger P (2008) Three new *Pseudopoda* species from northern India (Araneae, Sparassidae, Heteropodinae). Revue Suisse de Zoologie 115: 515–526. https://doi.org/10.5962/bhl.part.80441

Jäger P, Vedel V (2007) Sparassidae of China 4. The genus *Pseudopoda* (Araneae, Sparassidae) in Yunnan Province. Zootaxa 1623: 1–38. https://doi.org/10.11646/zootaxa.1623.1.1

Jäger P, Pathoumthong B, Vedel V (2006) First record of the genus *Pseudopoda* Jäger 2000 in Laos with description of new species (Arachnida, Araneae, Sparassidae). Senckenbergiana Biologica 86(2): 219–228. https://doi.org/10.11646/zootaxa.1623.1.1

Jäger P, Li S, Krehenwinkel H (2015) Morphological and molecular taxonomic analysis of *Pseudopoda* Jäger, 2000 (Araneae, Sparassidae, Heteropodinae) in Sichuan Province, China. Zootaxa 3999(3): 363–392. https://doi.org/10.11646/zootaxa.3999.3.3

Jiang TY, Zhao QY, Li SQ (2018) Sixteen new species of the genus *Pseudopoda* Jäger, 2000 from China, Myanmar, and Thailand (Sparassidae, Heteropodinae). Zookeys 791: 107–161. https://doi.org/10.3897/zookeys.791.28137

Jukes TH, Cantor CR (1969) Evolution of protein molecules. In: Munro HN (Ed.) Mammalian protein metabolism. Academic Press, New York, 21–32. https://doi.org/10.1016/B978-1-4832-3211-9.50009-7

Kapli P, Lutteropp S, Zhang J, Kobert K, Pavlidis P, Stamatakis A, Flouri T (2017) Multi-rate Poisson tree processes for single-locus species delimitation under maximum likelihood and Markov chain Monte Carlo. Bioinformatics 33(11): 1630–1638. https://doi.org/10.1093/bioinformatics/btx025

Kearse M, Moir R, Wilson A, Stones-Havas S, Cheung M, Sturrock S, Buxton S, Cooper A, Markowitz S, Duran C, Thierer T, Ashton B, Meintjes P, Drummond A (2012) Geneious Basic: an integrated and extendable desktop software platform for the organization and analysis of sequence data. Bioinformatics 28: 1647–1649. https://doi.org/10.1093/bioinformatics/bts199

Khmelik VV, Kozub D, Glazunov A (2005) Helicon Focus 3.10.3. https://www.heliconsoft.com/heliconsoft-products/helicon-focus/ [accessed on 2 May 2024]

Kimura M (1980) A simple method for estimating evolutionary rates of base substitutions through comparative studies of nucleotide sequences. Journal of Molecular Evolution 16: 111–120. https://doi.org/10.1007/BF01731581

Kumar S, Stecher G, Li M, Knyaz C, Tamura K (2018) MEGA X: Molecular Evolutionary Genetics Analysis across Computing Platforms. Molecular Biology and Evolution 35: 1547–1549. https://doi.org/10.1093/molbev/msy096

Li ZC, Zhang H, Jäger P, Liu J (2019) One new *Pseudopoda* group from Yunnan Province, China (Araneae, Sparassidae). Acta Arachnologica Sinica 28(2): 96–105.

Minh BQ, Schmidt HA, Chernomor O, Schrempf D, Woodhams MD, von Haeseler A, Lanfear R (2020) IQ-TREE 2: New Models and Efficient Methods for Phylogenetic Inference in the Genomic Era. Molecular Biology and Evolution 37: 1530–1534. https://doi.org/10.1093/molbev/msaa015

Nei M, Kumar S (2000) Molecular evolution and phylogenetics. Oxford University Press, Oxford, 333 pp. https://doi.org/10.1046/j.1365-2540.2001.0923a.x

Pons J, Barraclough TG, Gomez-Zurita J, Cardoso A, Duran DP, Hazell S, Kamoun S, Sumlin WD, Vogler AP (2006) Sequence-based species delimitation for the DNA taxonomy of undescribed insects. Systematic Biology 55(4): 595–609. https://doi.org/10.1080/10635150600852011

Puillandre N, Lambert A, Brouillet S, Achaz G (2012) ABGD, Automatic Barcode Gap Discovery for primary species delimitation. Molecular Ecology 21(8): 1864–1877. https://doi.org/10.1111/j.1365-294X.2011.05239.x

R Development Core Team (2024) R Foundation for Statistical Computing. http://www.R-project.org/ [Accessed on 15 May 2024]

Rambaut A (2012) FigTree Version 1.4.0. http://tree.bio.ed.ac.uk/software/figtree/ [accessed on 15 Mayl 2024]

Ronquist F, Teslenko M, van der Mark P, Ayres DL, Darling A, Hohna S, Larget B, Liu L, Suchard MA, Huelsenbeck JP (2012) MrBayes 3.2: efficient Bayesian phylogenetic inference and model choice across a large model space. Systematic Biology 61(3): 539–542. https://doi.org/10.1093/sysbio/sys029

Wang CX, Xu X, Li SQ (2017) Integrative taxonomy of *Leptonetela* spiders (Araneae, Leptonetidae), with descriptions of 46 new species. Zoological Research 38(6): 321–448. https://doi.org/10.24272/j.issn.2095-8137.2017.076

Wen LL, Li CC, Zhong Y (2024) One new species of *Pseudopoda* Jäger, 2000 from Shennongjia, Central China (Araneae, Sparassidae). Biodiversity Data Journal 12: e130445. https://doi.org/10.3897/BDJ.12.e130445

WSC (2025) World Spider Catalog. version 25.5. Natural History Museum, Bern. http://wsc.nmbe.ch [accessed on 05 January 2025]

Wu YR, Zhong R, Zhu Y, Jäger P, Liu J, Zhang H (2024) Description of three new species of the spider genus *Pseudopoda* Jäger, 2000 (Araneae, Sparassidae) from China, Laos and Thailand, and the female of *P. kavanaughi* Zhang, Jäger & Liu, 2023. ZooKeys 1202: 287–301. https://doi.org/10.3897/zookeys.1202.116007

Xu X, Liu FX, Chen J, Li DQ, Kuntner M (2015) Integrative taxonomy of the primitively segmented spider genus *Ganthela* (Araneae, Mesothelae, Liphistiidae): DNA barcoding gap agrees with morphology. Zoological Journal of the Linnean Society 175(2): 288–306. https://doi.org/10.1111/zoj.12280

Xu X, Liu FX, Ono H, Chen J, Kuntner M, Li DQ (2017) Targeted sampling in Ryukyus facilitates species delimitation of the primitively segmented spider genus *Ryuthela* (Araneae, Mesothelae, Liphistiidae). Zoological Journal of the Linnean Society 181(4): 867–909. https://doi.org/10.1093/zoolinnean/zlx024

Xu X, Yu L, Li F, Wang BJ, Liu FX, Li DQ (2022) Phylogenetic placement and species delimitation of the crab spider genus *Phrynarachne* (Araneae, Thomisidae) from China. Molecular Phylogenetics and Evolution 173: 107521. https://doi.org/10.1016/j.ympev.2022.107521

Yang ZZ, Chen YQ, Chen YL, Zhang YG (2009) Two new species of the genus *Pseudopoda* from Yunnan, China (Araneae, Sparassidae). Acta Arachnologica Sinica 18(1): 18–22.

Yang ZZ, Wu YY, Li ZM, Zhang BS (2022) Two new species of the genus *Pseudopoda* Jäger, 2000 and first description of the male of *Pseudopoda physematosa* (Araneae, Sparassidae) from Yunnan Province, China. Zootaxa 5188(4): 347–360. https://doi.org/10.11646/zootaxa.5188.4.3

Yao ZY, Wang X, Li SQ (2021) Tip of the iceberg: species diversity of *Pholcus* spiders (Araneae, Pholcidae) in the Changbai Mountains, Northeast China. Zoological Research 42(3): 267–271. https://doi.org/10.24272/j.issn.2095-8137.2021.037

Zhang BS, Zhang F, Zhang ZS (2013a) Four new species of the genus *Pseudopoda* Jäger, 2000 (Araneae, Sparassidae) from Yunnan Province, China. Zootaxa 3702: 273–287. https://doi.org/10.11646/zootaxa.3702.3.5

Zhang F, Zhang BS, Zhang ZS (2013b) New species of *Pseudopoda* Jäger, 2000 from Southern China (Araneae, Sparassidae). Zookeys 361: 37–60. https://doi.org/10.3897/zookeys.361.6089

Zhang H, Jäger P, Liu J (2017) One new *Pseudopoda* species group (Araneae, Sparassidae) from Yunnan Province, China, with description of three new species. Zootaxa 4318(2): 271–294. https://doi.org/10.11646/zootaxa.4318.2.3

Zhang H, Jäger P, Liu J (2019) Establishing a new species group of *Pseudopoda* Jäger, 2000 with the description of two new species (Araneae, Sparassidae). Zookeys 879: 91–115. https://doi.org/10.3897/zookeys.879.35110

Zhang H, Zhu Y, Zhong Y, Jäger P, Liu J (2023a) A taxonomic revision of the spider genus *Pseudopoda* Jäger, 2000 (Araneae, Sparassidae) from East, South and Southeast Asia. Megataxa 9(1): 1–304. https://doi.org/10.11646/megataxa.9.1.1

Zhang Q, Zhang JJ, Ma CY, Zhao FW (2023b) Main problems of biodiversity supporting bioeconomy in Honghe Hani and Yi Autonomous Prefecture. Forestry Construction 2: 52–59. https://doi.org/10.16473/j.cnki.xblykx1972.2022.02.016